

Neutrino-nucleus reactions and their role for supernova dynamics and nucleosynthesis

K. G. Balasi¹, K. Langanke^{2,3},
and G. Martínez-Pinedo^{3,2}

¹Demokritos National Center of Scientific Research,
Agia Paraskevi Attikis, 15310 Athens, Greece

²GSI Helmholtzzentrum für Schwerionenforschung,
Planckstr. 1, 64291 Darmstadt, Germany

³Institut für Kernphysik, Technische Universität Darmstadt,
Schlossgartenstr. 9, 64289 Darmstadt, Germany

March 30, 2015

Abstract

The description of nuclear reactions induced by supernova neutrinos has witnessed significant progress during the recent years. On one hand this progress is due to experimental data which serve as important constraints to model calculations, on the other hand it is related to advances in nuclear modelling itself and in computer hardware. At the energies and momentum transfers relevant for supernova neutrinos neutrino-nucleus cross sections are dominated by allowed transitions, however, often with non-negligible contributions from (first) forbidden transitions. For several nuclei allowed Gamow-Teller strength distributions could be derived from charge-exchange reactions and from inelastic electron scattering data. Importantly the diagonalization shell model has been proven to accurately describe these data and hence became the appropriate tool to calculate the allowed contributions to neutrino-nucleus cross sections for supernova neutrinos. Higher multipole contributions are usually calculated within the framework of the Quasiparticle Random Phase Approximation, which describes the total strength and the position of the giant resonances quite well. Both are the relevant quantities for a reliable calculation of the forbidden contributions to the cross sections.

The current manuscript reviews the recent progress achieved in calculating supernova-relevant neutrino-nucleus cross sections and discusses its verification by data. Moreover, the review summarizes also the impact which neutrino-nucleus reactions have on the dynamics of supernovae and on the associated nucleosynthesis. With relevance to the supernova dynamics these include the absorption of neutrinos by nuclei (the inverse of nuclear electron capture which is the dominating weak-interaction process during collapse), inelastic neutrino-nucleus scattering and nuclear de-excitation by neutrino-pair emission. For supernova nucleosynthesis we discuss the role of neutrino-induced reactions for the recently discovered νp process, for the r-process and for the neutrino process, for which neutrino-nucleus reactions have the largest impact. Finally we briefly review neutrino-nucleus reactions important for the observation of supernova neutrinos by earth-bound detectors.

1 Introduction

February 1987 was the birth of extrasolar neutrino astronomy when detectors in Japan and the United States registered neutrinos which travelled over 50 kpc from the Large Magellanic Cloud to Earth and gave the first indications that a star in this neighbor galaxy of the Milky Way had exploded as a supernova [1, 2]. This extraordinary scientific event also proved the general expectation that neutrinos are produced in enormous numbers in supernovae triggered by the core collapse of massive stars. In fact, about 99% of the gravitational binding energy released in the cataclysmic event is carried away by neutrinos, clearly overpowering the kinetic energy associated with the expansion of the supernova and the energy radiated away as light, despite the fascinating fact that supernovae can shine as bright as entire galaxies.

Although the neutrinos observed from supernova SN1987A were likely all electron antineutrinos, identified by the Cerenkov light produced by the relativistic positrons after a charged-current neutrino reaction on the protons in the water Cerenkov detectors, the amount of observed neutrinos and their energy spectrum (of order a few 10s of MeV) confirmed the general understanding of supernova dynamics [3]. These observations were supplemented by detailed studies of the SN1987A lightcurve, which as expected, followed the sequence of half-lives of radioactive nuclides like ^{56}Ni , ^{57}Ni or ^{44}Ti , which were copiously produced in the hot supernova environment [4].

Core-collapse, or Type II, supernovae are the final fate of massive stars when at the end of hydrostatic burning their inner core, composed of nuclei in the iron-nickel mass range, runs out of nuclear fuel and collapses under its own gravity triggering an explosion during which most of the star's material, partly processed in the hot environment in what is called explosive nucleosynthesis, is ejected into the Interstellar Medium [3]. In the general picture of core-collapse supernovae and their associated nucleosynthesis, neutrino reactions on nucleons and nuclei play an important role. Arguably, however, the most important impact neutrinos have on the supernova dynamics is the fact that, for the typical supernova neutrino energy scales, they virtually do not interact with matter for densities smaller than a few $10^{11} \text{ g cm}^{-3}$. This makes neutrinos the most efficient cooling mechanism during the late hydrostatic burning stages and the early collapse phase, where neutrinos could be thought of as free streaming with an appropriate energy loss correction for nuclear reactions mediated by the weak interaction like β decay or electron capture. This picture does not hold at higher densities, say in excess of $10^{12} \text{ g cm}^{-3}$, the neutrino interaction with matter is strong enough making a detailed bookkeeping of neutrinos and their interaction with matter a tedious, but necessary requirement for supernova modeling. During the collapse phase when densities larger than $10^{12} \text{ g cm}^{-3}$ are reached, it is the elastic scattering of neutrinos on nuclei which changes the neutrino transport through the dense matter to a diffusion problem with time scale larger than the competing collapse time scale. As a consequence neutrinos are trapped during the final stage of the collapse. By inelastic scattering on electrons and, to a lesser extent, on nuclei, neutrinos exchange energy with matter and get thermalized. Inelastic neutrino-nucleus scattering plays also an interesting role in a short episode after core bounce, where it alters the spectrum of electron neutrinos emitted during the so-called neutrino burst [5].

The supernova explosion is triggered by a shock wave which, when passing outwards through the Fe-Ni-core, dissociates the heavy nuclei into free nucleons. The interaction of neutrinos, produced by the hot matter of the freshly-born neutron star in the center, with the free protons and neutrons behind the shock are an effective additional energy source which, together with effects like convection and plasma instabilities, are required for successful explosions, as modern multi-dimensional supernova simulations show [6, 7].

It is also the competition of the various interactions of electron neutrinos with neutrons and of anti-electron neutrinos with protons, which determines the proton-to-neutron ratio of the matter ejected from the surface of the nascent proto-neutron star crucially influencing the subsequent nucleosynthesis of the ejected matter in this neutrino-driven wind model. Simulations indicate that there are periods

where the neutrino-driven wind matter is proton-rich (with an electron-to-nucleon ratio $Y_e > 0.5$) and where it is neutron-rich ($Y_e < 0.5$). In the former case the nucleosynthesis occurring when the ejected matter reaches cooler regions at larger distances from the neutron star surface gives rise to the recently discovered νp process. For several years the ejection of neutron-rich matter in the neutrino-driven wind has been considered as the favorite site for the astrophysical r-process. However, modern supernova simulations predict astrophysical conditions which allow for a 'weak r-process' [8], which can produce elements up to the second peak around mass number $A \sim 130$, which are, however, not sufficient for the production of r-process nuclides at the gold-platinum peak and the transactinides. As the nucleosynthesis in the neutrino-driven wind scenario occurs in the presence of enormous neutrino fluxes, neutrino-induced reactions on nuclei might play an important role in these processes. Particularly relevant are here neutrino-induced reactions with particle emission (neutron, protons, α) in the final channel as they implicitly alter the nuclear abundance distributions. Neutrino-induced particle emission of nuclei is also the key process in the neutrino nucleosynthesis process [9] which is responsible for the production of selected nuclides generated by particle spallation of more abundant nuclides in charged- or neutral-current reactions in the outer shells of the star.

Obviously neutrino-induced reactions by the various target nuclei are the means for detection of supernova neutrinos. After the observation of anti-electron neutrinos from SN1987A, it is the aim of operational and future detectors to individually detect the various neutrino types and proof the differences in the spectra of ν_e , $\bar{\nu}_e$ and ν_x (usually used to combine ν_μ and ν_τ neutrinos and their anti-particles which are expected to have quite similar spectra) predicted by supernova models.

Neutrino reactions on nuclei can be described in perturbation theory. For the energies and momentum transfers relevant for supernova neutrinos the task reduces to a nuclear structure problem where mainly allowed and first-forbidden transitions are of importance. Fermi transitions, of relevance for elastic neutrino scattering and for (ν_e, e^-) reactions, can only occur to Isobaric Analog States. Due to progress in computer hardware and impressive advances in shell model developments Gamow-Teller (GT) strength distributions can now be calculated for up to medium-mass nuclei taking the relevant nuclear degrees of freedom into account. This theoretical progress has been accompanied by novel experimental techniques which allow the determination of the GT_- strength (in which a neutron is changed into a proton as it is relevant for (ν_e, e^-) reactions) by (p, n) [10] and $(^3\text{He}, t)$ [11, 12] charge-exchange reactions and of the GT_+ strength (in which a proton is changed into a neutron as in the $(\bar{\nu}_e, e^+)$ reaction or in electron capture) by (n, p) [13] and, with significantly improved resolution, by the $(d, ^2\text{He})$ [14] and $(t, ^3\text{He})$ [15] reactions at intermediate energies. The GT_0 strength, important for inelastic neutrino-nucleus scattering, can be studied in (p, p') reactions, but it is also constrained by precision M1 data obtained in inelastic electron scattering for spherical nuclei where the orbital contribution to the M1 transition is small and the spin part is dominated up to a constant factor by the same operator as the GT_0 transitions. Importantly, the shell model studies reproduce the measured GT and M1 strength distributions quite well, except for a constant normalization factor and hence it is the method of choice to describe the Gamow-Teller contributions to the neutrino-nucleus cross sections. The calculation of first-forbidden (dipole) transitions require multi-shell studies which, due to computer limitations, have only been possible for light nuclei yet. Usually dipole contributions to the neutrino cross sections are derived within the Quasi-Particle Random Phase Approximation (QRPA) which can handle model spaces with a larger number of single particle orbitals than the shell model space, however, for the price of considering only (2 particle – 2 hole) correlations among nucleons. The QRPA is well suited to describe the energy centroid and total strength of giant resonances and hence gives a fair description of neutrino-nucleus cross sections if the neutrino energy is sufficiently large so that the cross sections are dominated by the contributions from giant resonances.

Neutrino-induced spallation reactions are usually described in a two-step process, calculating the neutrino-induced excitation spectrum within the framework of the shell model and QRPA, followed by a determination of the decay probability into the various particle (or γ) channels using the statistical

model. Exploiting this two-step strategy differential cross sections have been derived for nearly the entire nuclear chart which can now be routinely used in nucleosynthesis studies.

In this article we would like to review recent developments in the description of neutrino-nucleus reactions. Hereby we will focus solely on neutrino energies up to a few 10s of MeV, as they are relevant for supernovae. The description of reactions induced by higher-energetic neutrinos as they are important for atmospheric, accelerator or astrophysical neutrinos from other sources require different theoretical approaches; as outlined e.g. in Refs. [16, 17]. Our review can be viewed as an extension and update of the article by Kolbe *et al.* [18]. Hence we will only briefly repeat some of the material presented there, but focus mainly on the research performed later. Our review is organized as follows: in the next section we will briefly describe the current understanding of core-collapse supernovae, paying special attention to the role of neutrinos. In particular we will discuss the neutrino spectra during the collapse and arising from the cooling of the proto-neutron star. In Section 3 we summarize the basic cross section formulae for neutrino-nucleus reactions and discuss the models, mainly shell model and QRPA, used to derive the necessary nuclear input. We will also compare strength functions obtained with these models with experimental data. Furthermore we discuss in Section 3 on the basis of the statistical model the derivation of the decay probabilities into particle and γ channels as required to calculate partial cross sections for neutrino-induced spallation reactions and summarize some general results. Sections 4 and 5 are concerned with the description of specific neutrino-nucleus reactions and their role for the supernova dynamic and nucleosynthesis, respectively. Finally we summarize in Section 6 the progress achieved to describe neutrino-nucleus reactions of importance for operational and future supernova detectors.

2 Brief description of core-collapse supernovae

During their long lifetimes of millions and billions of years stars generate the energy necessary to achieve hydrostatic equilibrium by nuclear reactions in their interior [19, 20, 21]. The first nuclear reaction source which a star taps is hydrogen burning, the fusion of 4 proton nuclei to ^4He . Hydrogen burning occurs, in stars like our Sun, in a reaction sequence called pp-chains beginning with the formation of a deuteron by the fusion of two protons mediated by the weak interaction. In more massive stars than the Sun hydrogen burning occurs at slightly higher temperatures making hydrogen burning via the CNO cycle energetically more efficient than by the pp chains [22, 23]. It is interesting to note that hydrogen burning produces a nucleus (^4He) with an identical amount of protons and neutrons (i.e. $Y_e = 0.5$) from matter with an unbalanced proton-to-neutron ratio basically inherited from the Big Bang. It is an important feature of hydrostatic burning and nuclear stability that this value of $Y_e = 0.5$ is kept during the various burning stages.

The ashes of hydrogen burning, ^4He , can be burnt once the temperature of the star's interior has increased sufficiently by core contraction to enable the fusion of three ^4He nuclei to ^{12}C . This triple-alpha reaction and the subsequent $^{12}\text{C}(\alpha, \gamma)^{16}\text{O}$ reaction constitute helium burning. Both together determine the carbon/oxygen ratio in the Universe. Hence helium burning is essential for life as we know it.

In sufficiently massive stars the sequence of core contraction associated with a rise of the temperature repeats itself igniting successively the ashes of the previous burning phase. Thus following helium burning massive stars undergo in their centers the sequence of carbon, neon, oxygen and silicon burning until an 'iron core' is produced as the product of silicon core burning. At this phase of its hydrostatic burning, a massive star consists of concentric shells that are the remnants of its previous burning phases (hydrogen, helium, carbon, neon, oxygen, silicon) surrounding the iron core.

The temperature in the iron core (a few 10^9 K) is sufficiently high to establish an equilibrium of reactions mediated by the strong and electromagnetic interaction and their inverse. Under such conditions the matter composition is given by Nuclear Statistical Equilibrium (NSE). Importantly once such an equilibrium is achieved nuclear reactions (by strong and electromagnetic forces) cease as energy

sources. Hence the star has lost its nuclear energy source in the center and the iron core becomes eventually unstable under its own gravity. We note that the NSE matter composition depends on the astrophysical parameters (temperature and density). For the following discussion it is important that it also depends on the proton-to-neutron ratio, i.e. on the Y_e value, which can only be changed by reactions mediated by the weak interaction. Initially the ashes of silicon burning consists roughly of the same amount of protons and neutrons ($Y_e \approx 0.5$) favoring, in NSE, nuclei in the vicinity of the double-magic nucleus ^{56}Ni . Under (early) core conditions reactions mediated by the weak interaction are not in equilibrium with their inverse. This, as we will discuss next, will change the Y_e value during the collapse and relatedly the matter composition.

While the mass of the core is dominated by the nuclear component, the pressure is given by the electrons, which under core conditions, form a degenerate ultrarelativistic Fermi gas; both components are connected by the electron-to-nucleon ratio Y_e . Once the core density reaches values of order 10^9 g cm^{-3} or higher, the electron Fermi energy grows to values in excess of MeV, the core matter can efficiently lower its free energy by electron captures on nuclei. This process has three important consequences:

1) At densities below $10^{11} \text{ g cm}^{-3}$ the neutrinos produced by the capture process can leave the star unhindered carrying away energy. This is a very efficient cooling mechanism which, as noted in the fundamental paper by Bethe, Brown, Applegate and Lattimer (BBAL) [24] keeps the entropy of the matter low. As a consequence heavy nuclei survive during the collapse.

2) Electron capture reduces the number of electrons (i.e. Y_e gets smaller). As a result the pressure which the matter can stem against the gravitational collapse is reduced and the collapse is accelerated.

3) As electron captures change a proton in the nucleus into a neutron, the matter composition is driven towards more neutron-rich (and heavier) nuclei. With increasing neutron excess, nuclei become unstable against β decay. Under core conditions these decays are, however, hindered due to Pauli blocking by electrons and at sufficiently high densities (say in excess of $10^{10} \text{ g cm}^{-3}$) the phase space for beta decays closes and electron capture dominates by a large factor driving the core composition to neutron-rich, β -unstable nuclei

It should be mentioned that β decay is temporarily competitive with electron capture after silicon depletion and during silicon shell burning [25, 26]. Besides counteracting electron captures by increasing the Y_e value, β decays are also an important neutrino source and thus add to the cooling of the core and the reduction of the entropy [25]. Finally, we remark that it is quite fortuitous that for pre-supernova simulations β decay rates are only required for nuclei for which large-scale shell model calculations can be performed [27].

Exploiting progress in nuclear modelling electron capture rates at supernova conditions have recently been calculated using an appropriately chosen hierarchy of approaches [28]. At densities up to about $10^{10} \text{ g cm}^{-3}$ supernova weak-interaction rates are dominated by nuclei in the mass range $A = 45 - 65$ (pf -shell nuclei). At such densities the electron chemical potential is of the same order as the nuclear Q values requiring a detailed reproduction of the GT_+ distribution due to the strong phase space sensitivity of the rates. As we will discuss in the next Section, modern shell model calculations are capable to describe GT_+ distributions rather well. Shell model diagonalization in the pf model space has therefore been used to calculate the weak-interaction rates for the nuclei with $A \sim 50-65$ [29, 27, 30]. These rates explicitly consider that, due to the finite temperature in the star, electron capture can also occur from excited states, which can have different GT_+ distributions than the ground state. With continuing electron captures and at higher densities (above $10^{10} \text{ g cm}^{-3}$) nuclei become relevant for the capture rates which have proton numbers $Z < 40$ and neutron numbers $N > 40$; i.e. in the Independent Particle Model (IPM) the valence protons are in the pf shell, while the valence neutrons occupy already the next major shell (sdg shell). For such nuclei the IPM predicts a vanishing GT_+ strength as the GT operator acts only in spin-isospin space and all GT_+ transitions of the valence protons would be blocked due to the complete occupation of pf orbitals by neutrons. Hence electron captures on such nuclei are only possible due to correlations of nucleons across the $N = 40$ shell gap.

Such cross-shell correlations are a rather slowly converging process and usually require multi-particle-multi-hole excitations [31]. Taking this into account, the electron capture rates for heavier nuclei have been calculated within a hybrid approach. At first, the Shell Monte Carlo Approach (SMMC) [32, 33] has been used to determine occupation numbers of proton and neutron orbitals by performing SMMC calculations for individual nuclei at finite temperature within the complete pf - sdg shell and taking the appropriate nuclear correlations into account. Using these finite-temperature occupation numbers electron captures have been calculated using the RPA approach. The latter step is justified as at the conditions under which the nuclei with $A > 65$ are relevant the electron chemical potential is noticeably larger than the respective nuclear Q values making the capture rates mainly sensitive to the centroid and total value of the transition strength, but not to its detailed structure [28]. Forbidden transitions contribute increasingly to the capture rates with growing density and, relatedly, electron chemical potential. Inspired by the IPM supernova simulations have for a long time assumed that electron captures on heavy nuclei (with $N > 38$ [34]) vanish and that the capture occurs solely on free protons (which have the larger individual capture rate than heavy neutron-rich nuclei due to the smaller Q value, but are much less abundant in the core caused by the low entropy). More recent supernova simulations have incorporated the modern shell model rates and find that the capture on heavy nuclei dominates during the entire collapse [35, 36, 37]. By measuring the GT_+ strength for ^{76}Se (with 34 protons and 42 neutrons) it has been experimentally demonstrated that the strength is indeed unblocked by nuclear correlations across the $N = 40$ gap [38]. Data from transfer reaction measurements [39], in agreement with large-scale shell model calculations [40], indicate about 4 neutron holes in the pf shell in the ^{76}Se ground state, unblocking GT_+ transitions of valence protons.

Electron capture on nuclei is the main neutrino source during collapse. Fig. 1 shows the respective neutrino spectra produced at different moments during the core collapse of a $15 M_\odot$ and a $25 M_\odot$ star, respectively. The spectra have been calculated from the individual electron captures of about 3000 nuclei, averaged over an appropriate NSE distribution. The collapse snapshots are chosen to support the following discussion on neutrino trapping and thermalization. Due to the finite temperature of the environment and the presence of many nuclei the neutrino spectra are quite wide. At densities of a few $10^{11} \text{ g cm}^{-3}$ the spectrum is centered around neutrino energies of order 10 MeV. Due to the increase of electron chemical potential with density ($\sim \rho^{1/3}$) the neutrino spectra are shifted to higher energy with growing density. At $\rho > 10^{12} \text{ g cm}^{-3}$ the centroid is at neutrino energies $E_\nu \approx 20 \text{ MeV}$. Screening due to the astrophysical environment effectively reduces the chemical electron potential and enhances the nuclear Q value. These effects decrease the electron capture rates slightly and shift the neutrino spectra to lower energies (by about 2 MeV as is shown in Fig. 1).

An important change in the physics of the collapse occurs, when neutrinos start to get trapped in the core at densities $\rho_{\text{trap}} \approx 4 \times 10^{11} \text{ g cm}^{-3}$. The main process is elastic scattering of neutrinos on nuclei. The respective total cross section for this process is given by [3]

$$\sigma_{\text{el}}(E_\nu) = \frac{G_F^2}{4\pi} [N - (1 - 4 \sin^2 \theta_W)Z]^2 E_\nu^2 \quad (1)$$

where E_ν is the energy of the incident neutrino; G_F and θ_W are the Fermi coupling constant and the Weinberg angle ($\sin^2 \theta_W \approx 0.231$), respectively. As $(1 - 4 \sin^2 \theta_W) \approx 0.08$, elastic neutrino scattering occurs mainly as a coherent process on the neutrons in the nuclei. In Eq. 1 it has been assumed that the elastic form factors for protons and neutrons can be replaced by $F_{Z,N}(q^2) = F_{Z,N}(q^2 = 0) = 1$ which is justified at the momentum transfers involved. For odd- A and odd-odd nuclei with ground state angular momenta $J \neq 0$ and at finite temperature there can also be a GT contribution to the cross section. However, due to the strong fragmentation of the GT strength this is usually negligibly small. Furthermore under supernova conditions even-even nuclei dominate the nuclear composition. As is demonstrated in [3] neutrinos with energies about 20 MeV will have a mean free path of order 0.5 km at densities $10^{12} \text{ g cm}^{-3}$ which is significantly smaller than the core radius at the same density. As a

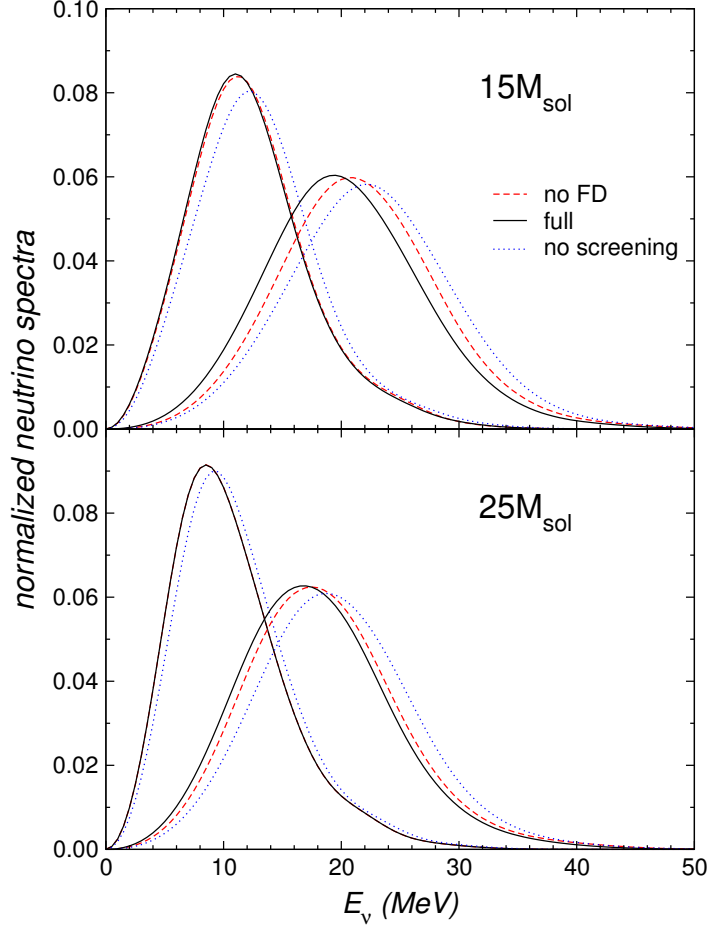


Figure 1: Neutrino spectra produced by electron captures on nuclei at two different densities ($3.76 \times 10^{11} \text{ g cm}^{-3}$ and $2.47 \times 10^{12} \text{ g cm}^{-3}$) during the collapse of a star with $15 M_{\odot}$ and at $1.13 \times 10^{11} \text{ g cm}^{-3}$ and $1.54 \times 10^{12} \text{ g cm}^{-3}$ for a $25 M_{\odot}$ star. For the solid line an NSE distribution has been assumed for the matter composition; the dashed line shows the spectrum if heavy nuclei (with $A > 100$) are neglected in the distribution. The dotted curve shows the spectra if screening corrections due to the astrophysical environment are not included. (from [28])

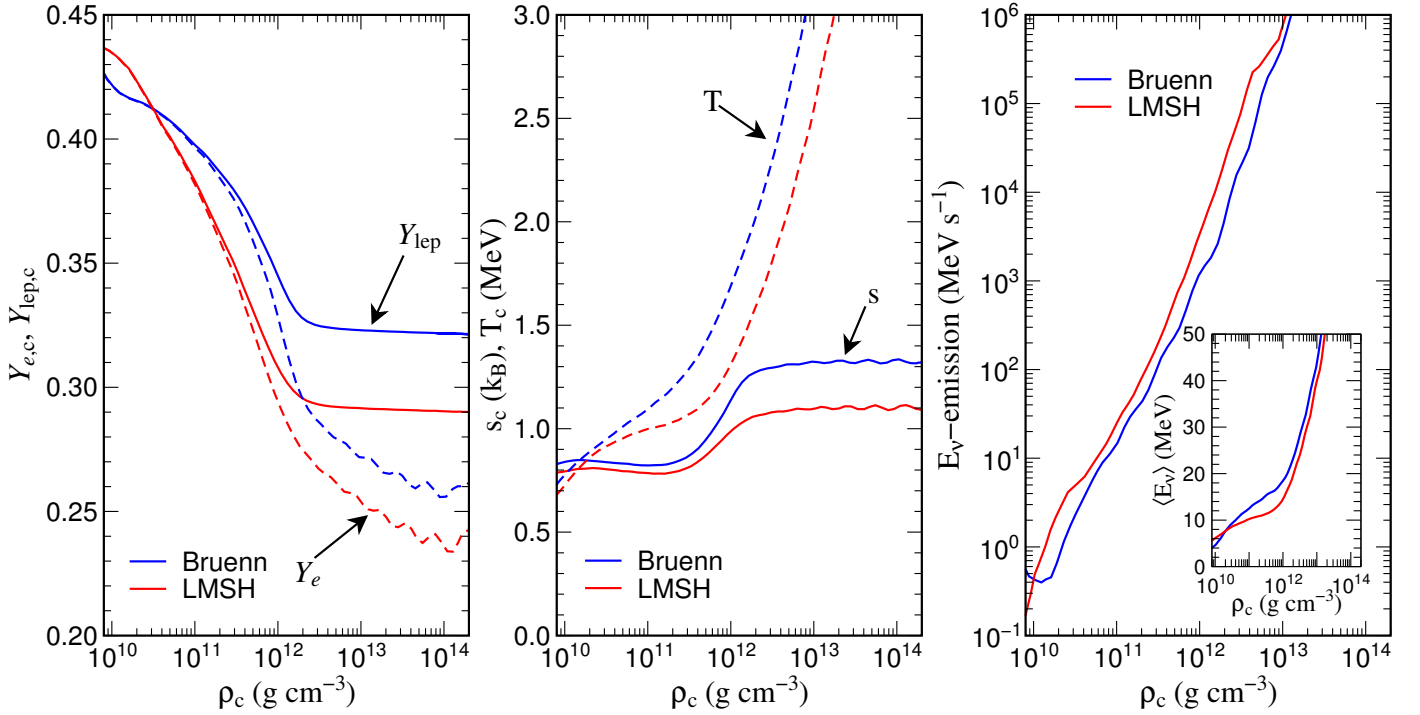


Figure 2: Comparison of the central values for the electron (Y_e) and lepton Y_{lep} abundances (left panel), temperature and entropy (middle panel) and electron neutrino emission rate (right panel) obtained in a spherical simulation of the collapse of an $18 M_\odot$ star using the shell model electron capture rates (LMSH) or neglecting capture on heavy nuclei with $N > 38$ (Bruenn rates [34]). The insert in the right panel compares the average neutrino energies. (courtesy Hans-Thomas Janka, adapted from [45])

consequence neutrinos scatter quite often in the core and their propagation has to be described by a diffusion process. Indeed, the diffusion time scale at $\rho = 10^{12} \text{ g cm}^{-3}$ is longer than the competing collapse time scale and neutrinos are effectively trapped during the final phase of the collapse.

Neutrinos exchange energy with the core matter by inelastic scattering, mainly on electrons. As electrons are highly degenerate at this stage of the collapse, they can only gain energy and hence neutrinos are down-scattered in energy. By inelastic scattering on nuclei neutrinos can both lose and gain energy (as is discussed in Section 4). Simulations, however, show that this process is less important during collapse than inelastic neutrino-electron scattering which is found to be quite efficient in thermalizing the neutrinos with the rest of the matter. This is effectively achieved at densities in excess of $10^{12} \text{ g cm}^{-3}$ as is demonstrated in Fig. 2 which shows results from a (spherical) collapse simulation of an $18 M_\odot$ star. The figure shows that the lepton abundance, i.e. the sum of abundances of electrons and electron neutrinos, reach a constant value once neutrinos are trapped and a Fermi sea of electron neutrinos builds up in the core. The figure also clearly demonstrates the impact of the modern electron capture rates (LMSH) on the collapse dynamics if compared to results based mainly on the IPM approach (neglecting electron capture on nuclei with neutron numbers $N > 38$ [34]). As electron captures on nuclei dominate over those on free protons the electron neutrino emission rate is larger, while the central core values for temperature, entropy and Y_e are smaller. At densities $\rho < 3 \times 10^{10} \text{ g cm}^{-3}$ nuclei from the mass region $A = 45 - 65$ dominate. For these nuclei the electron capture rates obtained by shell model diagonalization [27] are noticeably smaller than those inspired by the IPM (and corrected by data whenever available) [41, 42, 43, 44]. As neutron-rich nuclei have larger Q values than protons, the average neutrino energies are smaller in simulations incorporating the shell model capture rates.

After neutrino trapping, the collapse proceeds homologously [46], until nuclear densities ($\rho_N =$

$2.5 \times 10^{14} \text{ g cm}^{-3}$) are reached. Since nuclear matter has a much lower compressibility, the homologous core decelerates and bounces in response to the increased nuclear matter pressure. This drives a shock wave into the outer core; i.e. the region of the iron core which lies outside the homologous core and in the meantime has continued to fall inwards at supersonic speed. The core bounce with the formation of a shock wave is the mechanism that ultimately triggers a supernova explosion, but the exact mechanism of this physically appealing scenario are still uncertain and controversial. It appears as if the energy available to the shock is not sufficient, and the shock uses up its energy in the outer core mostly by the dissociation of nuclei into nucleons [3, 37]. This change in composition results to additional energy losses, because the electron capture rate on free protons is significantly larger than on neutron-rich nuclei due to the higher Q-values of the latter. A large fraction of the neutrinos produced by these capture behind the shock leave the star quickly in what is called the neutrino burst at shock break out, carrying away energy. This leads to further neutronization of the matter. The shock wave is weakened so much that it finally stalls and turns into an accretion shock.

After the core bounce, a compact remnant begins to form in the center. Depending on the stellar mass, this is either a neutron star (for progenitor stars with masses roughly smaller than $25 M_{\odot}$) or a black hole. The nascent proto-neutron star contains a large number of degenerate electrons and neutrinos, the latter being trapped as their mean free paths in the dense matter is significantly shorter than the radius of the neutron star. As the trapped neutrinos diffuse out, they convert most of their initially high degeneracy energy to thermal energy of the stellar medium [47]. The cooling of the proton-neutron star then proceeds by pair production of neutrinos of all three generations which diffuse out. After several tens of seconds the star becomes transparent to neutrinos and the neutrino luminosity drops significantly [48].

In what is called the ‘delayed neutrino-heating mechanism’ the stalled shock wave can be revived by neutrinos [49]. These carry most of the energy set free in the gravitational collapse of the core [47] and deposit some of it in the layers between the nascent neutron star and the stalled prompt shock, mainly by absorption on nucleons. This lasts for a few 100 ms, and requires about 1% of the neutrino energy to be converted into nuclear kinetic energy. The energy deposition increases the pressure behind the shock. However, it appears that energy transport by neutrinos is not enough to explode models with spherical symmetry [50, 51, 52]. However, multi-dimensional hydrodynamical simulations in two dimensions [53, 54, 55, 56] and in 3 dimensions [57, 58, 59, 60, 61] show that the region of low density, but rather high temperature (named ‘hot neutrino bubble’), which forms between the neutron star surface and the shock front, is convectively unstable developing large convective overturns which enhance the neutrino energy deposit behind the shock [54, 62, 63, 64]. This is additionally aided by instabilities of the shock to non-radial deformation (standing accretion shock instability SASI) which increases the time matter stays in the heating region [65, 66, 67, 68, 69, 70].

The simulations sensitively depend on the nuclear Equation of State (EoS) which is still not sufficiently well-known. It strongly influences the formation, the strength and the evolution of the shock wave, the latter indirectly via the compactness and the contraction of the nascent neutron star. For densities less than about $\rho_N/10$, nucleonic matter exists of individual nuclei. At larger densities matter exists in a variety of complex shapes caused by a competition of repulsive Coulomb forces and nuclear attraction until it reaches uniform nuclear matter. There are several EoS [71, 72, 73, 74, 75, 76, 77] frequently used in supernova simulations. A novel ansatz, based on the relativistic mean-field with density-dependent couplings and the explicit consideration of light-particle bound states, has recently been presented [78]. Refs. [79, 80] has studied the implications of an Equation of State with an explicit QCD phase transition to quark matter on the postbounce supernova evolution.

In the dense environment encountered in the late stage of the collapse or in the nascent neutron star, neutrino processes are modified by ion-ion correlations [81]. This includes the coherent elastic scattering of neutrinos on nuclei [82, 83, 84]. Correlations are particularly important for neutrino-pair bremsstrahlung, $NN \leftrightarrow NN\nu\bar{\nu}$. Calculations performed on the basis of Chiral Effective Field Theory

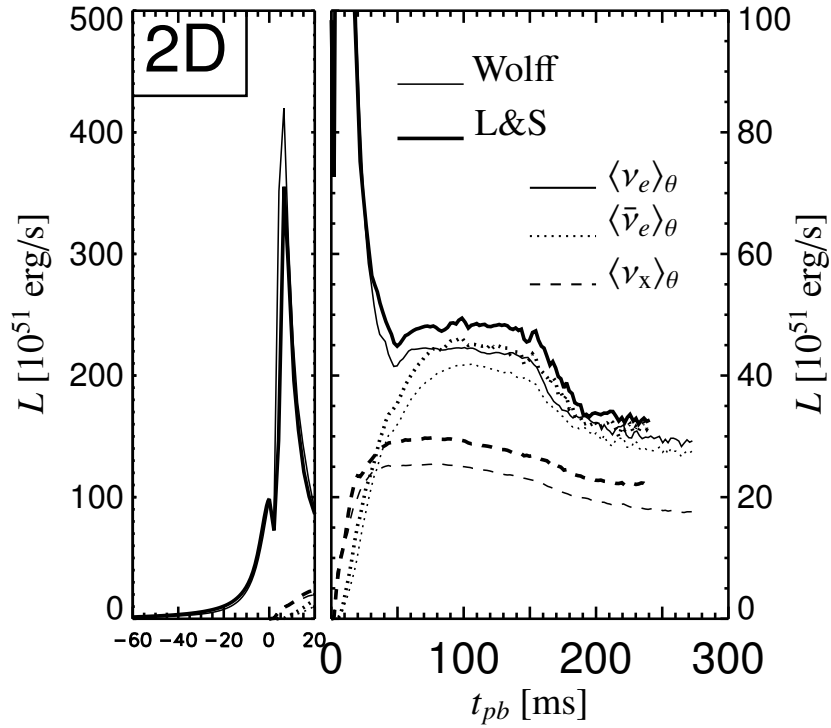


Figure 3: Results from 2D core-collapse simulations with two different equations of states (“Wolff” [73] and “L&S” [71]) for a $15 M_\odot$ star, using the neutrino transport technique of Refs. [89, 90]. The figure displays the neutrino luminosities with the prompt ν_e burst in the left window and the postbounce luminosities of ν_e (solid lines), $\bar{\nu}_e$ (dotted) and heavy-lepton ν ’s and $\bar{\nu}$ ’s (dashed) in the right window. The results of the 2D runs were averaged over latitudinal angles θ . (from [37])

have recently shown that noncentral contributions to the strong interaction, i.e. tensor and spin-orbit forces, reduce the neutrino pair production rate significantly compared to one-pion exchange approximations usually adopted in supernova simulations [85, 86]. Neutrino-pair bremsstrahlung, together with neutrino-pair annihilation into pairs of other flavor (mainly $\nu_e \bar{\nu}_e \rightarrow \nu_x \bar{\nu}_x$, $x = \mu, \tau$), is crucial for transport of μ and τ neutrinos [87, 88] and its inclusion in supernova simulations has resulted in noticeable changes of the spectrum of these two neutrino types towards smaller average energies.

Fig. 3 shows the time evolution of the luminosities in the different neutrino flavors obtained in a two-dimensional simulation for two different Equation of States. During the collapse phase the supernova overwhelmingly emits electron neutrinos, produced by electron capture on nuclei (the production rate of other neutrino types by nuclear deexcitation during collapse is much less and is discussed in Section 4). The sharp reduction in the ν_e luminosity just before bounce (at $t_{pb} = 0$) is related to neutrino trapping in the last phase of the collapse. It is followed by the sharp peak of the neutrino burst just after bounce, caused by photodissociation of nuclei into free nucleons and the associated fast electron captures on free protons. After about 50 ms the neutrino luminosities are mainly due to neutrino pair production caused by electron-positron annihilation in the dense and hot environment. Consequently supernova shine now in all neutrino flavors. As μ and τ neutrino pairs can couple to e^+e^- pairs only by neutral current, their production rate is smaller than the one of $\nu_e \bar{\nu}_e$ pairs.

The radius from which neutrinos can be considered to be ‘free streaming’ is called the neutrinosphere [3]. For electron neutrinos the neutrinosphere approximately corresponds to the region with trapping densities of a few $10^{11} \text{ g cm}^{-3}$, which is at radii of about 20 km in the later postbounce phase [91]. As neutrino cross sections depend on the neutrino energy, the neutrinosphere is ‘diffuse’; i.e. its radius decreases with neutrino energy.

On quite general grounds one expects a hierarchy in the average energies of neutrinos of different flavors: As μ and τ neutrinos have not sufficient energies to interact with matter by charged-current reactions, they decouple at smaller radii, and higher temperatures, than electron neutrinos. Furthermore, as the matter is neutron rich, anti-electron neutrinos, which by charged-current only interact with protons, decouple at smaller radii and higher temperature than electron neutrinos, which interact by charged-current reactions with neutrons. The hierarchy in temperatures at which the neutrino flavors decouple translates then into a hierarchy of average energies: $\langle E_{\nu_x} \rangle \gtrsim \langle E_{\bar{\nu}_e} \rangle > \langle E_{\nu_e} \rangle$. For current estimates for the average neutrino energies see refs. [6, 8].

It is one of the major aims for future supernova neutrino detections to confirm this hierarchy. However, these measurements will depend strongly on neutrino flavor oscillations along the way to the detector. One possibility are adiabatic flavor conversions [92] which implies noticeable mixing of the $\bar{\nu}_e$ and $\bar{\nu}_x$ spectra in case of the normal mass hierarchy and a complete swap for the inverted mass hierarchy [92]. For our nucleosynthesis discussion in Section 5 the flavor conversion induced by neutrino-neutrino refraction [93] is more important. In fact, several studies [94, 95, 96, 97] indicate that collective neutrino flavor oscillations, which occur in the high-neutrino-density environment surrounding the neutron star, swap the spectra of $\bar{\nu}_e$ and $\bar{\nu}_x$ neutrinos in certain energy intervals bounded by sharp spectral splits. This can have interesting consequences for the nucleosynthesis in the νp process (see Section 5),

3 Theoretical background and experimental validation

In this Section we want to discuss the theoretical background to describe neutrino-induced reactions on nuclei at neutrino energies relevant for supernova dynamics and nucleosynthesis. We will at first focus on charged- and neutral-current reactions on nuclei in their ground state. These reactions are directly relevant for studies of the neutrino-induced response of detectors for supernova neutrinos. The finite temperature in the supernova environment implies that nuclei exist in an ensemble with excited nuclear states thermally populated. This requires special attention. As charged-current (ν_e, e^-) and ($\bar{\nu}_e, e^+$) reactions are the inverse of stellar electron and positron captures, the relevant reaction rates can be obtained from the latter by applying the principle of detailed balance. In fact, in this way (ν_e, e^-) and ($\bar{\nu}_e, e^+$) reactions on nuclei are included in supernova simulations for a long time. Furthermore, charged-current reactions induced by muon and tau neutrinos are neglected in supernova simulations as their energies are not sufficient to initiate these processes at supernova conditions where individual nuclei exist. In the supernova neutral-current reactions on nuclei might alter the neutrino spectrum and/or contribute to the energy exchange between matter and neutrinos. Hence finite temperature effects are relevant and we will discuss below how these can be estimated and which influence they have on cross sections. The neutrino energies are often large enough to excite the nucleus to states above particle thresholds. In the hot supernova environment the subsequent particle decay can be neglected as the matter composition can be described in NSE. However, the decay is important for nucleosynthesis studies at lower temperatures as it alters the abundance distributions. The relevant decay probabilities will be described within the framework of the statistical model.

This Section is divided in 3 subsections in which we will derive the relevant cross sections, summarize briefly the hierarchy of nuclear models adopted to describe the nuclear structure problem at the various energy scales involved in the neutrino-nucleus reactions of interest and finally validate this ansatz by comparison to relevant experimental data.

3.1 Cross sections

For the semileptonic processes

$$\nu_e + {}_Z A_N \rightarrow {}_{Z+1} A_{N-1}^* + e^-; \quad \bar{\nu}_e + {}_Z A_N \rightarrow {}_{Z+1} A_{N-1}^* + e^+; \quad \nu + {}_Z A_N \rightarrow {}_Z A_N^* + \nu' \quad (2)$$

the excitation cross section from the ground states of a nucleus (defined by proton and neutron numbers Z and N , respectively) to a discrete final state is given in the extreme relativistic limit (final lepton energy $\epsilon_f \gg$ lepton mass $m_f c^2$) by [98, 99]:

$$\left(\frac{d\sigma_{i \rightarrow f}}{d\Omega_e} \right)_{\nu, \bar{\nu}} = \frac{G_F^2 \cdot \epsilon_f^2}{2\pi^2} \cdot \frac{4\pi \cos^2 \frac{\Theta}{2}}{(2J_i + 1)} \cdot F(Z \pm 1, \epsilon_f) \cdot \left[\sum_{J=0}^{\infty} \sigma_{CL}^J + \sum_{J=1}^{\infty} \sigma_T^J \right] \quad (3)$$

where

$$\sigma_{CL}^J = |\langle J_f || \mathbf{M}_J(q) + \frac{\omega}{q} \mathbf{L}_J(q) || J_i \rangle|^2 \quad (4)$$

and

$$\begin{aligned} \sigma_T^J = & \left(-\frac{q_\mu^2}{2q^2} + \tan^2 \frac{\Theta}{2} \right) \times [|\langle J_f || \mathbf{J}_J^{mag}(q) || J_i \rangle|^2 + |\langle J_f || \mathbf{J}_J^{el}(q) || J_i \rangle|^2] \\ & \mp 2 \tan \frac{\Theta}{2} \sqrt{\frac{-q_\mu^2}{q^2} + \tan^2 \frac{\Theta}{2}} \times \text{Re} [\langle J_f || \mathbf{J}_J^{mag}(q) || J_i \rangle \langle J_f || \mathbf{J}_J^{el}(q) || J_i \rangle^*] . \end{aligned} \quad (5)$$

Here G_F is the Fermi coupling constant, Θ the angle between the incoming and outgoing lepton, and $q_\mu = (\omega, \vec{q})$ ($q = |\vec{q}|$) the four-momentum transfer. The minus-(plus) sign in Eq. (4) refers to the neutrino (antineutrino) cross section. The quantities \mathbf{M}_J , \mathbf{L}_J , \mathbf{J}_J^{el} and \mathbf{J}_J^{mag} denote the multipole operators for the charge, and the longitudinal and the transverse electric and magnetic parts of the four-current, respectively. Following Ref. [98] they can be written in terms of one-body operators in the nuclear many-body Hilbert space. The cross section involves the reduced matrix elements of these operators between the initial state J_i and the final state J_f .

The Fermi function $F(Z, \epsilon_f)$ appears in the cross section for the charged-current process and accounts for the Coulomb interaction between the final charged lepton and the residual nucleus. It can be derived relativistically as the Coulomb correction obtained from a numerical solution of the Dirac equation for an extended nuclear charge [100, 101]:

$$\begin{aligned} F(Z, \epsilon_f) &= F_0(Z, \epsilon_f) \cdot L_0 \\ \text{with } F_0(Z, \epsilon_f) &= 4(2p_l R)^{2(\gamma-1)} \left| \frac{\Gamma(\gamma + iy)}{\Gamma(2\gamma + 1)} \right|^2 \cdot e^{\pi y}, \end{aligned} \quad (6)$$

where Z denotes the atomic number of the residual nucleus in the final channel, ϵ_f the total lepton energy (in units of $m_l c^2$) and p_l the lepton momentum (in units of $m_l c$), R is the nuclear radius (in units of $\lambda = \hbar/(m_l c)$) and γ and y are given by ($\alpha =$ fine structure constant):

$$\gamma = \sqrt{1 - (\alpha Z)^2} \quad \text{and} \quad y = \alpha Z \frac{\epsilon_f}{p_l}. \quad (7)$$

The numerical factor L_0 in (5), which describes the finite charge distribution and screening corrections, is nearly constant (≈ 1.0), and can be well approximated by a weakly decreasing linear function in p_l [101].

At higher energies, the Fermi function for s waves becomes a poor approximation when higher partial waves also contribute for $p_l R \geq 1$. Guided by the distorted-wave approximation of quasielastic electron scattering, in that case the Coulomb effects can be treated in the ‘Effective Momentum Approximation’ in which the outgoing lepton momentum p_l is replaced by the effective momentum

$$p_{\text{eff}} = \sqrt{E_{\text{eff}}^2 - m_l^2}, \quad E_{\text{eff}} = E_l - V_C(0), \quad (8)$$

where $V_C(0) = 3e^2 Z/(2R)$ is the Coulomb potential at the origin. In the formalism above [102], the Coulomb effect is taken into account not only by using the effective momentum, but also by replacing the phase space factor $p_l E_l$ by $p_{\text{eff}} E_{\text{eff}}$ (see also [103] where this procedure is called modified effective

momentum approximation, and shown to work quite well). In practice, a smooth interpolation between these two regimes of treatment of the Coulomb effects is used.

The total cross section is obtained from the differential cross sections by summing over all possible final nuclear states and by numerical integration over the solid angle $d\Omega$.

Supernova neutrino energies are sufficiently high to excite nuclei in the final channel to energies above particle thresholds. The nuclear state will then subsequently decay by particle emission. Under certain conditions the final nucleus might even be excited to energies high enough to allow for multi-particle emissions. Such a situation occurs in neutral-current reactions induced by supernova ν_x neutrinos as their expected average energies of about 18 MeV often suffices to excite nuclei above the 2-particle emission threshold. Such a decay is also relevant for charged-current reactions induced by supernova ν_e neutrinos if the Q value is large enough. Such a situation will certainly occur for r-process nuclei if they are subject to charged-current reactions with supernova ν_e neutrinos. As nuclei on the r-process path also have very small neutron separation energies, the state excited by the neutrino process in the daughter nucleus will decay by the emission of several neutrons [104, 105]. It has been pointed out that neutrino-induced fission of r-process nuclei will also be accompanied by multiple neutrons [106, 107].

Neutrino-induced reactions with subsequent particle emission can be described in a two-step process. In the first step a nuclear level f at energy E_f with angular momentum J_f and parity π_f is excited. The respective reaction cross section is described by Eq. 3. The subsequent particle decay is calculated on the basis of the statistical model. At relatively low excitation energies, where one-particle decays dominate, these calculations are preferably done on the basis of statistical model codes which explicitly consider experimentally known nuclear spectra. There are several such codes existing: SMOKER [108], MOD-SMOKER and SMARAGD [109], TALYS [110]. There have been a few applications where such codes have been extended to treat also the cascade of two-particle emissions. However, these treatments are computationally quite demanding, thus multi-particle emissions are usually studied within a Monte-Carlo treatment of the decay cascades. Such a dynamical code is ABLA07 [111] that describes de-excitation of the compound nucleus through the evaporation of light particles (protons, neutrons, α and γ) and fission. The particle evaporation is considered in the framework of the Weisskopf formalism [112], while in the description of fission the ABLA code treats explicitly the relaxation process in deformation space and the resulting time-dependent fission width using an analytical approximation [113] to the solution of the Fokker-Planck equation. The wide range of excitation energies and the large variety of nuclei of interest demands for a consistent treatment of level densities as a function of excitation energy and deformation. The nuclear level density is calculated according to the Fermi-gas formula taking into account the shell corrections, collective excitations and pairing correlations; details on the implementation of these effects in the nuclear level density, their damping with excitation energy and their deformation dependence are described in details in Refs. [114, 115, 116]. The angular-momentum-dependent fission barriers are taken from the finite-range liquid-drop model [117]. In order to describe the fission-fragment mass and charge distributions, as well as their kinetic energies, the ABLA code is coupled to the semi-empirical Monte-Carlo fission model PROFI [118].

3.2 Hybrid model for allowed and forbidden contributions

Reactions of low-energy neutrinos with $E_\nu \leq 20$ MeV off nuclei are dominated by allowed $J = 0^+$ and $J = 1^+$ transitions (see Fig. 4). In the limit of vanishing momentum transfers $q = 0$, which is justified at the low neutrino energies involved, these two transitions between initial (i) and final (f) nuclear states reduce to the Fermi and Gamow-Teller transitions, respectively:

$$B_{if}(F) = T(T + 1) - T_{z_i}T_{z_f}, \quad (9)$$

where the transition is only possible between Isobaric Analog states and where we have neglected the reduction in the overlap between nuclear wave functions due to isospin mixing which is estimated to be

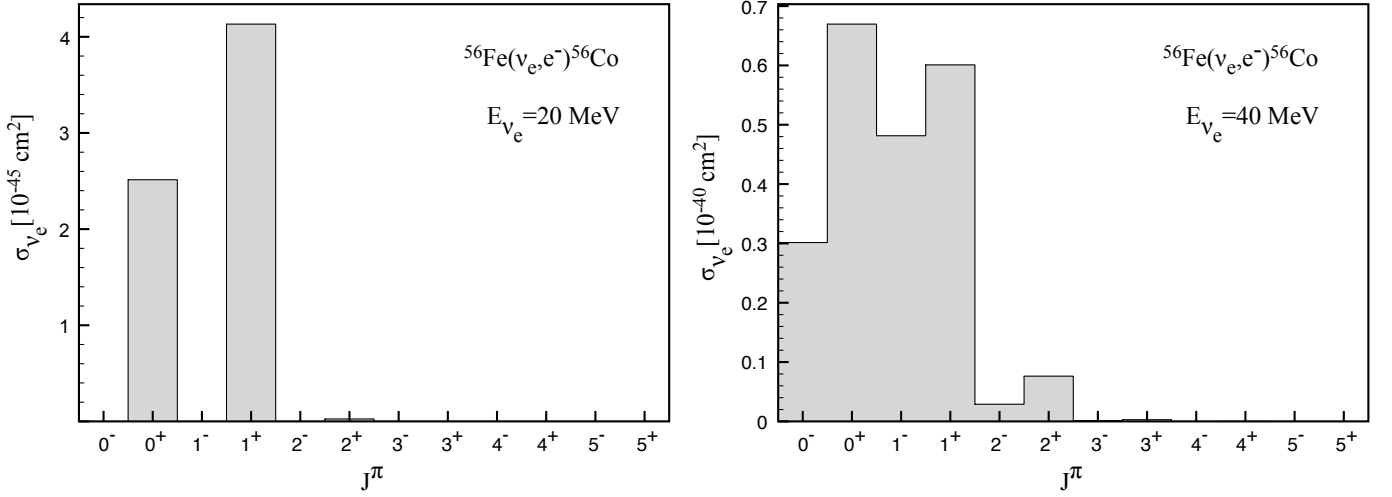


Figure 4: Multipole decomposition of (ν_e, e^-) cross sections on ^{56}Fe for two different neutrino energies. (from [119])

small ($\approx 0.5\%$ [120]), and

$$B_{if}(GT) = \left(\frac{g_A}{g_V}\right)_{\text{eff}}^2 \frac{\langle f || \sum_k \sigma^k t_{\pm}^k || i \rangle^2}{2J_i + 1}, \quad (10)$$

where the matrix element is reduced with respect to the spin operator σ only (Racah convention [121]) and the sum runs over all nucleons. For the isospin rising and lowering operators, $t_{\pm} = (\tau_x \pm i\tau_y)/2$, we use the convention $t_{+}p = n$; thus, ‘+’ refers to electron capture and β^+ transitions and ‘-’ to positron capture and β^- transitions. Finally, $(g_A/g_V)_{\text{eff}}$ is the effective ratio of axial and vector coupling constants that takes into account the observed quenching of the GT strength [122]. One often uses [123, 124, 125]

$$\left(\frac{g_A}{g_V}\right)_{\text{eff}} = 0.74 \left(\frac{g_A}{g_V}\right)_{\text{bare}}, \quad (11)$$

with $(g_A/g_V)_{\text{bare}} = -1.2599(25)$ [120]. If the parent nucleus (with isospin T) has a neutron excess, then the GT_- operator can connect to states with isospin $T-1, T, T+1$ in the daughter, while GT_+ can only reach states with $T+1$. This isospin selection is one reason why the GT_+ strength is more concentrated in the daughter nucleus (usually within a few MeV around the centroid of the GT resonance), while the GT_- is spread over 10-15 MeV in the daughter nucleus and is significantly more structured.

The GT response is in turn sensitive to nuclear structure effects and hence its contribution to the cross section has to be derived from a model which is capable to describe the relevant nuclear structure and correlation effects. This model is the diagonalization shell model [31]. Higher multipoles will, however, contribute to the cross section for larger neutrino energies. For each of these multipoles the response of the operator will be fragmented over many nuclear states. However, most of the strength resides in a collective excitation, the giant resonance, whose centroid energy grows with increasing rank λ roughly like $\lambda\hbar\omega \approx 41\lambda/A^{1/3}$ MeV. As the phase space prefers larger final neutrino energies, the average nuclear excitation energy grows noticeably slower than the initial neutrino energy. As a consequence, initial neutrino energies are noticeably larger than the energy of a giant resonance, when the later will contribute to the neutrino-nucleus cross section. Fortunately, the neutrino-nucleus cross section depends then mainly on the total strength of the multipole excitation and its centroid energy, and not on the detailed energy distribution of the strength (as this is the case for the Gamow-Teller response at low neutrino energies). Thus the higher multipole contributions to the neutrino-nucleus

cross section can be derived within the RPA making use of the fact that the RPA describes the energy centroid and total strength of multipoles other than the Gamow-Teller quite well.

In such a hybrid model, the total reaction cross section consists then of two parts

$$\sigma_{\nu}^{\text{tot}}(E_{\nu}) = \sigma_{\nu}^{\text{sm}}(E_{\nu}) + \sigma_{\nu}^{\text{rpa}}(E_{\nu}), \quad (12)$$

where the shell model part, σ^{sm} , describes the allowed contributions to the cross section for (ν_e, e^-) (GT₋) and $(\bar{\nu}_e, e^+)$ (GT₊) reactions and is given by:

$$\sigma(E_{\nu}) = \frac{G_F^2 \cos^2 \theta_C}{\pi} \sum_f k_e^f E_e^f F(\pm Z \pm 1, E_e^f) (B_f(F) + B_f(GT_{\pm})) \quad (13)$$

where G_F is the Fermi constant, θ_C the Cabibbo angle, and k_e and E_e the momentum and energy of the outgoing electron or positron. The sum is over the final (f) nuclear states with energies E_f . There is no Fermi contribution to $(\bar{\nu}_e, e^+)$ reactions on nuclei with neutron excess. For inelastic neutrino scattering to an excited nuclear state at energy E_f the allowed contribution to the cross section is given by:

$$\sigma_{\nu}(E_{\nu}) = \frac{G_F^2 \cos^2 \theta_C}{\pi} \sum_f E_{\nu',f}^2 B_f(GT_0) \quad (14)$$

where energy conservation yields $E_{\nu',f} = E_{\nu} - E_f$. These allowed contributions replace the $\lambda = 0^+$ and $\lambda = 1^+$ contributions in the cross section formula above. All other multipole contributions can be derived adopting the RPA as the nuclear model to describe the initial and final nuclear states. We mention that, for light nuclei like ^{12}C , shell model calculations are now also possible for the first-forbidden transitions ($\lambda = 0^-, 1^-, 2^-$) requiring model spaces spanned by $3\hbar\omega$ [126, 127, 128].

3.3 Inelastic neutrino-nucleus reactions at finite temperature

So far, our formalism assumes that the target nucleus is in the ground state corresponding to an environment with temperature $T = 0$. This is, of course, appropriate for neutrino-induced reactions in earthbound detectors and it is a reasonable approximation for the supernova environment in which neutrino-nucleus reactions occur in nucleosynthesis processes ($T < 100$ keV). However, the $T = 0$ approximation is not valid if we want to study inelastic neutrino-nucleus reactions in the hot supernova environment (with temperatures $T \gtrsim 1$ MeV). (We recall that charged-current reactions under these conditions can be derived from electron and positron captures by detailed balance.) Here nuclei exist as a thermal ensemble with excited nuclear states at energy E_i with spin J_i populated with a Boltzmann weight of $G_i = (2J_i + 1) \exp(-E_i/kT)$. There are two interesting effects which occur at finite T : i) neutrinos can be up-scattered in energy; i.e. the neutrino picks up energy from the nucleus which by the scattering reaction deexcites; ii) at zero temperature for even-even nuclei with their $J = 0^+$ ground states GT transitions can only be induced by neutrinos with minimum energies to bridge the gap to the first excited $J = 1^+$ state in the nucleus. Transitions to excited states at lower excitation energies can be induced by higher multipoles, but the respective cross sections are usually quite small. As a consequence inelastic neutrino-nucleus cross sections for even-even nuclei drop quite fast with decreasing small neutrino energies. This is not expected to be the case for inelastic neutrino-nucleus reactions at finite temperatures. Due to the exponential increase in the nuclear level density states at modest excitation energies are likely to have states in their energy vicinity with which they can be connected by GT transitions. Furthermore, it is even likely that GT transitions (or with less strength by other multipoles) can lead to levels at lower energies, a transition which is in principle possible for all neutrino energies. In summary, we expect on general grounds that the cross section is in particular at low neutrino energies modified at finite temperature.

Unfortunately an evaluation of the inelastic cross section at finite temperature by explicitly summing over the thermally populated states is computationally unfeasible due to the many states involved at temperatures of order MeV. There are two suggestions how to overcome this problem and treat inelastic neutrino scattering at finite temperature. We briefly discuss both in turn.

Refs. [129, 130] apply Brink's hypothesis which states that for a given excited nuclear level i the strength distribution built on this state, $S_i(E)$, is the same as for the ground state, $S_0(E)$, but shifted by the excitation energy E_i : $S_i(E) = S_0(E - E_i)$. The validation of Brink's hypothesis has been in detailed studied in ref. [131], however, for electron capture on sd-shell nuclei (see also [27]). Upon applying the Brink hypothesis, the down-scattering part becomes independent of temperature and can be solely derived from the ground state GT distribution. With this approximation, the Gamow-Teller (shell model) contribution to the cross section becomes:

$$\sigma_\nu^{\text{sm}}(E_\nu) = \frac{G_F^2}{\pi} \left[\sum_f E_{\nu',0f}^2 B_{0f}(GT_0) + \sum_f E_{\nu',if}^2 B_{if}(GT_0) \frac{G_i}{G} \right], \quad (15)$$

where G_F is the Fermi constant, and $E_{\nu',if}$ is the energy of the scattered neutrino, $E_{\nu',if} = E_\nu + (E_i - E_f)$, with E_i, E_f denoting the initial and final nuclear energies.

The first term in Eq. (15) arises from Brink's hypothesis. By construction, this Brink term does not allow for neutrino up-scattering. These contributions to the cross section are comprised in the second term, where the sum runs over both initial (i) and final states (f). The former have a thermal weight of $G_i = (2J_i + 1) \exp(-E_i/kT)$, where J_i is the angular momentum, E_i is energy of the initial state, and T is temperature; $G = \sum_i G_i$ is the nuclear partition function. The up-scattering contributions are the more important i) the lower the nuclear excitation energy (Boltzmann weight in the thermal ensemble), ii) the larger the GT transition strength B_{if} , and iii) the larger the final neutrino energy. Guided by these general considerations Ref. [130] has approximated the second term in Eq. (15) by explicitly considering GT transitions between nuclear states with $E_i > E_f$, where the sum over the final nuclear states is restricted to the lowest nuclear levels. As is usual in astrophysical applications, experimental data (in this case mainly excitation energies) have been used whenever available.

As stressed above, the derivation of the first (down-scattering) term in the cross section explicitly assumes that the distributions on excited states is the same as for the ground state. This is likely not the case as the vanishing of pairing correlations with increasing temperature should effect the relative excitation energy of the strength centroid and move it slightly down in energy. In fact Shell Model Monte Carlo studies, performed at finite temperature, confirm this conjecture [132]. To account for this effect, Dzhioev *et al.* developed a model which extends the QRPA approach to finite temperature (Thermal Quasiparticle Random-Phase Approximation, TQRPA [133, 134]). In the applications the authors consider multipole contributions up to $\lambda = 3$. However, it is illustrative to assume that the scattering process is given solely by the contribution from the allowed $J = 1^+$ multipole. Then the cross section induced by neutrinos with energy E_ν at temperature T can be written as

$$\sigma(E_\nu, T) = \frac{G_F^2}{\pi} \sum_i (E_\nu - \omega_i)^2 \Phi_i + \frac{G_F^2}{\pi} \sum_i (E_\nu + \omega)^2 \exp\left(-\frac{\omega_i}{kT}\right) \Phi_i. \quad (16)$$

Analog to Eq. (15) the first term corresponds to the down-scattering, and the second to the up-scattering contributions. The sum in the down-scattering term runs over all 1^+ thermal phonon states with positive energy $\omega_i < E_\nu$. The Boltzmann factor suppresses the contribution from highly thermally populated states in the up-scattering term. These transitions are, however, somewhat favored by the phase factor $(E_\nu + \omega)^2$ [134]. In Eq. (16) Φ_i denotes the transition strength of the GT operator. We note that the TQRPA approach obeys detailed balance which, however, is slightly violated in the approach based on Eq. (15).

Using iron isotopes as example we will discuss results from both approaches in Section 4.

3.4 Nuclear models and their validation by data

Measurements of neutrino-nucleus cross sections are very rare. For charged-current reactions there exist the set of measurements for solar electron neutrinos on the nuclei comprising the various solar neutrino detectors. These data - despite being very valuable for solar physics and the proof of neutrino oscillations - are only of restricted use to check the applicability of nuclear models to describe neutrino-nucleus reactions for supernova neutrinos. Solar neutrinos have an energy spectrum, which is well understood from the reactions mediated by the weak interaction in solar hydrogen burning and distorted by matter-enhanced oscillations in the Sun. However, solar neutrino energies are too low to excite giant nuclear resonances which in turn are expected to dominate the cross sections for supernova neutrinos. This means that transitions induced by solar neutrinos are strongly state-dependent and are quite a challenge to model. There have been a few theoretical studies performed for solar neutrinos within the framework of effective field theory [135], shell model and RPA.

For the deuteron, which has been the target nucleus in the SNO detector, neutrino-scattering calculations have been performed in effective field theory (EFT). This approach allows to split the neutrino-induced cross section into two pieces $\sigma(E) = a(E) + L_{1A}b(E)$ where $a(E)$ and $b(E)$ are known and all unknown effects can be lumped together in one unknown parameter L_{1A} (isovector two-body axial current) which must be determined by experiment [136, 137]. Although $a(E)$ contributes dominantly to the cross section, the current uncertainty in L_{1A} (about 50%) is still large [138, 139, 140, 141]. Similar results have been obtained based on the phenomenological Lagrangian approach [142]

For the two nuclei ^{12}C and ^{56}Fe there exist measurements of cross sections induced by ν_e neutrinos [143, 144, 145, 146, 147, 148]. The neutrinos are produced by muons decaying at rest and have therefore spectra which are slightly shifted to larger neutrino energies than supernova neutrinos. Nevertheless the respective neutrino-nucleus cross sections are expected to be dominated by contributions from allowed (Fermi and GT) and first-forbidden transitions and are therefore valuable test cases for nuclear models. In turn measurements of these transition strengths serve as strong indirect constraints of the ability of nuclear models to describe neutrino-nucleus scattering at supernova neutrino energies.

In Ref. [18] it is argued on the basis of general considerations that, depending on the neutrino energies, the nuclear structure problem has to be treated with different demands and details. As we will show below these requirements are fulfilled by a hierarchy of models which is actually the basis of the hybrid model defined above: the nuclear shell model for low neutrino energies and the Random Phase Approximation (or its variants) for higher energies.

i) Low energy neutrino scattering requires the detailed reproduction of the nuclear response (mainly allowed transitions) at low nuclear excitation energy. The method of choice here is the shell model which, for a fixed model space of valence nucleons, accounts for nucleon-nucleon correlations among these valence particles via an effective interaction. Shell model wave functions have good quantum numbers for angular momentum, parity and isospin. Modern shell model codes allow now diagonalization in model spaces with up to a few billion configurations. Based on a Monte Carlo strategy of importance sampling shell model calculations for low energy spectra have been extended to even larger model spaces. Hence shell model diagonalization is now possible for medium-mass nuclei in the iron-nickel region in the full pf shell as is desirable for calculations of GT transitions. For lighter nuclei, like ^{12}C and ^{16}O , shell model calculations can be performed in multi- $\hbar\omega$ model spaces allowing also for fully correlated studies of first-forbidden transitions. Such transition strengths are calculated employing the Lanczos technique for a finite number (of order 100) iterations. As a consequence the lowest transitions correspond to well-defined (shell model) states, while at higher excitation energies the calculated strength corresponds to the summed strength per energy interval (which depends on the number of iterations considered). For a review on the shell model and its abilities and applications the reader is referred to Ref. [31].

ii) The RPA has been developed to describe the collective excitations of a nucleus by considering the one-particle one-hole excitations of the correlated ground state. Compared to the shell model,

the RPA calculations usually use model spaces with a (significantly) larger set of single particle, but they consider, however, only a strongly truncated part of the possible configurations. This has the consequence that the strength is less fragmented in RPA than in shell model calculations.

It is important that in the shell model and in the RPA the total strength is fixed by sum rules. Of particular relevance for the description of neutrino-nucleus reactions at supernova neutrino energies are the Ikeda sum rule for the Gamow-Teller strength

$$\sum_i GT(Z \rightarrow Z + 1)_i - \sum_i GT(Z \rightarrow Z - 1)_i = 3(N - Z), \quad (17)$$

and the Thomas-Reiche-Kuhn sum rule for the dipole strength

$$\sum_i (E_i - E_0) B(E1; 0 \rightarrow i) = \frac{9}{4\pi} \frac{\hbar^2}{2M_n} \frac{NZ}{A} e^2. \quad (18)$$

where M_n is the nucleon mass. For nuclei with large neutron excess, the Ikeda sum rule basically fixes the total GT_- strength relevant for (ν_e, e^-) reactions.

It is known from studies of β decays and of GT distributions [123, 125] that both shell model and RPA calculations systematically overestimate the GT transition strengths. For the shell model calculations this shortcoming can be overcome by introducing a constant quenching factor via the introduction of an effective axial-vector coupling constant which for pf shell nuclei has empirically been determined as $g_A^{\text{eff}} = 0.74g_A$ [125]. GT strengths, obtained in RPA calculations, are often quenched by the same factor, although this procedure in RPA studies is hampered by the limited consideration of configurations within the model space.

Replacing the full $\lambda = 1^+$ operator by its approximation in the $q = 0$ limit (the GT operator) is only justified for small incident neutrino energies. At modest neutrino energies the consideration of the finite momentum transfer reduces the cross section. In Ref. [149] it is suggested to correct cross sections calculated from the shell model GT distribution by the ratio of RPA calculations performed for finite momentum transfer and for $q = 0$, respectively. For neutrinos produced by muon decay at rest the correction is of order 20%. For supernova neutrino energies the correction is smaller.

Ref. [18] gives a detailed comparison of data obtained for charged-current reactions on ^{12}C induced by muon-decay-at-rest (DAR) ν_e neutrinos with various model calculations. The exclusive reaction to the $J = 1^+$ ground state of ^{12}N is given by a GT transition. In general models agree quite well with experiment (see Table I in Ref. [18]). However, it must be noted that the calculations are usually constrained by other experimental data which fix the GT matrix element (like the β decays of the ^{12}N and ^{12}B ground states or the muon capture to the ^{12}B ground state). Hence these calculations should be understood as proving that the exclusive DAR from Karmen [143, 144] and from LSND [145, 146, 147] are consistent with other measurements probing the nuclear matrix element.

In fact the description of the GT transition between the ^{12}C and ^{12}N ground states (or to the other members of the $T = 1$ multiplett in the $A = 12$ nuclei including the ^{12}B ground state and the $J = 1^+$ state in ^{12}C at 15.11 MeV) is a very demanding nuclear structure problem involving the subtle breaking of the SU(4) symmetry (in the limit of good SU(4) symmetry the GT transition vanishes). Clearly RPA correlations are insufficient and overestimate the transition strength by about a factor of 4 [150, 151, 126]. Hayes *et al.* performed shell model calculations in successively larger model spaces up to $6\hbar\omega$ and gained two important insights into the problem [152]: i) enlarging the model space increasingly breaks the SU(4) symmetry. Relatedly the GT matrix elements increases moving towards the experimental value. However, this convergence process is quite slow. ii) The inclusion of a three-body interaction noticeable improves the agreement with data. The findings of Ref. [152] have recently been confirmed in no-core shell model (NCSM) calculations using chiral NN+3N interactions [153, 154]. In fact, the NSCM calculation of Maris *et al.* [154], performed in a model space with $8\hbar\omega$

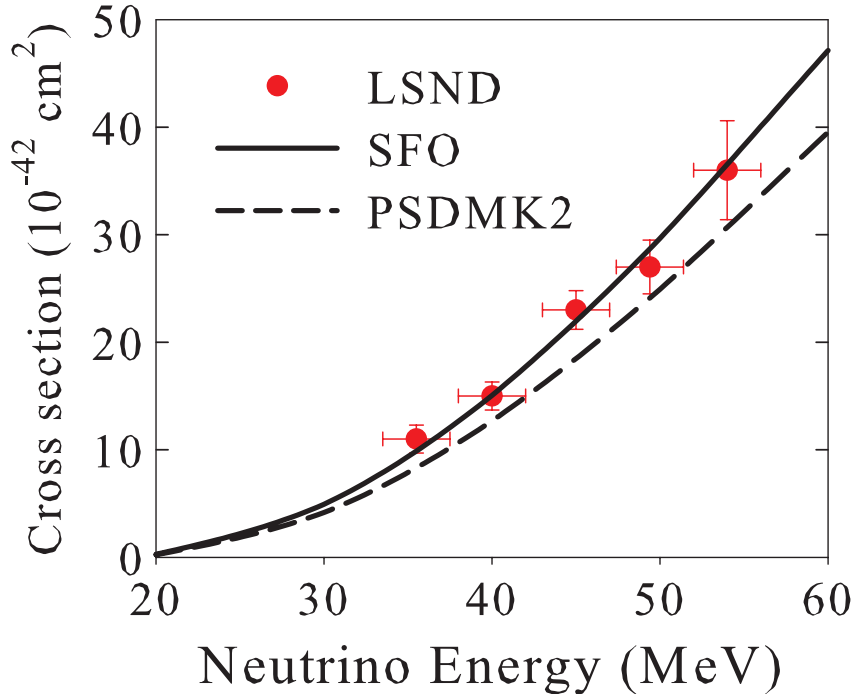


Figure 5: Comparison of the exclusive $^{12}\text{C}(\nu_e, e^-)^{12}\text{N}_{gs}$ cross section data of the LSND collaboration [146] with shell model calculations performed with two different residual interactions (from [128]).

now slightly overestimates the transition by about 15%. A good reproduction of the GT transition strength, and relatedly of the exclusive $^{12}\text{C}(\nu_e, e^-)^{12}\text{N}_{gs}$ has also been obtained in a diagonalization shell model calculation performed in a $3\hbar\omega$ model space [128] using a novel residual interaction [155]. In fact, using a slightly quenched value for the axial-vector coupling constant Otsuka *et al.* [155] find very good agreement with the LSND exclusive cross sections (see Fig. 5).

The inclusive $^{12}\text{C}(\nu_e, e^-)^{12}\text{N}$ cross section induced by DAR neutrinos leads to many excited states in ^{12}N . The typical momentum transfer in this process, $q \simeq 50$ MeV, is noticeably larger than the average excitation energy, $\omega \simeq 20$ MeV. Under these conditions the cross section is dominated by forbidden transitions, but it is not too sensitive to details of the strength distribution. As discussed above, RPA studies should be adequate to reproduce the cross sections which is indeed the case as it is in details outlined in Ref. [18]. Further proof that ^{12}C cross sections, which are dominated by contributions from collective excitations, are well described by RPA calculations are given by studies of the muon capture on ^{12}C [150] and by inclusive electron scattering. The successful reproduction of muon capture rates by RPA calculations is not restricted to ^{12}C , but has been extended to the data set across the full nuclear chart [156, 157].

The KARMEN collaboration has reported a measurement of the $^{56}\text{Fe}(\nu_e, e^-)^{56}\text{Co}$ cross section for DAR neutrinos, $\sigma = (2.56 \pm 1.08 \pm 0.43 \cdot 10^{-40}) \text{ cm}^2$ [148]. Table 1 compares this cross section with results from a hybrid model study and from different variants of the RPA. All calculations are consistent with the data within their relatively large uncertainty. We note, however, that the RPA cross sections show a spread of about a factor of 2.5. Looking at the results of the hybrid model in more details one finds the largest contributions from the allowed transitions. The $\lambda = 1^+$ part ($1.12 \times 10^{-40} \text{ cm}^2$) has been calculated from the shell model GT strength distribution with the standard quenching factor and corrected for effects of finite momentum transfer [149]. The $\lambda = 0^+$ contribution to the Isobaric Analog State at excitation energy of 3.5 MeV in ^{56}Co is readily calculated exploiting the appropriate Fermi sum rule yielding a cross section of $0.53 \times 10^{-40} \text{ cm}^2$. Higher multipoles, which have been treated within an RPA approach, contribute a cross section of $0.73 \times 10^{-40} \text{ cm}^2$. The shell model $\lambda = 1^+$ cross section

Table 1: Comparison of $^{56}\text{Fe}(\nu_e, e^-)^{56}\text{Co}$ cross sections for DAR neutrinos calculated with different variants of the Random Phase Approximation, with the hybrid model and with data (exp) [148].

model	cross section (in 10^{-40} cm 2)
QRPA [158]	2.646
PQRPA [158]	1.973
RPA [159]	2.77
QRPA [160]	3.52
RQRPA [119]	1.4
Hybrid [149]	2.38
exp [148]	$(2.56 \pm 1.08 \pm 0.43)$

is about 32% smaller than the one obtained within the RPA approach showing some sensitivity to the detailed GT distribution.

Such GT distributions - as other relevant strength distributions for dipole transitions or M1 transitions - serve as indirect constraints to validate the nuclear input into neutrino-nucleus cross section calculations. For ^{56}Fe Ref. [161] have measured the forward-angle cross section in a charge-exchange (p, n) reaction. These data are proportional to the GT $_-$ distribution, which is of importance for the KARMEN measurement of the (ν_e, e^-) cross section. In Fig. 6 the measured forward-angle cross section is compared to the results obtained from a shell model calculation [29], where the latter has been folded with the experimental resolution. Overall a reasonable agreement is observed. The total GT $_-$ strength has been calculated as 9.3 units, while Ref. [161] quotes 9.9 ± 2.4 units. In agreement with experiment, the calculation places the main strength at energies between 6 and 15 MeV, however, it misses some of the detailed fragmentation in the data. For low excitation energies the forward-angle cross sections have been recently determined using the ($^3\text{He}, t$) charge-exchange reaction with a noticeably improved resolution compared to the pioneering (p, n) experiments [162, 163], again showing a rather good agreement with the shell model calculation.

The left panel of Fig. 7 compares the GT $_-$ strength calculated within a relativistic QRPA approach with a shell model calculation [164]. The shell model calculation uses a different residual interaction than adopted in [29], but yields very similar results. The total GT $_-$ strength with the GXPF1J interaction is 9.5 units, but it is also well reproduced by the QRPA study 9.7 units [164]. (Note that also the Ikeda sum rule is quenched.) The QRPA strength distribution has some strength at excitation energies below 5 MeV, similar to the shell model, and it places the largest portion of the strength in a resonance centred around 10 MeV. As expected, the shell model and experimental distributions show a significantly stronger fragmentation of this resonant strength which is not recovered in the QRPA study due to lack of correlations.

As we have stressed above the detailed distribution of the GT $_-$ strength matters in the description of neutrino-nucleus reactions if the incident neutrino energy is of the order of the nuclear excitation energy (considering the Q value of the reaction). This is nicely demonstrated in Fig. 7. For the distributions dominated by low energy neutrinos (at $T = 2$ and 3 MeV) the QRPA predicts slightly smaller cross sections than the hybrid model. But for the neutrino distributions with temperatures $T > 4$ MeV the cross sections are very similar indicating that the (average) neutrino energies are large enough that the cross section is only sensitive to the total strength and to the energy centroid of the distribution (which are quite similar in the QRPA and shell model), but not to the details of the distribution. Also the hybrid model calculation of Ref. [165], using a different shell model residual interaction and another RPA variant, yields cross sections which are very close to the one obtained in Ref. [164]. We note that the relative importance of correlations for the description of the total GT $_-$ strength decreases with

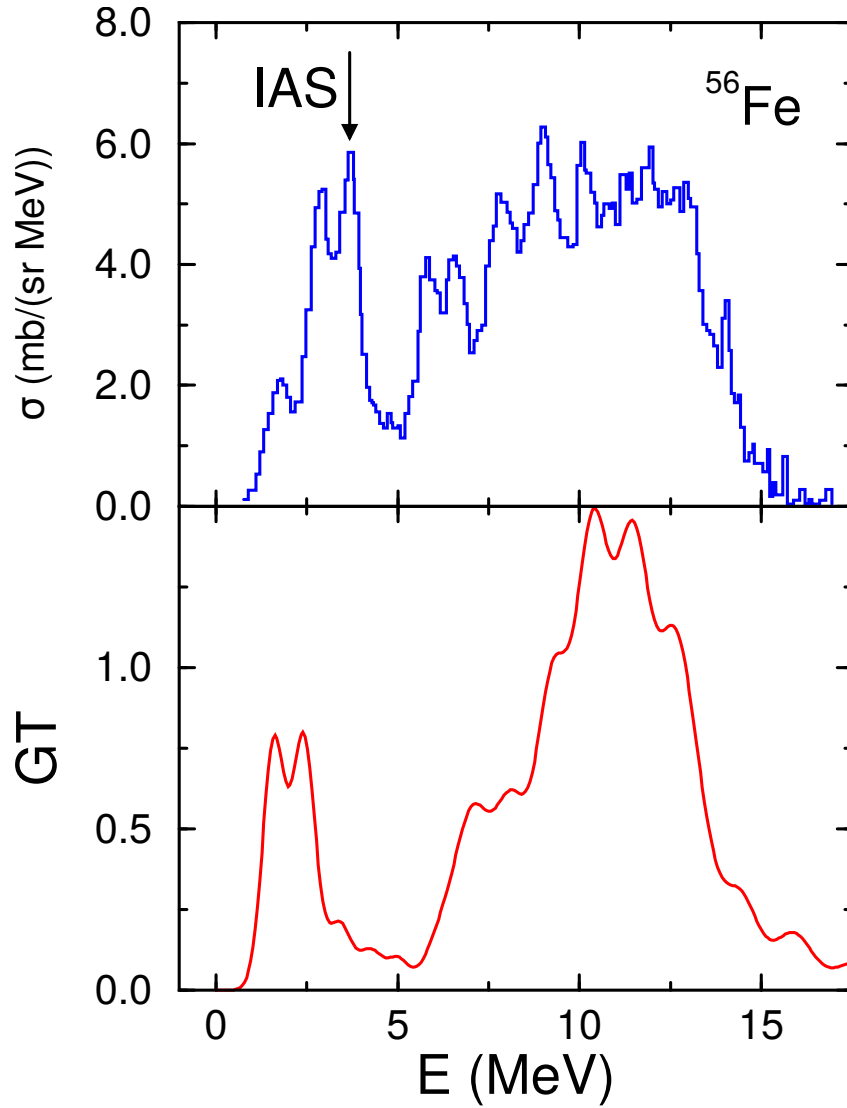


Figure 6: Comparison of the GT strength distributions for ^{56}Fe obtained by (p, n) charge-exchange experiment [161] and a shell model calculation (folded with the experimental resolution). The data also include the Fermi contribution from the Isobaric Analog State (IAS) (from [29]).

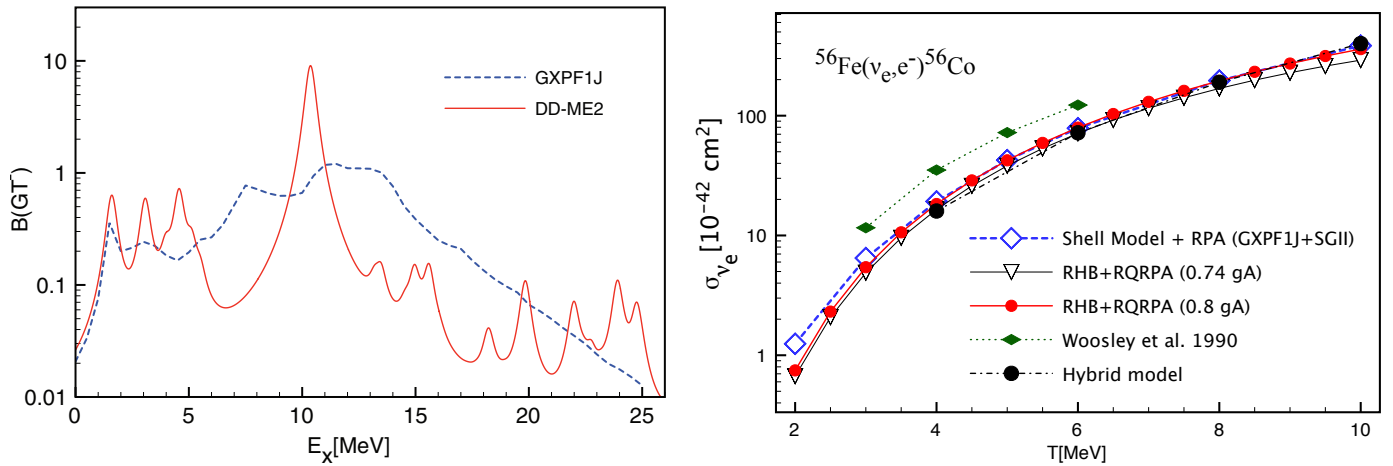


Figure 7: (left panel) GT_- strength distribution for ^{56}Fe , calculated within a relativistic QRPA approach (RQRPA with interaction DD-ME2) and a shell model study with the GXPF1J residual interaction. Both calculations have been folded with a Lorentzian of width 0.5 MeV. (right panel) Comparison of (ν_e, e^-) cross sections on ^{56}Fe calculated within relativistic QRPA approaches with different quenchedings of the axial-vector coupling constant (RHB+RQRPA) and within hybrid models where the GT_- strength has been calculated within the shell model and the other multipole contributions within the RPA. The cross sections have been folded with a Fermi-Dirac distribution with temperature T (corrected version from [164]).

growing neutron excess as for nuclei with modest and large neutron excess this strength is dominated by the (quenched) $3(N - Z)$ part stemming from the Ikeda sum rule.

We expect that the results found for ^{56}Fe applies quite generally: i.e. for charged-current (ν_e, e^-) reactions, RPA and hybrid model calculations will give reliable estimates for supernova neutrinos provided they give a reasonable account of the total GT_- strength and of the energy centroid.

As the GT_+ strength for nuclei with neutron excess is unconstrained by the Ikeda sum rule, its reproduction is a larger challenge to nuclear models than the GT_- strength. Importantly the shell model could be established as a reliable tool for such calculations in recent years [29, 31]. Using again ^{56}Fe as an example, Fig. 8 compares the experimental GT_+ strength with various calculations performed within the shell model and the QRPA. At first we notice the significantly improved resolution obtained in the $(t, ^3\text{He})$ charge-exchange experiment [168] (a similar resolution is achieved in the $(d, ^2\text{He})$ experiments) compared to the pioneering work using the (n, p) reaction with an energy resolution of about 1 MeV [166, 167]. Secondly, the shell model gives a fair account of the total GT_+ strength as well as of the distribution, although both residual interactions place slightly too much strength into the energy interval between 2 and 4 MeV. The shell model calculations, which agree quite well with each other, however, differ from the QRPA predictions. The latter yields noticeably more total strength than the data (about 5.5 units and 2.6 ± 0.8 units, respectively). Furthermore the lack of correlations in the QRPA has the consequence that not sufficient strength is pulled to excitation energies below 2 MeV, in contrast to data and the shell model. Such shortcomings can lead to significant differences in the $(\bar{\nu}_e, e^+)$ cross sections for low anti-neutrino energies.

Satisfyingly the shell model has been proven to describe all measured GT_+ distributions for pf shell nuclei quite well [169]. This ability makes it the method of choice to describe astrophysically important weak-interaction processes like electron capture or $(\bar{\nu}_e, e^+)$ reactions if the astrophysical conditions make the respective cross sections sensitive to a detailed description of the GT_+ distribution. As an example, Fig. 9 compares electron captures rates calculated from the measured GT_+ distributions for all pf shell nuclei, for which these data exist, and from QRPA and shell model strength distributions (for two

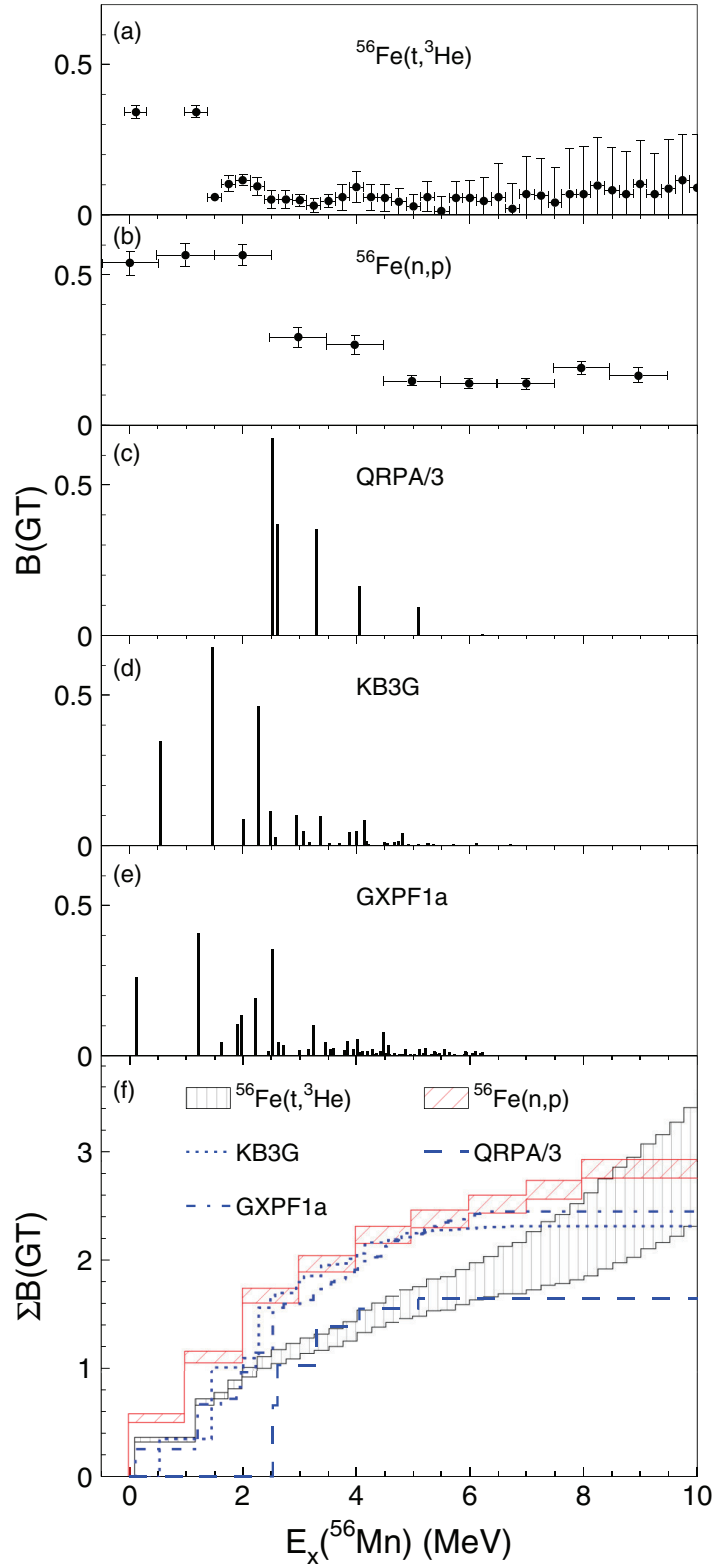


Figure 8: Comparison of GT_+ strength for ^{56}Fe deduced from (n,p) [166, 167] and $(t, ^3\text{He})$ [168] charge-exchange experiments with distributions calculated within the QRPA approach (c) and by the shell model (d and e) with different residual interactions (KB3G and GXPF1a). Panel f) shows the running sums of the strengths. The QRPA results have been divided by a factor of 3 (from [168]).

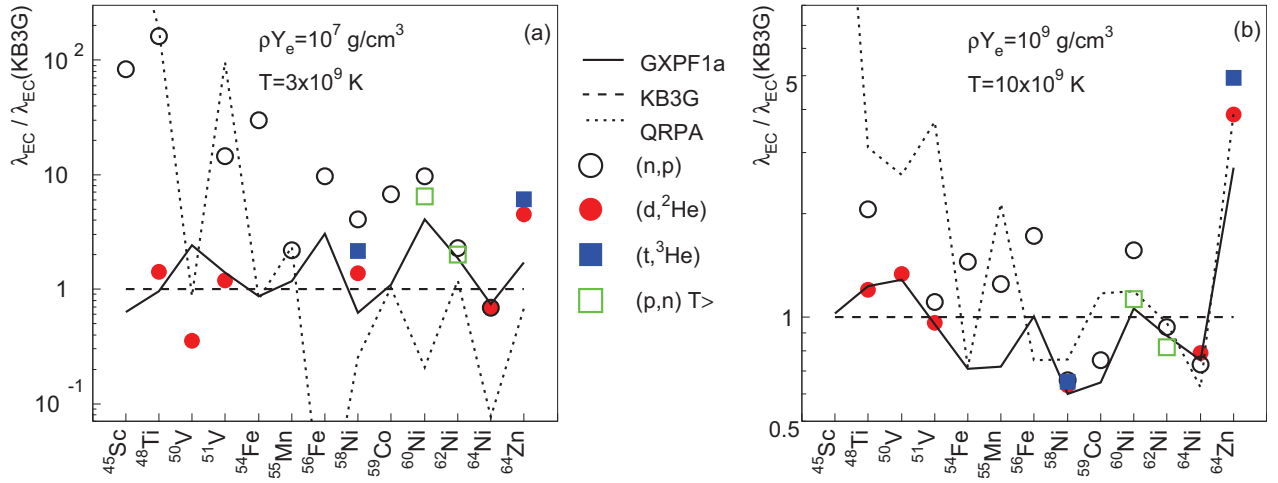


Figure 9: Comparison of electron-capture rates for 13 pf -shell nuclei calculated on the basis of theoretical (connected by lines) and experimental (indicated by markers) GT strength distributions. All rates are plotted relative to those calculated by the shell-model with the KB3G interaction. The rates are shown for two combinations of stellar density and temperature: (a) $\rho Y_e = 10^7 \text{ g cm}^{-3}$ and $T = 3 \times 10^9 \text{ K}$ and (b) $\rho Y_e = 10^9 \text{ g cm}^{-3}$ and $T = 10 \times 10^9 \text{ K}$ (from [169]).

different residual interactions). The astrophysical conditions in the right panel correspond to the early onset of collapse where the electron Fermi energy is of the same order of magnitude as the reaction Q value making the capture rate sensitive to details of the GT_+ distribution. Fig. 9 shows a very satisfying agreement between the rates obtained from data and shell model distributions. The capture rates obtained from the QRPA calculations agrees usually also within a factor of 2.

The sensitivity of the rates to the details of GT_+ distributions decreases with increasing Fermi energy (or density). Fig. 9 confirms this fact by showing a noticeably larger variation between the different calculations and the data for supernova conditions at smaller density. In particular two points are noteworthy: i) the better energy resolution achieved in the $(d, {}^2\text{He})$ and $(t, {}^3\text{He})$ reactions usually leads to smaller rates than those obtained from the (n, p) data, in good agreement with the shell model; ii) the missing fragmentation of the QRPA strengths can lead to large differences in either directions. We stress, however, that the pf shell nuclei shown in the figure have small abundances at the relatively low densities and hence do not contribute much to the overall electron capture rate.

A similar study as performed for electron capture in Ref. [169] would be also desirable for $(\bar{\nu}_e, e^+)$ cross sections for supernova neutrinos. As energies of supernova $\bar{\nu}_e$ neutrinos are larger than the electron Fermi energies for both collapse situations depicted in Fig. 9. we expect from the general considerations above that the respective $(\bar{\nu}_e, e^+)$ cross sections are less sensitive to the details of the GT_+ distribution than shown at the conditions of Fig. 9 and that the shell model, and also the QRPA, should give a fair account of the GT contribution to the cross sections, supplemented by higher multipole contributions obtained from RPA calculations. This statement is likely correct for the chosen pf shell nuclei, but it can unfortunately not be generalized. For these pf shell nuclei the neutron number is smaller than 40 and hence GT_+ transitions, in which a proton is changed into a neutron, is even possible within the IPM. However, for nuclei with proton numbers below a major oscillator shell closure (say $Z < 20$ or $Z < 40$) and neutron numbers above ($N > 20$ or $N > 40$, respectively) GT_+ transitions are Pauli blocked in the IPM. However, they can open up by correlations which move nucleons across the shell closure. Thus such correlations can enable GT_+ transitions for protons in the upper oscillator shell or into neutron holes in the lower oscillator shell. Detailed calculations have shown that describing cross-shell correlations is a slowly converging process requiring many-particle many-hole configurations

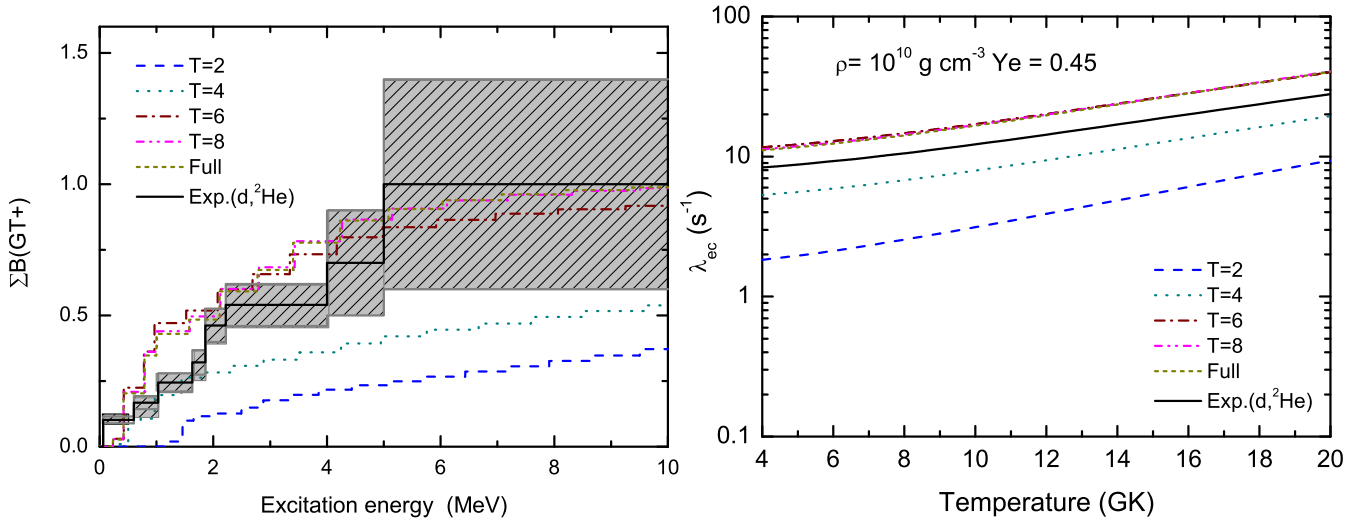


Figure 10: (left panel) Running GT_+ sum for different values of the particle-hole excitations across the $N = 40$ shell gap. (right panel) Electron capture rates calculated with normalized GT strength distributions at different truncation levels (from [40]).

usually beyond those considered in QRPA studies [170, 171]. To illustrate this point we use the electron capture rate on ^{76}Se with $N = 42$ and $Z = 34$ as an example (see Section 2). The left panel of Fig. 10 shows the shell model results for the ^{76}Se GT_+ strength. Note that the shell model space is adequate to describe the correlations of valence nucleons across the shell gap, it lacks, however, some spin-orbit partners making the use of the universal quenching factor inappropriate. In Ref. [40] the quenching has been simply chosen to match the total experimental GT_+ strength [38]. This choice does not affect our argument here which is the evolution of the strength with truncation level; i.e. with the number of nucleons allowed to be promoted from the pf shell across the shell gap by correlations. In particular, truncation level $t = 2$ includes up to two-particle two-hole correlations like in QRPA calculations. We observe from Fig. 10 that, with increasing correlations, i) the total GT_+ strength grows, mainly due to an increase of neutron holes in the pf shell, and ii) more strength is shifted to lower excitation energies. This has an important effect on the capture rates. This is illustrated in the right panel of Fig. 10 at conditions with electron Fermi energies of nearly 10 MeV, where the rates differ by up to an order of magnitude between the calculation with truncation level $t = 2$ and the converged calculation. We mention that in the IPM the GT_+ strength and the rates vanish. As the average energies of supernova $\bar{\nu}_e$ neutrinos are slightly larger than the electron Fermi energy in our example, we expect that the differences in $(\bar{\nu}_e, e^+)$ cross sections for supernova neutrinos will be still appreciable, but somewhat smaller.

The only neutral-current cross section measured for nuclei beyond the deuteron is the transition from the ground state to the $T = 1$ state at 15.11 MeV in ^{12}C [144, 172]. This is the Isobaric Analog State of the ^{12}B and ^{12}N ground states. Thus from a nuclear structure point of view this measurement yields the same informations as the exclusive charged-current reactions on ^{12}C discussed above. Hence we have to use indirect experimental information to validate cross section calculations for inelastic neutrino-nucleus scattering. Due to the relatively low energies of supernova neutrinos allowed transitions dominate inelastic (ν, ν') cross sections and the relevant nuclear quantity is the GT_0 strength distribution. This strength can be experimentally studied for example in (p, p') experiments. However it is also intimately related to M1 excitations of nuclei which have been studied with great precision by inelastic electron scattering [173]. We will now use such electron scattering data to show that the shell model is capable to describe the allowed response needed to determine inelastic cross sections for supernova neutrinos.

$M1$ transitions are mediated by the operator

$$\mathbf{O}(M1) = \sqrt{\frac{3}{4\pi}} \sum_k [g_l(k)\mathbf{l}(k) + g_s(k)\mathbf{s}(k)]\mu_N \quad (19)$$

where the sum runs over all nucleons. The orbital and spin gyromagnetic factors are given by $g_l = 1$, $g_s = 5.585694675(57)$ for protons and $g_l = 0$, $g_s = -3.82608545(90)$ for neutrons [174]; μ_N is the nuclear magneton. Using isospin quantum numbers $t_z = \tau_3/2 = \pm 1/2$ for protons and neutrons, respectively, Eq. (19) can be rewritten in isovector and isoscalar parts. Due to a strong cancellation of the g -factors in the isoscalar part, the $M1$ transitions are of dominant isovector nature. The respective isovector $M1$ operator is given by

$$\mathbf{O}(M1)_{\text{iv}} = \sqrt{\frac{3}{4\pi}} \sum_k [\mathbf{l}(k)\mathbf{t}_z(k) + (g_s^p - g_s^n)\mathbf{s}(k)\mathbf{t}_z(k)]\mu_N \quad (20)$$

We note that the spin part of the isovector $M1$ operator is the zero component of the GT operator,

$$\mathbf{O}(GT_0) = \sum_k 2\mathbf{s}(k)\mathbf{t}_z(k) = \sum_k \boldsymbol{\sigma}(k)\mathbf{t}_z(k), \quad (21)$$

however, enhanced by the factor $\sqrt{3/4\pi}(g_s^p - g_s^n)/2 = 2.2993$. The allowed contribution to the inelastic neutrino-nucleus scattering at low energies, where finite momentum transfer corrections can be neglected, from an initial nuclear state (i) to a final state (f) is then given by

$$\sigma(E_\nu, i \rightarrow f) = \frac{G_F^2 g_A^2}{\pi(2J_i + 1)} (E_\nu - \omega)^2 |\langle f | \sum_k \boldsymbol{\sigma}(k)\mathbf{t}_z(k) | i \rangle|^2 \quad (22)$$

where E_ν is the energy of the scattered neutrino and ω is the difference between final and initial nuclear energies. The nuclear dependence is contained in the $B(GT_0) = g_A^2 |\langle f | \sum_k \boldsymbol{\sigma}(k)\mathbf{t}_z(k) | i \rangle|^2 / (2J_i + 1)$ reduced transition probability between the initial and final nuclear states. In shell model calculations of the $M1$ strength the spin part is quenched by the same factor used for studies of the GT strengths [175].

Thus, experimental $M1$ data yield the desired GT_0 information, required to determine inelastic neutrino scattering on nuclei at supernova energies, to the extent that the isoscalar and orbital pieces present in the $M1$ operator can be neglected. On general grounds one expects, as stated above, that the isovector component dominates over the isoscalar piece. Furthermore, it is wellknown that the major strength of the orbital and spin $M1$ responses are energetically well separated in the nucleus. In pf shell nuclei, which are of interest for supernova neutrino-nucleus scattering, the orbital strength is located at excitation energies $E^* \simeq 2 - 4$ MeV [176], while the spin $M1$ strength is concentrated between 7 and 11 MeV. A separation of spin and orbital pieces is further facilitated by the fact that the orbital part is strongly related to nuclear deformation [177]. For example, the famous scissors mode [178], which is the collective orbital $M1$ excitation, has been detected in well-deformed nuclei like ^{56}Fe [179]. Thus one can expect that in spherical nuclei the orbital $M1$ response is not only energetically well separated from the spin part, but also strongly suppressed.

Examples of spherical pf shell nuclei are ^{50}Ti , ^{52}Cr and ^{54}Fe . In Fig. 11 we show the total $M1$ strength and its spin and orbital contributions from a shell model calculation for ^{52}Cr and compare it to the experimental data [180]. We observe a very good agreement between data and calculation for the $M1$ strength distribution, with the strength mainly located at excitation energies between 7-10 MeV. We also find that the calculated $M1$ strength is dominated by its spin contribution which exceeds the orbital part by more than an order of magnitude. Finally, the calculation yields no indication for a scissors mode or any orbital strength at low excitation energies, as expected for spherical nuclei. Thus, the calculation

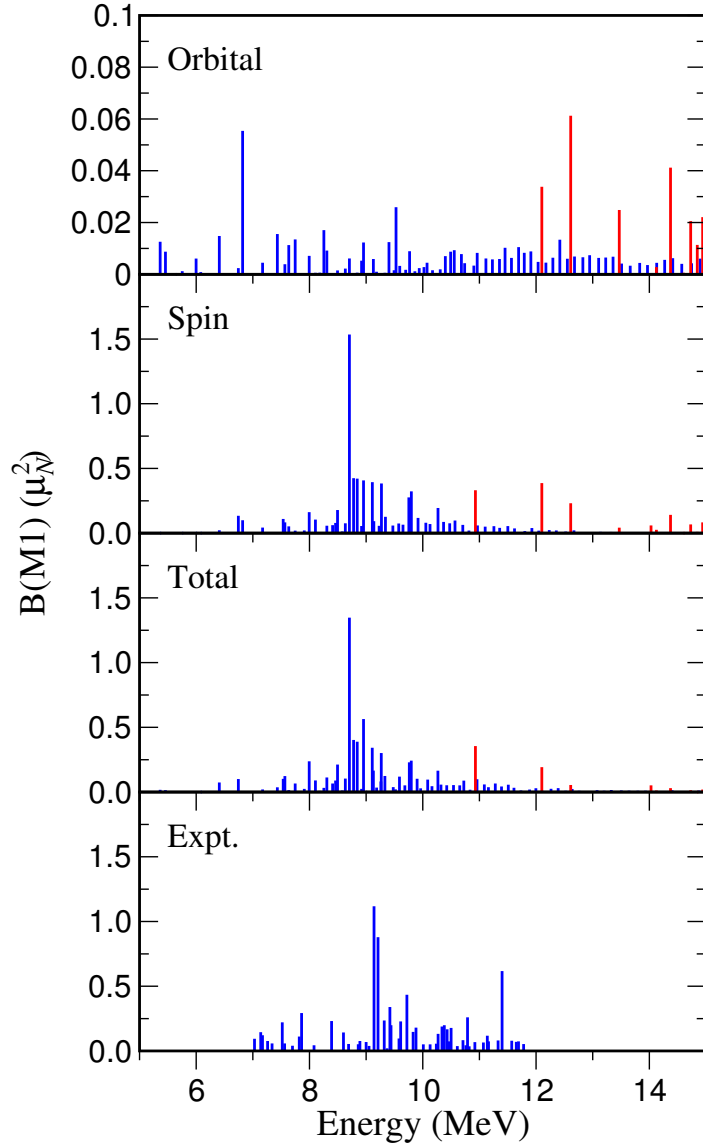


Figure 11: Comparison of experimental ^{52}Cr $M1$ strength distribution (bottom panel) with shell-model result (upper panels) showing the orbital, spin components and the total. Note the different scales of the ordinate for the spin and orbital pieces, respectively. The shell-model calculations show isospin $T = 2$ states as blue spikes and $T = 3$ as red spikes (adapted from [180]).

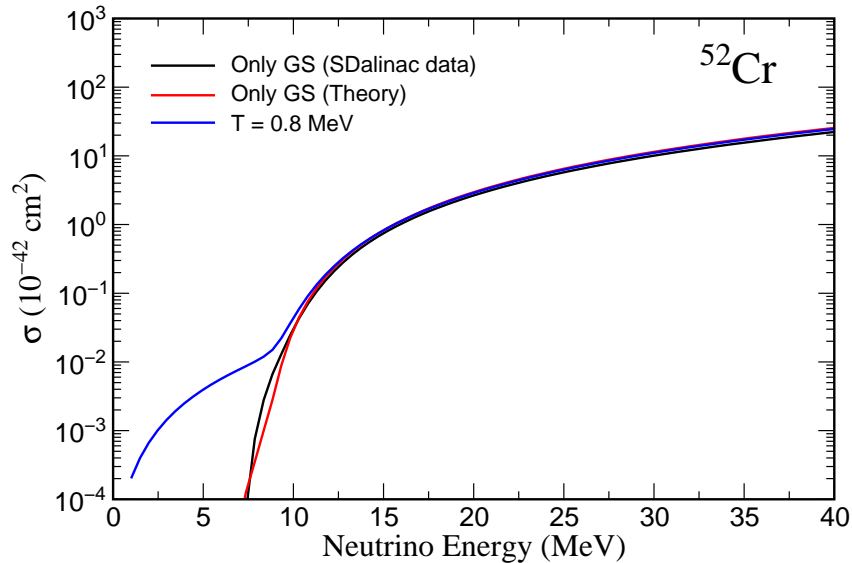


Figure 12: Neutrino-nucleus cross sections on ^{52}Cr calculated from the $M1$ data (black line) and the shell-model GT_0 distribution (red line). The blue line shows the cross section for a temperature of 0.8 MeV (adapted from [180]).

strongly supports the argument of Ref. [180] that, except for an overall normalization, the $M1$ strength for spherical nuclei reflects in a good approximation the GT_0 distribution. Based on this assumption, Ref. [180] has calculated the allowed contributions to the inelastic neutrino scattering on ^{52}Cr from both the $M1$ data (properly normalized to represent the GT_0 strength) and the GT_0 strength calculated in the shell model. Both cross sections are compared in Fig. 12 and show excellent agreement for scattering from the ground state. For the cross section at finite temperature contributions of thermally populated states have to be included. These have been calculated from appropriate shell model GT_0 strength distributions and added to the ground state cross section as described above, eq. (15). Fig. 12 indicates that the contributions from excited states have noticeable effects at low neutrino energies. This is particularly enhanced for spherical nuclei like ^{52}Cr where there is no significant GT_0 strength at low nuclear excitation energies. For neutrino energies which are sufficient to excite the GT_0 resonance, related to the spin part in the $M1$ strength, from the ground state the finite temperature corrections become negligible. For applications to supernova neutrinos contributions from forbidden transitions have to be added to the cross section. These can be calculated within RPA approaches and become increasingly relevant with growing neutrino energies.

The importance of a detailed reproduction can be deduced from a study presented in Ref. [134]. These authors performed a comparison of inelastic neutrino-nucleus cross sections for ^{56}Fe calculated within the hybrid model (shell model for allowed contributions and RPA for other multipoles, [165] and with studies in which all multipole contributions are determined within different variants of the QRPA [181, 182, 134]. The cross sections are summarized in Table 2 for different incident neutrino energies. We note some differences in the cross section predictions between the QRPA calculations. As mentioned in Ref. [182] these are related to the choices of single particle energies and the residual interaction. and should become less important with increasing neutrino energy. However, the calculations also treated the quenching of the various multipole contributions differently: only quenching the GT_0 contribution (like in the hybrid model) [134] or quenching all multipole contributions [182]. As Ref. [134] took special care in reproducing the centroid and strength of the GT_0 distribution and of the dipole giant resonance by slight adjustment of the residual interaction, this study allows a detailed comparison to the hybrid model calculation [165]. We find indeed a very good agreement between the cross sections

except at the lowest neutrino energy $E_\nu = 10$ MeV. Here the cross section is sensitive to a detailed description of the GT_0 strength: the shell model describes the fragmentation of the strength while the QRPA calculations predict it to be quite strongly concentrated around excitation energies of $E_x = 10$ MeV (see Figs. 15 and 13 below).

Table 2: Comparison of cross sections (in units of 10^{-42} cm²) for inelastic neutrino scattering on the ground state of ⁵⁶Fe calculated within the hybrid model [165] and different variants of the QRPA. The incident neutrino energy is E_ν . Exponents are given in parenthesis (from [134]).

E_ν [MeV]	hybrid model [165]	QRPA [134]	QRPA [182]	QRPA [181]
10	1.91(-1)	1.69(-2)	1.87(-1)	1.01(+0)
20	6.90(+0)	5.64(+0)	9.78(+0)	5.79(+0)
30	2.85(+1)	2.41(+1)	4.08(+1)	1.87(+1)
40	7.86(+1)	6.65(+1)	1.05(+2)	5.51(+1)
50	1.72(+2)	1.49(+2)	2.16(+2)	1.43(+2)
60	3.20(+2)	2.87(+2)	3.89(+2)	3.09(+2)
70	5.25(+2)	4.83(+2)	6.33(+2)	5.63(+2)
80	7.89(+2)	7.36(+2)	9.59(+2)	8.82(+2)
90	1.11(+3)	1.03(+3)	1.38(+3)	1.22(+3)
100	1.49(+3)	1.36(+3)	1.92(+3)	1.52(+3)

4 Applications to supernova dynamics

As we have stressed before neutrino-induced processes play a crucial role in the dynamics of core-collapse supernovae. In accordance with the main theme of this review we will focus here on two types of neutrino-nucleus reactions which both have recently for the first time been incorporated in supernova simulations and their impact on the dynamics has been explored. The first subsection deals with inelastic neutrino-nucleus scattering. We have outlined in the last section how progress in nuclear modelling, constrained by experimental data from inelastic electron scattering and charge-exchange experiments, has made possible to reliably estimate respective cross sections for scattering on ground states, despite the absence of direct data, and has shown ways to extend the calculations to finite temperature as is appropriate for supernova simulations. In the first subsection we will discuss the results of the nuclear model calculations, focussing on the effects introduced by finite temperature, and then turn to the impact elastic neutrino-nucleus scattering has in supernova simulations. In the second subsection we deal with nuclear deexcitation by neutrino pairs; i.e. the transition of a nucleus from a state at higher energy to a state at lower energy by neutrino pair production. Obviously this is only possible at finite temperature and can therefore not be directly studied in the laboratory. However, from a nuclear structure point of view this neutral current process is dominated by the same allowed Gamow-Teller and forbidden response as inelastic neutrino scattering, but in different kinematics. We will discuss two quite distinct approaches to derive the respective cross sections. Both yield, however, similar results. Supernova simulations, which include nuclear deexcitation by neutrino pair emission, indicate that this process does not impact the dynamics of the collapse. The process is, however, a source of ν_x and $\bar{\nu}_e$ neutrinos during the collapse phase.

4.1 Inelastic neutrino-nucleus scattering and its impact in supernova simulations

Inelastic neutrino-nucleus scattering, $A_i + \nu \rightarrow A_f + \nu'$, changes the nucleus A from an initial state A_i with energy E_i to a final state A_f with energy E_f . In this process the neutrino either gains energy if $E_f < E_i$ or it loses energy if $E_f > E_i$. The energy exchange between the nucleus and the neutrino can have potentially interesting consequences for the supernova dynamics. Inelastic neutrino-nucleus scattering might i) transfer energy to nuclei outside the shock front after bounce before arrival of the shock [183] enabling an easier revival of the shock, ii) add to inelastic neutrino-electron scattering speeding up the thermalization of neutrinos with matter after neutrino trapping during the collapse phase, and iii) change the neutrino opacity which will in turn modify the spectra of neutrinos released in the supernova and subsequently observed by earthbound detectors.

Investigations of inelastic neutrino-nucleus scattering in SN simulations has been pioneered in an exploratory study [184], approximating the matter composition by a representative nucleus, ^{56}Fe . The reaction cross sections were based on a nuclear model appropriate for temperature $T = 0$, combining a truncated shell model evaluation of the allowed Gamow-Teller response to the cross section with estimates of forbidden components derived from the Goldhaber-Teller model. The study concluded that inelastic neutrino-nucleus scattering rates can compete with those of neutrino-electron scattering at moderate and high neutrino energies ($E_\nu > 25 \text{ MeV}$), while they are significantly smaller for low E_ν . No significant effects of neutrino-nucleus interactions on the stalled shock by preheating the accreted matter were found in [184].

Approximating the composition of supernova matter by the ground state of the even-even nucleus ^{56}Fe is too simple an assumption for the calculation of inelastic neutrino-nucleus interaction rates for two reasons. i) Gamow-Teller transitions, which as we recall dominate the cross sections at the neutrino energies of interest, can only connect the 0^+ ground state of ^{56}Fe to final states with spin and parity $J = 1^+$. As the lowest 1^+ state in ^{56}Fe is at an excitation energy of $E_x = 3 \text{ MeV}$, there exists a threshold for inelastic neutrino scattering on ^{56}Fe (similarly on other even-even nuclei) and the cross sections are rather small for low neutrino energies. Supernova matter consists of a mixture of many nuclei with even and odd proton and neutron numbers. Since odd- A and odd-odd (i.e., with odd proton and neutron numbers) nuclei miss the strong pairing gap that lowers the ground state in even-even nuclei relative to excited states, and have usually $J_i \neq 0$, Gamow-Teller transitions from the ground state to levels at rather low excitation energies are possible, reducing the threshold for inelastic neutrino scattering on the ground state and generally increasing the cross sections at low E_ν . ii) More importantly, however, supernova matter has a non-zero temperature of order 1 MeV or higher, requiring the description of nuclei as a thermal ensemble. This completely removes the energy threshold for inelastic neutrino scattering, as we have shown in Section 3.

The finite temperature effect on the inelastic neutrino cross section off the two even-even nuclei ^{56}Fe and ^{82}Ge has been in detailed explored recently by Dzhioev and collaborators [134] using the TQRPA approach. As their general findings for the two nuclei are similar, we concentrate on ^{56}Fe here. The temperature evolution of the GT_0 strength is exhibited in Fig. 13. The ground state ($T = 0$) distribution shows that the strength is overwhelmingly concentrated at excitation energies around 10 MeV , corresponding to a spin excitation. The strength at low energies around 4 MeV is significantly lower. We note that these states are more pronouncedly seen in M1 data as they predominantly reflect orbital excitations, including the scissors mode at 3.45 MeV . At finite temperature the GT_0 distributions show several effects [134] which are relevant for the subsequent discussion of neutrino-nucleus scattering. For positive neutrino energy transfer ($E > 0$ in Fig. 13) the main effect is a shift of the strength towards smaller energies, by about 1.5 MeV . This shift is attributed to the pairing phase transition [134]: at temperatures above the critical one no extra energy has to be invested into breaking Cooper pairs and as a consequence the GT_0 strength moves to lower energies. This

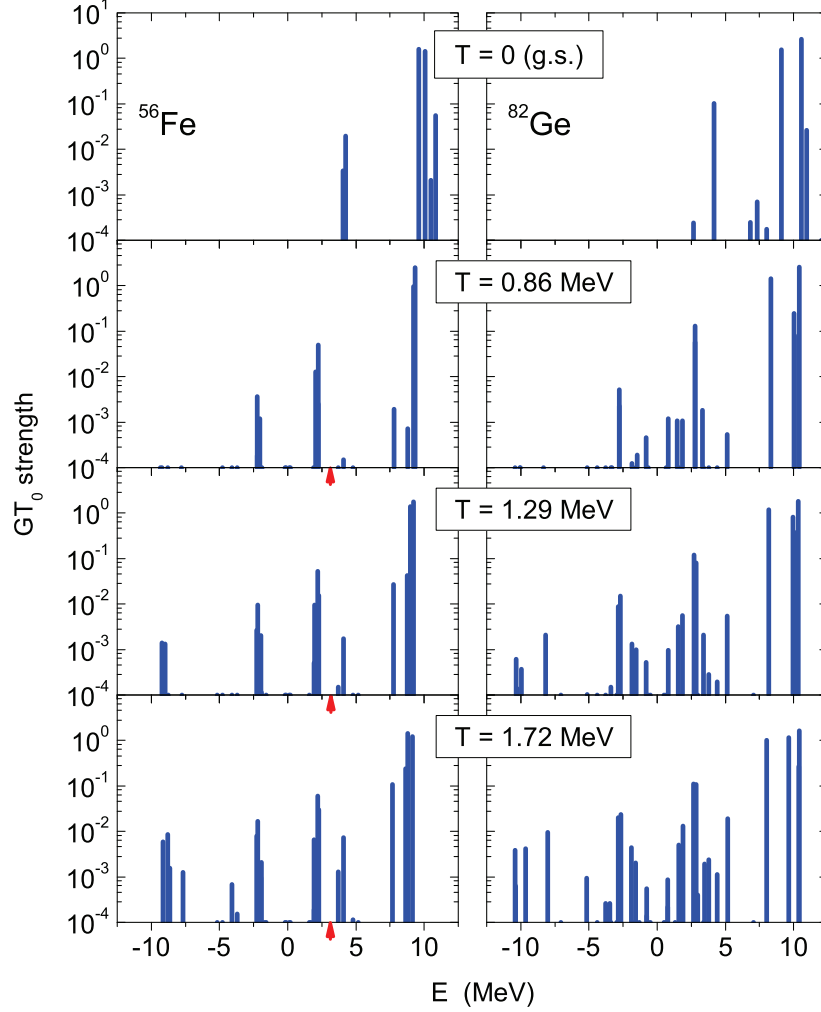


Figure 13: Temperature evolution of the GT_0 strength distributions for ^{56}Fe (left panels) and ^{82}Ge (right panels) calculated in the TQRPA approach. The x axis denotes the neutrino energy transfer to the nucleus. The red arrows indicate the threshold for inelastic neutrino scattering on ^{56}Fe at temperature $T = 0$ which is given by the excitation energy of the lowest $J = 1^+$ state. Here the experimental value 3.12 MeV is chosen, which is slightly lower than the calculated value (from [134]).

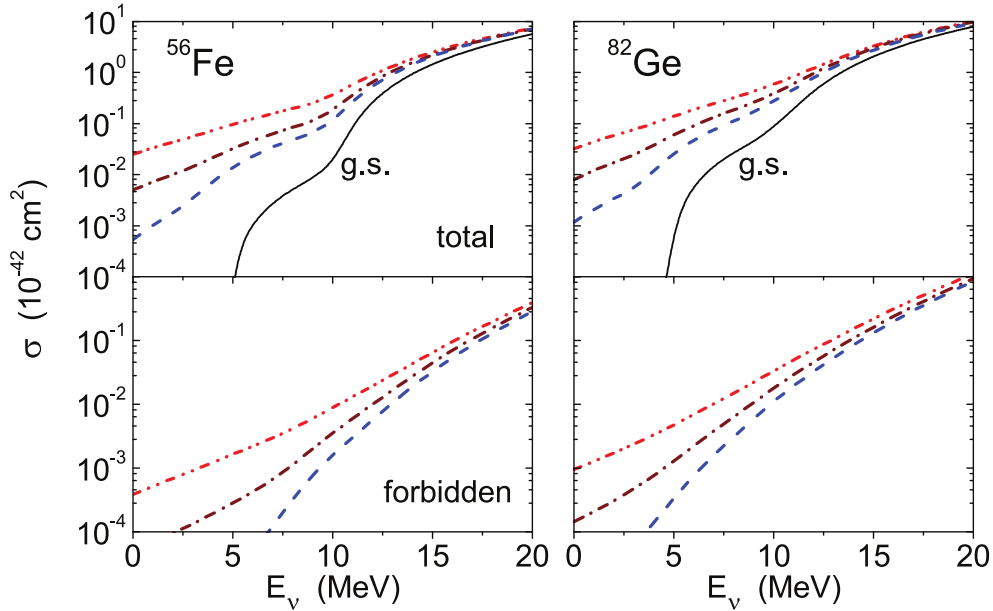


Figure 14: (upper panels): Cross sections for inelastic neutrino-nucleus scattering on ^{56}Fe (left) and ^{82}Ge (right) at different temperatures: $T = 0$ (full line), $T = 0.86$ MeV (blue dashed line), $T = 1.29$ MeV (brown dot-dashed line), $T = 1.72$ MeV (red double-dot-dashed line). (lower panels): Contribution of the forbidden multipoles to the cross sections at selected temperatures (from [134]).

behavior will not be present in calculations which are based on Brink's hypothesis. Furthermore, at finite temperature strength appears now also at negative neutrino energy transfers ($E < 0$). This relates to thermally populated nuclear states which decay to states at lower energies. Obviously the downward transitions increase noticeably with temperature. The strength observed at $E = -9$ MeV can be attributed to the deexcitation of the GT_0 resonance. Dzhioev *et al.* point out that the assumption of Brink's hypothesis also affects the downward strength distribution. In their approach the shift of the upward strengths to lower energies due to the melting of pairing makes it easier to thermally populate these states which, in turn, leads to an enhanced downward strength as well. Furthermore we remark that the smearing of the Fermi surface at finite temperature allows for a larger fragmentation of the strength, which affects more the low lying transitions (and ^{82}Ge).

The Gamow-Teller transitions and contributions from forbidden multipoles up to $\lambda = 3$ have been used to calculate inelastic neutrino-nucleus cross sections for ^{56}Fe and ^{82}Ge at different temperatures [134]. The results are shown in Fig. 14. There are several interesting observations. i) At $T = 0$, i.e. using the ground state transitions, the cross section drops at low neutrino energies. This is related to the gap in the GT distribution requiring neutrinos to have a certain minimum energy (about 4 MeV in the TQRPA ^{56}Fe calculation) to excite the lowest $J = 1^+$ state. ii) There is no gap in the cross sections at the finite temperatures mainly caused by the fact that deexcitation of thermally populated nuclear states contributes to the cross section at all neutrino energies. Obviously the contributions of the thermally populated states increase with temperature, so does the scattering cross section at low energies. iii) With increasing neutrino energies the cross sections at different temperatures converge. At neutrino energies $E < 15$ MeV, excitation of the GT_0 resonance dominates the cross section. At the energies shown in Fig. 14 the shift of the centroid energy due to the melting of pairing leads to a small increase in cross section at the finite temperatures compared to the $T = 0$ case. Due to the energy dependence of the phase space factor the relative enhancement of the cross section caused by this energy shift of the centroid decreases with increasing neutrino energy. iv) At the neutrino energies shown, which are typical for supernova neutrinos, the cross sections is dominated by the GT contribution

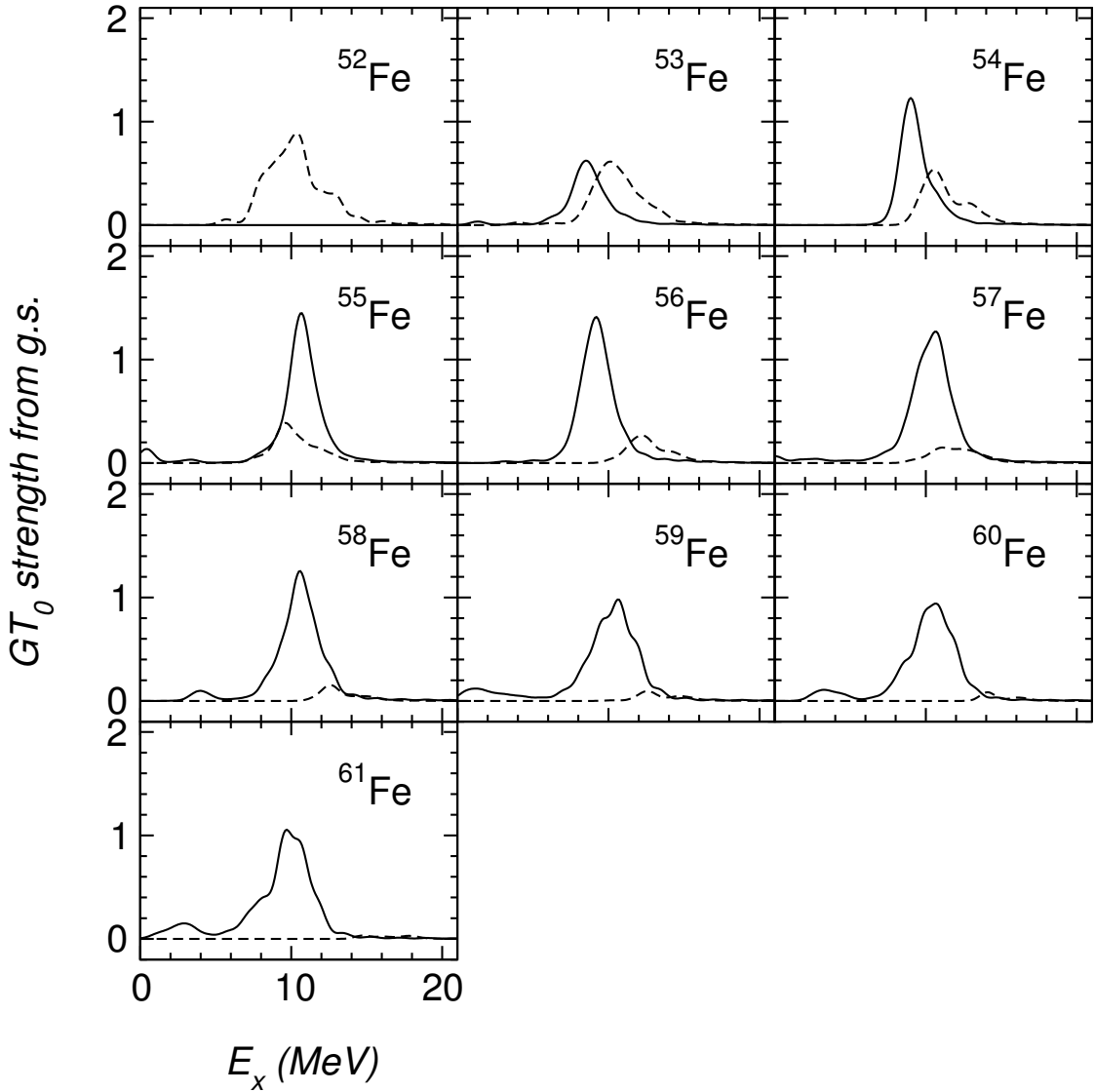


Figure 15: Gaussian-smoothed neutral Gamow-Teller (GT_0) distributions from the ground state in Fe isotopes. Solid lines indicate $\Delta T = 0$ strength, and dashed lines $\Delta T = 1$. E_x is the nuclear excitation energy (from [130]).

at all temperatures. Forbidden transitions contribute less than 10%.

We mentioned above briefly that the GT distributions and the inelastic neutrino-nucleus cross sections at supernova neutrino energies are quite similar for ^{56}Fe and ^{82}Ge . This is actually more globally true. Neutral-current (ν, ν') cross sections, folded over appropriate supernova neutrino energy distributions and calculated for $T = 0$, show relatively small variations from nucleus to nucleus [9, 104, 105]. The reason is related to the fact that the cross section at the supernova energies is dominated by GT transitions and that the GT strength is strongly concentrated in a resonance at excitation energies around 9-10 MeV for medium-mass and heavy nuclei. To support this point we show the GT_0 distributions from shell model calculations [130] for the iron isotopes $^{52-61}\text{Fe}$ in Fig. 15 (see also [185]). In fact for all isotopes the dominant part of the strength resides in a resonance around 10 MeV. Also the total resonant strength does not vary much. Very similar strength functions are found for the manganese, cobalt and nickel isotopic chains [130]. It is worth mentioning that the GT_0 distributions for this set of Mn, Fe, Co and Ni isotopes does not depend on the pairing structure of the ground state (even-even, odd- A , odd-odd).

We recall that the hybrid model (introduced in Section 3) explicitly incorporates Brink’s hypothesis for the downscattering part of the cross section. Hence it does not account for the energy shift in the GT_0 strength due to the melting of pairing, in contrast to the TQRPA approach. As a consequence the TQRPA cross sections for ^{56}Fe (the only nucleus which has been studied in both approaches) are somewhat larger (by about a factor of 2-3) at $E_\nu < 10$ MeV than those calculated in the hybrid model [134]. For higher energies the cross sections of the two models become nearly identical.

Juoadagalvis *et al.* have calculated inelastic neutrino scattering cross sections on Mn, Fe, Co and Ni isotopes at finite temperatures [130]. The study has been performed within the hybrid model (taking the GT_0 distributions from the shell model and other multipole contributions from RPA calculations). The finite temperature effects have been derived by inverting the shell model GT_0 distributions for the lowest excited states. The cross sections for the iron isotopes are shown in Fig. 16. We again observe the same trend in the cross sections as discussed above for TQRPA calculations. At low neutrino energies the cross sections is given by the contributions arising from deexcitation of thermally populated states and there are small variations in the cross section between the different isotopes. Once the neutrino energy is large enough to excite the GT_0 resonance the cross sections for all isotopes become very similar (which is due to the similarity of the GT_0 distributions) and finite-temperature effects become rather small. At energies $E_\nu < 20$ MeV forbidden contributions are at least an order of magnitude smaller than the GT contribution, become, however, increasingly more important with energy.

The effect of inelastic neutrino-nucleus scattering on the supernova dynamics has been in details explored in Ref. [5] by simulating the collapse of a $15 M_\odot$ progenitor star (model s15a28 of [186]). The simulation has been performed in spherical symmetry with the neutrino-hydrodynamics code VERTEX of the Garching group [89, 90] using a state-of-the-art description of the interactions of neutrinos and antineutrinos of all flavors as defined in [90, 35, 84].

The inelastic neutrino-nucleus scattering cross sections were derived on the basis of the hybrid model for a pool of about 50 nuclei covering the $Z = 24 - 28$ chains [130, 5]. Importantly, for temperatures $T > 1$ MeV, these calculations do not show large variations between the individual cross sections, for the reasons explained above. This justifies to approximate the relevant neutrino-nucleus cross sections by replacing the supernova matter composition by the results drawn from the restricted pool of nuclei. Hence, Ref. [5] defined an average neutrino-nucleus cross section as $\langle \sigma_{\nu n} \rangle = \sum_i Y_i \sigma_i / \sum_i Y_i$, where the sum is restricted to the pool of nuclei for which individual cross sections exist. The abundances of the individual nuclei Y_i were determined from an appropriate NSE matter distribution [187]. A rate table of the cross section has been derived as a function of temperature, density and electron-to-baryon ratio Y_e allowing for cross section determination at all encountered astrophysical conditions during the simulation. As an example the pool-averaged total cross section is shown in Fig. 17 at 3 different temperatures. (The densities and Y_e values are different at the different temperatures. They influence the average cross section by change of the NSE distribution with very minor impact.) The average cross section reflects the general trends discussed at length above.

Keeping track of neutrino energies is a crucial ingredient in supernova simulations. Inelastic neutrino scattering on nuclei changes the energy of the incident neutrino. This change depends on the incident energy and on temperature. The right panel in Fig. 17 shows the normalized outgoing neutrino spectra at different initial neutrino energies and for temperature $T = 1$ MeV. For $E_\nu = 6$ and 10 MeV down-scattering contributes significantly to the cross section; i.e., the de-excitation of thermally populated nuclear levels produces neutrinos with $E'_\nu > 10$ MeV. Down-scattering becomes essentially irrelevant at higher neutrino energies. For $E_\nu = 30$ MeV the cross section is dominated by the excitation of the GT_0 centroid, giving rise to a cross section peak around $E'_\nu = 20$ MeV. For even higher neutrino energies forbidden transitions contribute noticeably to the cross section. The peaks in the differential cross sections for $E_\nu = 50$ MeV correspond to excitations of the centroids of the GT_0 and dipole transition strengths. With increasing population of excited nuclear states the down-scattering contributions get relatively enhanced with increasing temperature [130, 134].

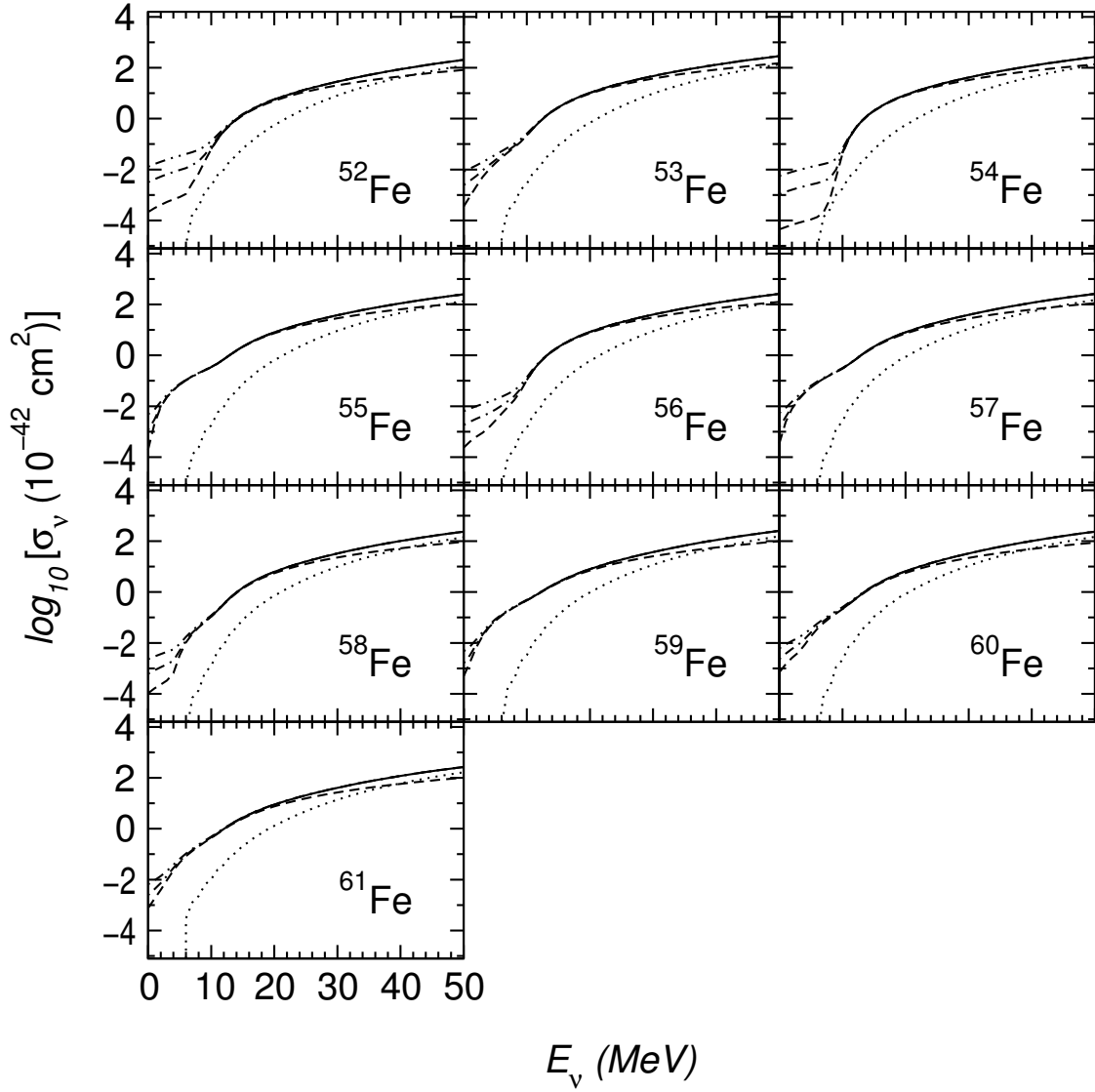


Figure 16: Neutral current neutrino-nucleus inelastic cross-sections for Fe isotopes. The dashed lines show shell model contributions at three different temperatures ($T = 0.86$ MeV dashed line, 1.29 MeV dash-dotted line, and 1.72 MeV dash double-dotted line); the dotted line is the RPA contribution; the solid line corresponds to the total cross sections. At low neutrino energies the total cross section coincides with the SM contributions (from [130]).

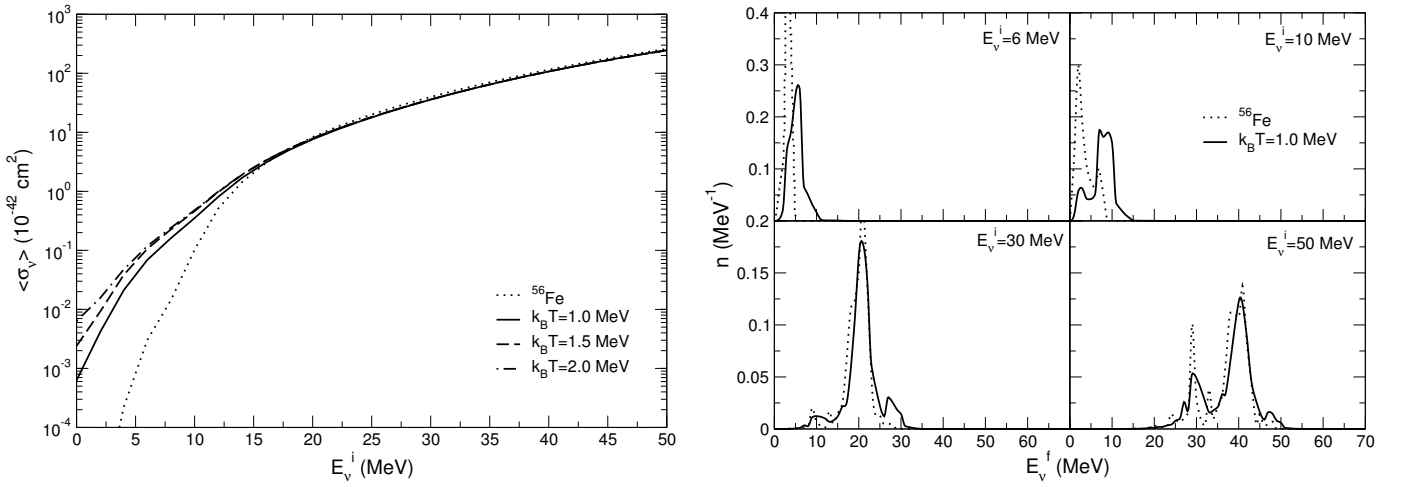


Figure 17: (left panel) Inelastic neutrino scattering cross sections for supernova conditions (see text) at 3 different temperatures. (right panels) Normalized neutrino spectra derived from inelastic neutrino scattering on a supernova matter composition for 4 different initial neutrino energies and at temperature $T = 1 \text{ MeV}$. For a comparison the dotted lines in the various panels give the respective quantities for the individual nucleus ^{56}Fe at $T = 0$ (based on the simulations presented in [5]).

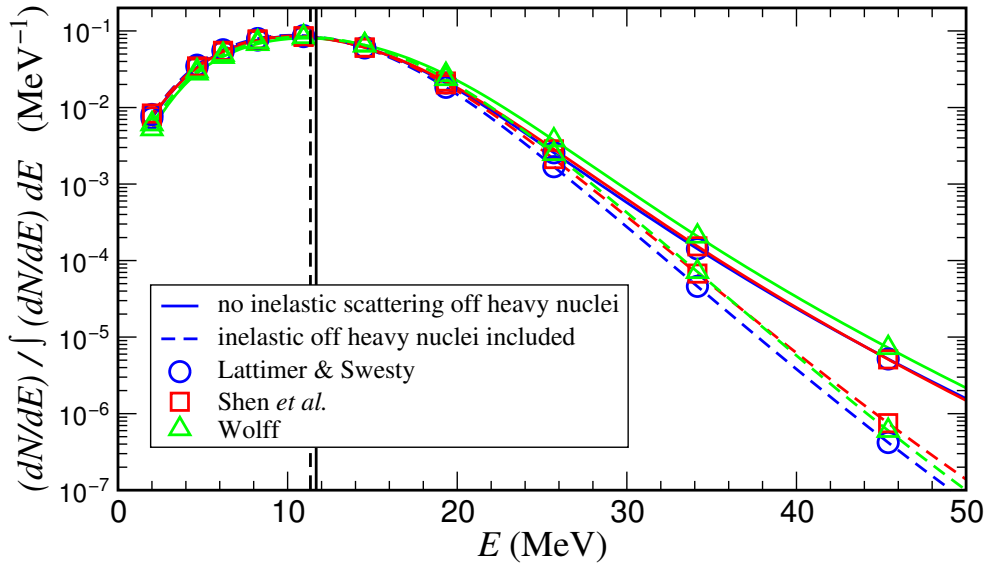


Figure 18: Normalized ν_e number spectra radiated during the shock breakout burst as seen by a distant observer at rest. Results are shown for simulations with three different nuclear EoSs. For better comparison of the strongly time-dependent spectra during this evolution phase, integration in a window of 8 ms around the peak luminosity was performed. Inelastic neutrino scattering off nuclei (dashed lines) leads mostly to energy losses of high-energy neutrinos and thus reduces the high-energy tails of the spectra. The vertical line marks the mean spectral energy (from [5]).

Table 3: Electron neutrino cross sections for scattering off electrons and for charged-current interactions with nuclei of different detector materials, averaged over the supernova neutrino spectrum of Fig. 18, using the results obtained with the Lattimer-Swesty EoS. The different cross sections were taken from: e [188], d [189], ^{12}C [151], ^{16}O [190], ^{40}Ar [18], ^{56}Fe and ^{208}Pb [104] (from [5]).

Material	$\langle\sigma\rangle$ (10^{-42} cm 2)		Reduction
	With IS	Without IS	
e	0.114	0.123	7%
d	5.92	7.08	16%
^{12}C	0.098	0.17	43%
^{12}C (N_{gs})	0.089	0.15	41%
^{16}O	0.013	0.031	58%
^{40}Ar	17.1	21.5	20%
^{56}Fe	8.81	12.0	27%
^{208}Pb	147.2	201.2	27%

Despite causing a higher neutrino opacity by increasing the neutrino-matter interaction, inelastic neutrino-nucleus scattering has virtually no impact on the supernova evolution [5]. As suggested by Haxton [183] the scattering increases the neutrino-matter coupling and thus the total energy transfer rate mainly to matter (nuclei and electrons) ahead of the shock by a factor 2-3 during the first 50 ms after shock bounce. However, the time period during which this additional heating acts on the supersonically infalling matter is too short to have consequences on the supernova simulation. The simulation of [5] thus confirms the expectation of Bruenn and Haxton [184] that neutrino preheating of matter ahead of the shock does not add significantly to the shock revival.

Inelastic neutrino-nucleus scattering has, however, a significant influence on the spectra of neutrinos emitted after bounce, in particularly during the period of the so-called ν_e neutrino burst (which, as we recall, is caused by fast electron captures on free protons after photodissociation of nuclei by the shock, see Section 2). During this period matter ahead of the shock still consists of heavy nuclei in NSE. Furthermore the density is still high with a relatively large optical depth for neutrinos. Under these conditions neutrinos interact frequently with nuclei by inelastic scattering. Due to the energy dependence of the cross section the scattering occurs more often for high-energy neutrinos, which will spend part of their energy by mainly exciting the GT_0 or giant dipole resonances (see Fig. 17). In fact, inelastic neutrino-nucleus scattering shifts the mean spectral energy of the ν_e burst spectrum only slightly by about 0.5 MeV, but it strongly suppresses the high-energy tail of the spectrum. This is shown in Fig. 18 which compares the ν_e burst spectrum in supernova simulations with and without consideration of inelastic neutrino-nucleus scattering. A similar suppression of the high-energy tail, caused by inelastic neutrino-nucleus scattering, is also observed for $\bar{\nu}_e$ and ν_x neutrinos during this early phase of the explosion. At later times inelastic neutrino scattering on nuclei becomes negligible for the neutrino emission spectra as the abundance of heavy nuclei has dropped drastically due to dissociation of nuclei

The observation of the ν_e burst neutrinos is one of the aims of supernova neutrino detectors [191, 192, 193]. The change of the ν_e burst spectrum due to inelastic neutrino-nucleus scattering will have consequences on the expected event rates for such detectors. We note again that, due to the energy dependence of neutrino-nucleus cross sections, the weight of high-energy neutrinos gets enhanced in the event rates. In Table 3 we compare the relevant detection cross sections for several target nuclei calculated for the ν_e burst spectra obtained with and without consideration of inelastic neutrino-nucleus

scattering. The largest reduction occurs for ^{12}C and ^{16}O which are detector materials in Borexino, MiniBooNe, KamLAND, SNO+, and Super-Kamiokande. For these nuclei only neutrinos with relatively high energies ($E > 17$ MeV for ^{12}C and $E > 15$ MeV for ^{16}O) can trigger charged-current reactions. As the neutrino scattering cross section on electrons increases linearly with energy, the reduction of the event rate for electrons, is less. Ref [5] estimates the improved event rates (including the effect of inelastic neutrino-nucleus scattering) arising from the ν_e burst of a supernova going off at 10 kpc distance.

In summary, supernova simulations imply that inelastic neutrino-nucleus scattering has no impact on the supernova evolution, but noticeably changes the ν_e burst spectrum. The latter effect is mainly caused by scattering on nuclei induced by high energy neutrinos, for which the respective cross sections are likely under control and can be calculated with sufficient accuracy, also at finite temperature. Finite temperature corrections significantly affect the cross sections for low-energy neutrinos. Here recent developments achieved within the TQRPA approach [134] are very promising and show that the cross section estimates based on the finite-temperature treatment in the hybrid model [130] are probably somewhat too small. This uncertainty in the low-energy neutrino-nucleus cross section has, however, probably no impact on the supernova evolution or the emitted neutrino spectra.

4.2 Deexcitation of hot nuclei by neutrino-pair emission in supernova environment

During the final phase of the collapse the temperature in the inner core can reach values above 1.5 MeV. Under such conditions the average excitation energy of a nucleus with mass number $A \sim 120$, (a representative value for the matter composition of heavy nuclei) is about $\langle E_x \rangle = 35$ MeV. It has been argued that the deexcitation of such highly excited states can be a significant neutrino-pair producing process [194] which can compete with electron-positron annihilation or nucleon-nucleon bremsstrahlung. As the presence of electron neutrinos does not block the production of muon and tau neutrino-antineutrino pairs, the nuclear deexcitation process might further reduce the entropy of the collapsing core if the neutrinos produced by the process can leave the core during the dynamical timescale of the collapse [194]. Recently nuclear deexcitation by neutrino-pair emission has, for the first time, been incorporated into a supernova simulation [195]. We will here briefly summarize the results of this study.

The formalism how to derive the rate for nuclear deexcitation, $A_i \rightarrow A_f + \nu + \bar{\nu}$, and its inverse reaction neutrino-pair absorption, $A_i + \nu + \bar{\nu} \rightarrow A_f$, and how to incorporate it into supernova simulations is presented in Ref. [195]. For our discussion here it is sufficient to recall that both processes are mediated by neutral current. In fact for neutrino-pair absorption the nuclear input is given by the same allowed and forbidden strength functions which determine inelastic neutrino-nucleus scattering. Our discussions above have shown that the hybrid model and the TQRPA calculations both indicate that these allowed and forbidden strengths are both concentrated around the GT_0 and giant dipole resonances. Furthermore the calculations (and the available M1 data) show that the position and total strengths do only mildly vary between nuclei. The authors of Ref. [195] used these findings to approximate the strength for the absorption process by:

$$S^{\text{abs}}(\Delta) = S_{Ag_A}(\Delta) + S_{Fg_F}(\Delta) \quad (23)$$

where $\Delta = E_\nu + E_{\bar{\nu}}$ is the energy sum of the neutrino-antineutrino pair. The normalized strength functions g_A for allowed transitions and g_F for forbidden transitions have been chosen as Gaussians. The centroids of these Gaussians μ_A, μ_F have been chosen guided by the shell model and TQRPA calculations for allowed transitions ($\mu_A = 9$ MeV, [134, 130, 185]) and by RPA calculations for forbidden transitions ($\mu_F = 22$ MeV, [165, 134]). Assuming that the strengths for excited states is somewhat more fragmented and wider spread in energy the standard deviations σ_A, σ_F have been adopted slightly larger

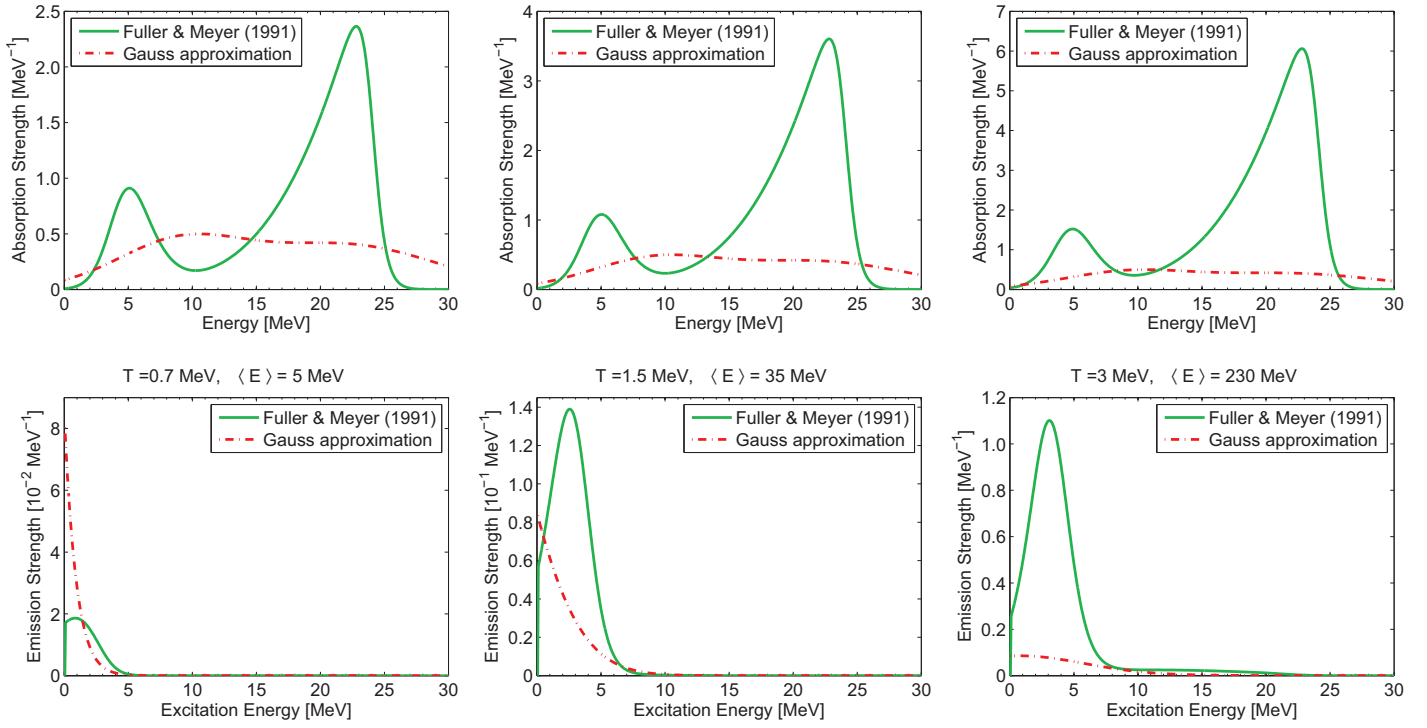


Figure 19: Strength for absorption (top panels) and emission (bottom panels) of neutrino pairs based on the Fermi-gas model of ref. [194] (green lines) and the Gaussian ansatz, eq. (23), (red lines) at temperatures of $T = 0.7$ MeV (left panel), $T = 1.5$ MeV (middle panel), and $T = 3.0$ MeV (right panel). The average thermal energy at the different temperatures is given above the lower panels (from [195]).

than for the ground state; i.e $\sigma_A = 5$ MeV, $\sigma_F = 7$ MeV. Finally the total allowed strength, $S_A = 5$ and the total forbidden strength, $S_F = 7$, has been adopted from shell model [130, 185] and RPA calculations [165]. Finally we mention that the approximate ansatz for the absorption strength function, eq. (23), explicitly assumes the Brink hypothesis which makes the strength independent of the initial nuclear excitation energy and consequently the absorption strength becomes independent of temperature.

The process of relevance for supernova simulations is nuclear deexcitation by neutrino pair emission. As this is the inverse of the neutrino-pair absorption process, the relevant strength function S^{emi} can be obtained by detailed balance

$$S^{emi}(\Delta, T) = S^{abs}(\Delta) \times \exp\left(-\frac{\Delta}{kT}\right). \quad (24)$$

While the absorption strength is independent of temperature by construction, the emission strength function depends on temperature by the Boltzmann factor $\exp(-\Delta/kT) = \exp(-(E_\nu + E_{\bar{\nu}})/kT)$.

The ansatz Eq. (23) is a rather simple approximation. For example, it assumes that it is the same for all nuclei and it neglects the dependence of the widths on temperature. An alternative approach to describe the nuclear deexcitation rate has been suggested by Fuller and Meyer [194]. These authors derived analytical expressions for the allowed and forbidden contributions to the emission and absorption strength functions at finite temperature based on the Fermi gas model. The parameters in their expressions were adjusted to reproduce results obtained in an independent single-particle shell model. We note that the strength functions proposed in Ref. [194] depend on temperature as well as on charge and mass number of the nucleus.

The absorption and emission strengths of the two models are plotted in Fig. 19. The absorption

strength functions of Ref. [194] show two distinct peaks for allowed and forbidden transitions, while the Gaussian ansatz (Eq. 23) distributes the strength over a wider energy range. While the Gaussian ansatz is independent of charge and mass number of the nuclei, the absorption strength of Ref. [194] is proportional to the number of nucleons and increases with temperature as the NSE composition gets shifted to heavier nuclei with growing temperature. For example, the average mass number is $\langle A \rangle = 124$ at $T = 1.5$ MeV using the Lattimer-Swesty Equation of State [71] and $\langle A \rangle = 205$ at $T = 3$ MeV. In summary, the two absorption strengths are quite distinct and can be understood as extreme cases allowing to explore how sensitive supernova simulations are to an accurate description of the strength. Nevertheless it might be desirable that the absorption strength function will be calculated within the TQRPA approach for several nuclei and at different temperatures.

The emission strength function is obtained by multiplying the absorption strength with the appropriate Boltzmann factor, see Eq. 24. The differences between the two absorption strength functions lead to strong deviations in the emission strength functions. We note that there is also emission strength at energies above the thermal average energy due to the thermal population of states at higher energies. In the emission decay rate the high-energy tails of the emission strength function get enhanced by an E^5 factor in the phase space factor, while this factor relatively decreases the contributions from lower energies.

Recently the downwards strength function has been calculated for fixed excitation energies for several nuclei within the diagonalization shell model [196]. To translate the downward strength into a thermal emission strength, the excitation energy has been adequated with the average thermal energy of a Fermi gas model. Hence by construction this approach does not allow for the production of neutrino pairs with a sum energy larger than the thermal average energy. Due to the phase space factor such high-energy pairs do noticeably contribute to the deexcitation rate.

The impact of nuclear deexcitation on the supernova evolution has been studied in core-collapse supernova simulations of an $11.2 M_\odot$ progenitor star [195]. Three simulations have been performed which differ only in the treatment of the neutrino pair de-excitation process. In the first two simulations this process has been implemented following the prescription of Ref. [194] and by adopting the Gaussian approximation model to the absorption strength function, as described above. The third simulation served as a control study, in which the neutrino-pair nuclear deexcitation has been switched off.

The most important result of these simulations is that the global quantities such as temperature and electron fraction profiles are the same in all simulations. This implies that the neutrino-pair nuclear deexcitation process has no impact on the global supernova evolution [195]. This is confirmed in Fig. 20 which shows that the luminosities of electron neutrinos, arising mainly from electron capture, are about 4 orders of magnitude larger than those of heavy-flavor neutrinos during the collapse phase.

Fig. 20 also shows that the evolution of the ν_e luminosities and average energies are the same in all three simulations: the luminosity increases from about 10^{51} erg s $^{-1}$ to 10^{53} erg s $^{-1}$ at ν_e trapping shortly before core bounce caused by the increasing density which enlarges the electron Fermi energy and the electron capture rates. Relatedly, the average energies of ν_e neutrinos increase from 6 MeV to 10 MeV which, however are smaller than those of the neutrinos directly produced by the capture process, reflecting the importance of down-scattering by interaction with matter.

Nuclear deexcitation by neutrino-pair emission produces all neutrino types, while electron capture is a pure source of electron neutrinos. Indeed the de-excitation process is the dominating source of ν_x neutrinos and, to a lesser extent, of electron antineutrinos during collapse (see Fig. 20). Due to the charged-current contribution the production of electron neutrino pairs is larger than that of the other two flavors. At high densities of order 10^{13} g cm $^{-3}$ also nucleon-nucleon bremsstrahlung becomes a significant source of neutrinos other than ν_e which causes the steep rise of the $\nu_{\mu,\tau}$ and $\bar{\nu}_e$ luminosities at times just before bounce in Fig. 20. At densities below 10^6 g cm $^{-3}$ electron-positron annihilation is another relevant neutrino-pair production process. The average energies of the heavy-flavor neutrinos increase slightly during the collapse (as temperature increases), but they are noticeably smaller than

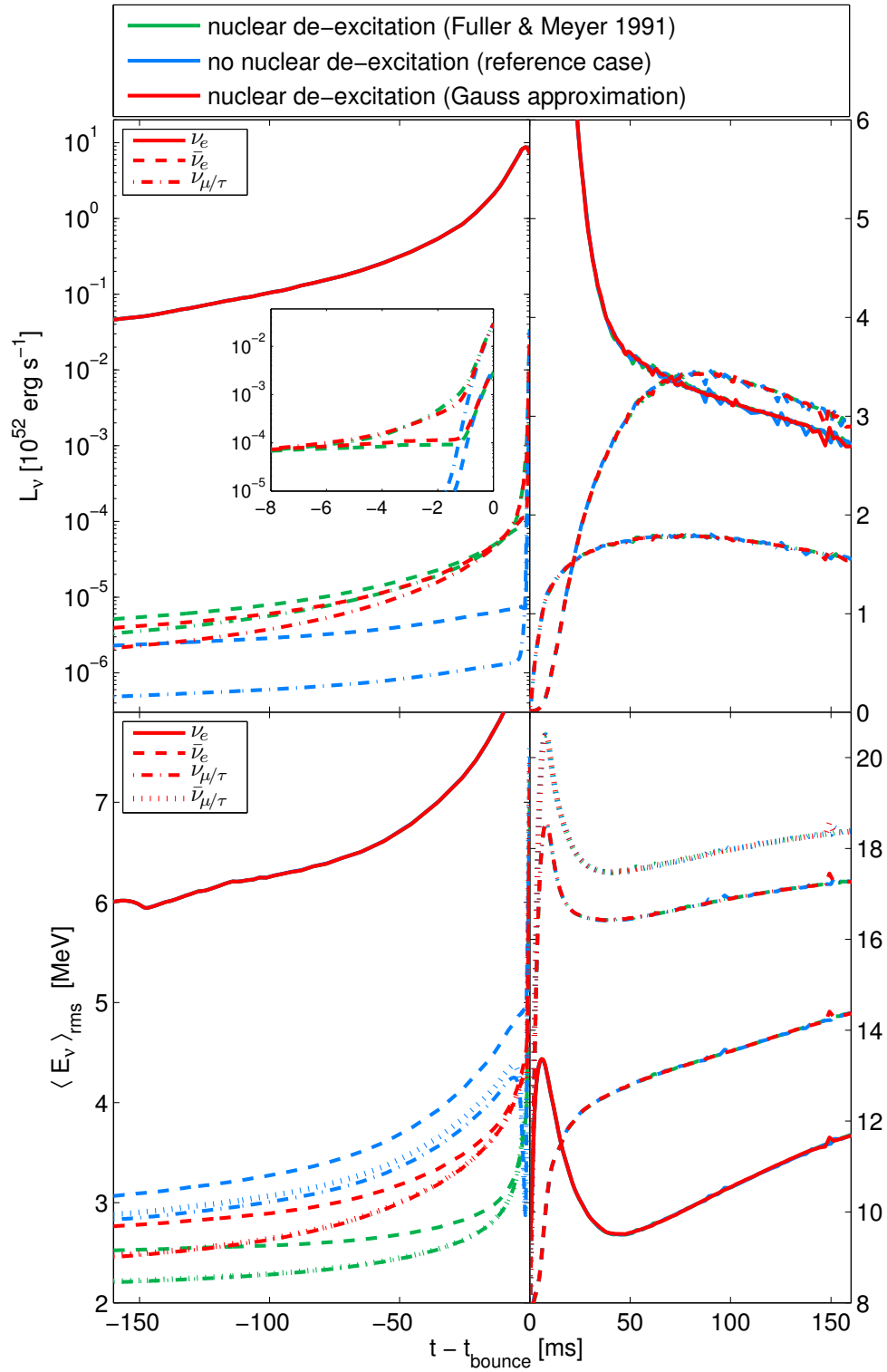


Figure 20: Evolution of neutrino luminosities and average energies from a core-collapse supernova simulation of an $11.2 M_\odot$ progenitor star including the production of neutrino pairs from heavy-nuclei de-excitations, based on Ref. [194] (green lines) and the Gauss ansatz (see text, red lines), in comparison to a simulation that uses identical input physics, but neglects the nuclear deexcitation process (blue lines) (from [195]).

the values of electron neutrinos produced by electron capture. For densities $\rho > 5 \times 10^{11} \text{ g cm}^{-3}$ neutrino-matter interactions also become relevant for heavy-flavor neutrinos.

At core bounce where normal matter density is reached, heavy nuclei dissociate into a state of homogeneous matter of nucleons and hence the production of neutrino pairs from nuclear deexcitation disappears. At shock formation and during the initial shock propagation out of the stellar core, the infalling heavy nuclei that hit the expanding shock wave also dissociate. Consequently at the conditions behind the expanding shock front, weak processes are determined by interactions with free neutrons and protons. Hence, the inclusion of heavy-nuclei de-excitations has no impact on the supernova dynamics or the neutrino signal after core bounce, e.g., in terms of the energy loss (as suggested in ref. [194]). Although a small fraction of heavy nuclei exist ahead of the expanding bounce shock before being dissociated (see the discussion in the preceding subsection), the conditions are such that other pair processes dominate over the pair production from nuclear de-excitation. Moreover, the supernova dynamics is dominated by charged-current processes on free nucleons behind the bounce shock in the dissociated regime. Consequently, neutrino pair heavy-nuclei de-excitations has no impact in the entire post-bounce period and the evolution of the neutrino luminosities and average energies in our three simulation become identical.

By studying the radial profiles of the collapsing core at different times during collapse, Ref. [195] gives a detailed account of the evolution of the luminosities and average energies of the various neutrino flavors and the competition of the different neutrino sources. It turns out that the two approaches which have been adopted to describe nuclear deexcitation give qualitatively similar results, they differ, however, in details. This is relevant if one is interested in an accurate description of the heavy-flavor and electron antineutrinos during collapse. An improved calculation of the absorption strength function within a formalism like the Thermal QRPA of Ref. [134] might be useful to this end.

5 Neutrino-nucleus reactions and supernova nucleosynthesis

As discussed above, the continuous emission of neutrinos from the protoneutron star drives a low-mass outflow (the neutrino-driven wind). Due to the high temperature involved the matter is ejected as free protons and neutrons. Upon reaching cooler regions further away from the neutron star, the matter can assemble into nuclei. The outcome of this nucleosynthesis depends crucially on the proton-to-neutron ratio and can either support the νp process (if $Y_e > 0.5$) or an r process ($Y_e < 0.5$). We will discuss both processes in the two following subsections. Furthermore neutrinos can also contribute to the astrophysical production of certain nuclides, in what is called the ν process, when they pass through the outer shell of the star. The ν process is discussed in the third subsection.

The proton-to-neutron ratio is mainly determined by the neutrino and antineutrino charged-current reactions with the free neutrons and protons [197]. Assuming that the neutrino luminosities are about equal for electron neutrinos and antineutrinos a detailed analysis of these reactions shows that the matter is expected to be proton rich if $4\Delta > (\langle E_{\bar{\nu}_e} \rangle - \langle E_{\nu_e} \rangle)$, where $\Delta = 1.29 \text{ MeV}$ is the proton-neutron mass difference and $\langle E_{\bar{\nu}_e} \rangle, \langle E_{\nu_e} \rangle$ are the average energies of electron antineutrinos and neutrinos, respectively [198]. It is important that in the kinematics of the neutrino-nucleon reactions corrections due to the nuclear interaction are included. The dominant contribution is due to mean-field corrections, induced by the astrophysical environment and accounted for in the Equations of State [199, 200]. Introducing the mean-field potentials for protons, U_p , and neutrons, U_n , the energy of neutrinos is reduced by $U_n - U_p$, while the energy of antineutrinos is enlarged by the same amount. We note that these corrections act like the Q value in electron capture reactions on nuclei which grows with increasing neutron excess throttling the capture rate. In fact, for the neutron-rich environment in core-collapse supernovae, e.g. shortly after bounce, $U_n - U_p > 0$ and as a consequence, the emissivity of neutrinos (antineutrinos) is increased (decreased) if the mean-field corrections are taken into account.

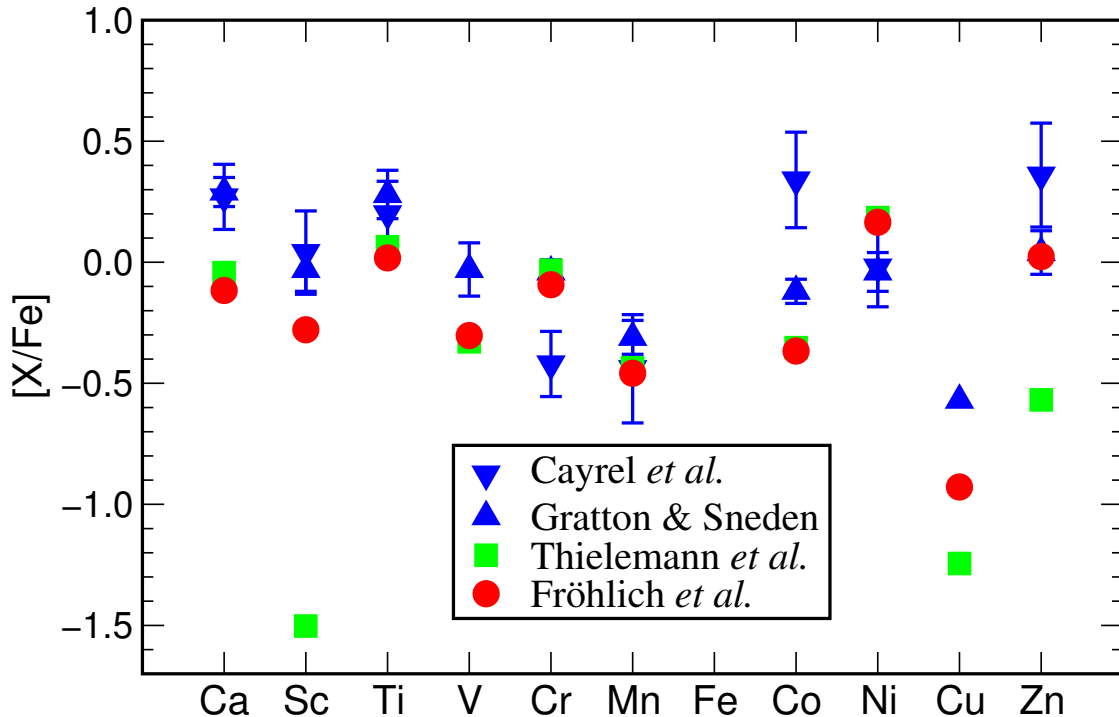


Figure 21: Comparison of elemental abundances in the mass range Ca to Zn produced in proton-rich environment (Fröhlich *et al.*, [198]) with previous calculations (Thielemann *et al.*, [212]) and observational data [213, 214] (adapted from [198]).

Remembering that the charged-current neutrino reactions on nucleons set the neutron-to-proton ratio of the matter ejected in the neutrino-driven wind, the changes of the neutrino and antineutrino energies due to the mean-field corrections have an essential impact on the neutrino-driven wind nucleosynthesis: the early ejecta are slightly neutron rich, while at later times the ejecta become proton rich [200].

In Ref. [201] it has been shown that in the outer layers of the protoneutron star a substantial amount of light nuclei (deuterons, ^3H , ^3He , and ^4He) is present. The interaction of neutrinos with these light nuclei has an impact on the average energies of neutrinos and antineutrinos. The relevant neutrino cross sections on the light nuclei have been calculated on the basis of ab-initio few-body methods like the hyperspherical harmonics approach [202, 203, 204]. These cross sections are more accurate than previous calculations performed on less sophisticated nuclear models (e.g. [9, 205]), but do not differ too dramatically.

5.1 The νp process

Supernova simulations indicate that during some period after bounce the hot matter ejected from the surface of the freshly born neutron star is proton-rich (i.e. $Y_e > 0.5$) (e.g. [50, 206, 207, 208, 8]). The alpha rich freeze-out of such proton-rich matter favors the production of α nuclei (mainly ^{56}Ni) with some free protons left [209]. We note that this freeze-out also results in enhanced abundances of selected nuclei in the Ca-Fe mass range bringing them into better agreement with observation [198, 210, 211] (see Fig. 21).

Heavier nuclides can be synthesized from the freeze-out abundance distribution by subsequent proton captures, competing with β^+ decays. We note that this reaction sequence is realized in the so-called rapid-proton capture process (i.e. explosive hydrogen burning on the surface of neutron stars in X-ray

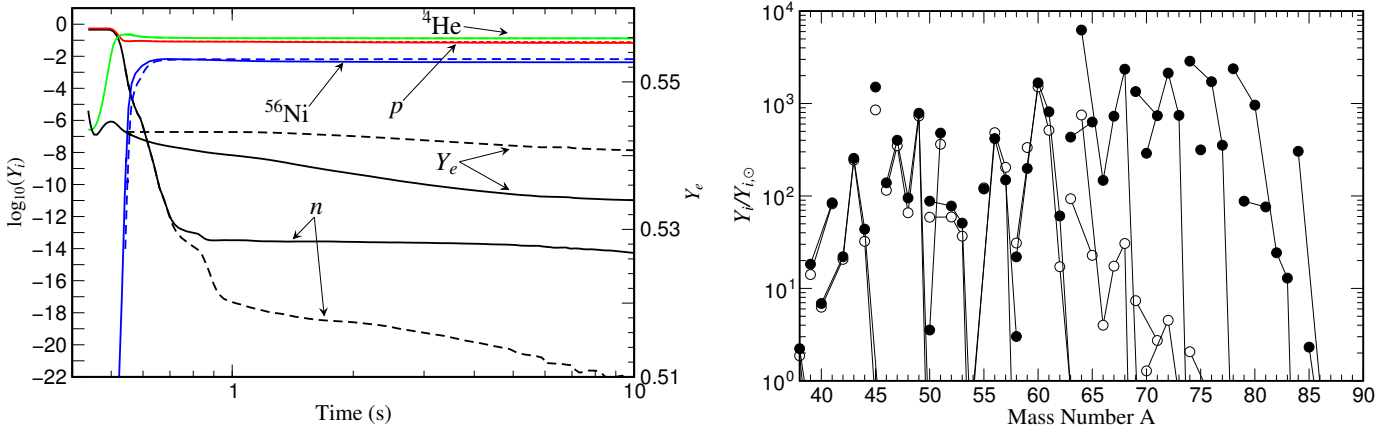


Figure 22: (left) Evolution of the abundances of neutrons, protons, alpha-particles, and ^{56}Ni . The solid (dashed) lines display the nucleosynthesis results which include (omit) neutrino and antineutrino absorption interactions after nuclei are formed. The abscissa measures the time since the onset of the supernova explosion. (right) Isotopic abundances (relative to solar) obtained within the supernova νp process nucleosynthesis. The filled circles represent calculations where (anti)neutrino absorption reactions are included in the nucleosynthesis while for the open circles neutrino interactions are neglected. The two panels base on a nucleosynthesis trajectory from the model B07 from Ref. [198] (from [210]).

bursts) [215]. However, in this scenario the mass flow to heavier nuclides is strongly hampered by the increasing Coulomb barrier of the produced elements and, in particular, by the so-called waiting point nuclei. These are α nuclei like ^{56}Ni , ^{64}Ge , ^{68}Se ... which have relatively long β half lives and for which the proton capture is strongly hindered due to the small or negative proton binding energies of the final nuclei (e.g. ^{57}Cu , ^{65}As , ^{69}Br , ...). In the case of unbound daughters it is suggested that the mass flow might overcome the waiting point nuclei by two-proton captures [216].

In contrast to the nucleosynthesis in X-ray bursts, the process occurs in the supernova environment in the presence of extremely intense neutrino fluxes which influences and alters the matter flow to heavier nuclei substantially. While the energy of supernova ν_e neutrinos is too small to induce sizable reaction rates on $N \sim Z$ nuclei, this is different for antineutrinos that are captured in a typical time of a few seconds in the conditions of the hot neutrino bubble, both on protons and nuclei, at the distances at which nuclei form (~ 1000 km). This time scale is much shorter than the beta-decay half-life of the most abundant heavy nuclei (e.g. ^{56}Ni , ^{64}Ge), which serve as obstacles in the mass flow to heavier nuclei if neutrino interactions are not included. As protons are more abundant than heavy nuclei, antineutrino capture occurs predominantly on protons, causing a steady supply of free neutrons with a residual density of 10^{14} – 10^{15} cm^{-3} for several seconds, when temperatures are in the range 1–3 GK (see left panel in Fig. 22). The neutrons produced via antineutrino absorption on protons can easily be captured by neutron-deficient $N \sim Z$ nuclei (for example ^{64}Ge), which have large neutron capture cross sections. The amount of nuclei with $A > 64$ produced is then directly proportional to the number of antineutrinos captured. While proton capture, (p, γ) , on ^{64}Ge takes too long, the (n, p) reaction dominates (with a lifetime of 0.25 s at a temperature of 2 GK), permitting the matter flow to continue to nuclei heavier than ^{64}Ge via subsequent proton capture up to the mass range $A \sim 80 - 100$ (for a mass-flow diagram see, for example, Ref. [217]). This nucleosynthesis process, operating in proton-rich supernova environment, is called the νp -process [210]. The abundance distribution obtained by νp -process nucleosynthesis is compared in the right panel of Fig. 22 to a simulation in which the effects of (anti)neutrino captures are switched off. Huther has explored the influence of the various neutrino-induced neutral- and charged-current reactions on the νp process abundances. He finds that the impact of the neutrino and antineutrino reactions on nuclei is negligible [218].

How far the massflow within the νp process can proceed strongly depends on the environment conditions, most noticeable on the Y_e value of the matter. Obviously the larger Y_e , the larger the abundance of free protons which can be transformed into neutrons by antineutrino absorption, and the faster the bridging of the waiting point nuclei like ^{64}Ge by (n, p) reactions. Other important parameters are the location (radius) of the matter during the formation of nuclei and the ejection velocity which both influence the antineutrino fluence which the ejected matter experiences. A location closer to the surface of the proto-neutron star and/or a slow ejection velocity leads to an extended antineutrino exposure that allows for an increased production of heavy elements [219, 220]. The sensitivity of the νp -process on parameters like the Y_e value has been explored in [210, 217, 221]. These studies show that nuclei heavier than $A = 64$ are only produced for $Y_e > 0.5$, showing a very strong dependence on Y_e in the range 0.5–0.6. A clear increase in the production of the light p -nuclei, $^{92,94}\text{Mo}$ and $^{96,98}\text{Ru}$, is observed as Y_e gets larger. Thus the νp process offers an explanation for the production of these light p -nuclei, which was unknown before.

The late-time abundance of free neutrons depends sensitively on the $\bar{\nu}_e$ luminosities and spectra. As has been shown recently [94, 93, 95], the $\bar{\nu}_e$ spectrum is affected by collective neutrino flavor oscillations which are expected to occur in the high-neutrino-density environment surrounding the neutron star [93] and can swap the $\bar{\nu}_e$ and $\bar{\nu}_{\mu,\tau}$ spectra above a certain split energy of order 15-20 MeV, where the split energy depends on the relative fluxes of $\bar{\nu}_e$ and $\bar{\nu}_x$ and on the neutrino mass hierarchy [222]. Assuming such a swap scenario for the case of the normal neutrino mass hierarchy (see left part of Fig. 23), Ref. [223] has studied the impact of collective neutrino flavor oscillations on the νp process nucleosynthesis adopting anti-neutrino spectra from recent supernova simulations [90]. As in general, $\bar{\nu}_x$ neutrinos have larger mean energies and a larger high-energy tail than electron antineutrinos, the spectrum swap induced by collective neutrino oscillations increases the neutron production rate by antineutrino capture on protons during the νp process. Ref. [223] estimates this increase to vary by a factor between 1.5 to 1.25 depending on a split energy between 0 and 25 MeV. Obviously the enhanced production of free neutrons boosts the matter flow to heavier nuclides and results in larger νp process abundances. This is demonstrated in the right part of Fig. 23 which compares the νp -process abundances calculated with a neutron production rate increased by a factor of 1.4 due to collective neutrino oscillations and the standard case without such oscillations. The production of the light p -nuclides $^{92,94}\text{Mo}$ and $^{96,98}\text{Ru}$ is enhanced by a factor 2-3. The largest production increase is observed for nuclides $A > 96$ which is traced back to a faster (n, p) reaction time-scale for the $N = 50$ nucleus ^{96}Pd which acts like a 'seed' for the production of nuclides with $A > 96$ [224]. The faster (n, p) reactions also have an effect on the abundances of waiting point nuclei like ^{64}Ge or ^{68}Se . These nuclei are less of an obstacle in the mass flow in the calculations which consider collective neutrino oscillations and hence less matter is accumulated at the waiting points. More recently, Wu *et al* [97] have performed a detailed analysis of the impact of collective oscillations on neutrino-wind nucleosynthesis accounting for the full temporal variation of neutrino spectra and matter density profiles.

The νp process constitutes a mass flow from seed nuclei, mainly ^{56}Ni , to heavier nuclides by (p, γ) reactions, supplemented by (n, p) or β^+ reactions running through many nuclei at the proton-deficient side of the nuclear chart. Many of the β^+ half-lives, for the ground states, are experimentally known. However, their potential modifications for the astrophysical environment with finite temperature as well as the rates for the proton capture and (n, p) reactions have to be theoretically modelled, which is usually performed on the basis of the statistical model. A particularly important ingredient in such statistical model calculations are the nuclear masses, which define the reaction Q values and thus the competition between reactions and their inverse. Nuclear mass measurements have benefited tremendously in recent years by the establishment of nuclear Penning traps or by storage ring experiments at radioactive ion-beam facilities which also allowed the determination of masses of νp -process nuclei with unprecedented precision. With relevance to the νp process such measurements have been performed for nuclei in the mass range $A \sim 90$ at the SHIPTRAP at GSI and JYFLTRAP in Jyväskylä [225, 226], for nuclei

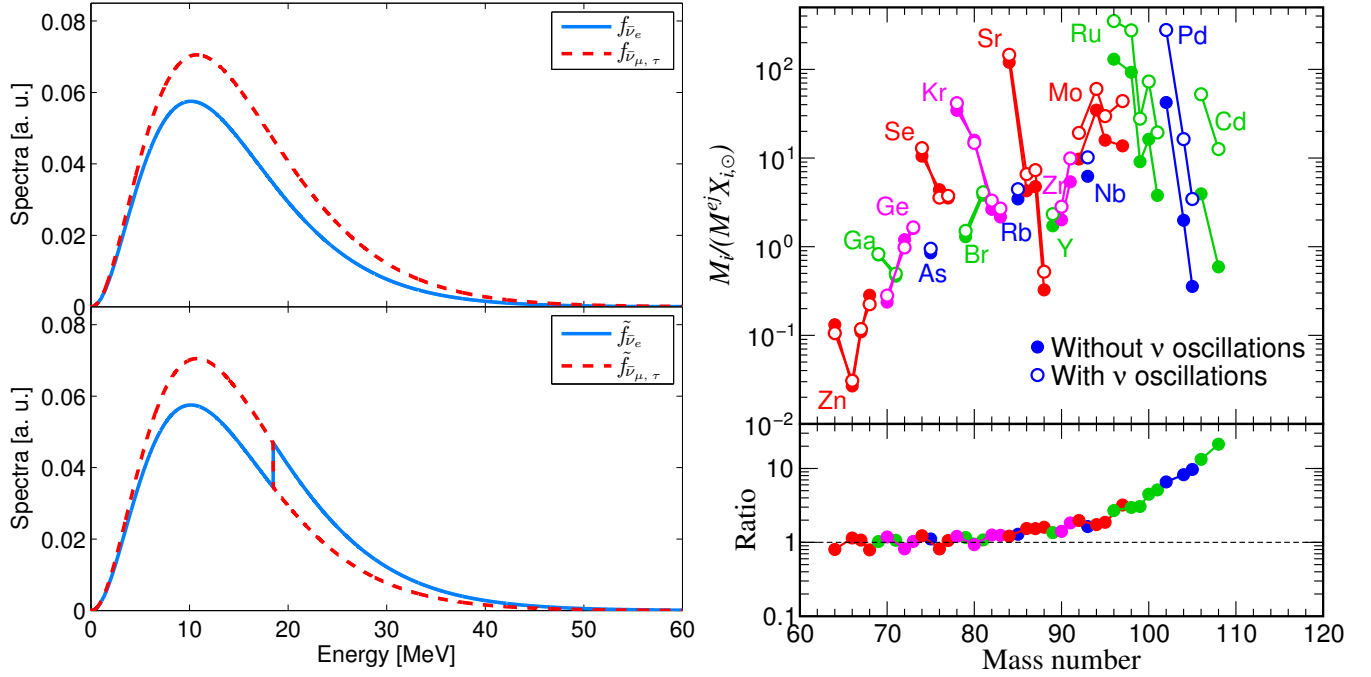


Figure 23: Left: (upper panel) $\bar{\nu}_e$ and $\bar{\nu}_x$ spectra $f_{\bar{\nu}_e}$ and $f_{\bar{\nu}_x}$ based on the simulations of ref. [90] as given in table 1 of ref. [217]. The $\bar{\nu}_e$ spectra have been arbitrarily normalized to one while the $\bar{\nu}_x$ spectra are normalized to 1.3 to keep the relative ratio of the number luminosities. (lower panel): modified spectra $\tilde{f}_{\bar{\nu}_e}$ and $\tilde{f}_{\bar{\nu}_x}$, including the effects of collective neutrino oscillations, which induce a swap of the $\bar{\nu}_e$ and $\bar{\nu}_x$ spectra for energies above E_s . Right: Abundances of νp nucleosynthesis calculations with (open circles) and without (full circles) considering the effects of collective neutrino flavor oscillations (normalized to solar). The lower panel shows the ratios for the two nucleosynthesis studies as function of mass number (from [223]).

around $A = 64$ at the CSRe storage ring in Lanzhou [227], for proton-deficient nuclei in the mass range $A \sim 90$ at the Canadian Penning trap [228]. The impact of these mass measurements on the νp process has been explored in Refs. [224, 225]. Studies which investigated the sensitivity of the νp process abundances on the uncertainties in the (n, p) rates have been reported in [219, 229]. The results are similar to those found for the effect of the collective neutrino oscillations: faster (n, p) rates speed up the mass flow to heavy nuclides and hence increase the abundances for nuclides with $A > 96$, while they decrease the abundances for nuclides in the mass range $A \sim 64 - 96$.

5.2 The r-process

More than 50 years ago the astrophysical r-process (short for rapid neutron capture process) was introduced to explain the origin of the transactinides and of half of the nuclides heavier than iron [19, 230]. The process is characterized by fast neutron captures, in comparison to the competing β decays, which, in turn, requires astrophysical objects with extreme neutron densities for the r process to operate [108]. On the nuclear chart the r-process path runs through nuclei with extreme neutron excess far off the valley of stability. Most of these nuclei have yet not been produced in the laboratory and their properties, which are required input to r-process simulations, have to be modelled theoretically. The most relevant nuclear input are masses (reaction Q values) and β half lives which influence the r-process path and the duration of the process, respectively [108]. Particularly important for the r-process mass flow to heavier nuclei are the waiting point nuclei associated with the magic neutron numbers $N = 82$ and 126 (and possibly 184), which are also related to the peaks observed in the r-process abundance distributions around mass numbers $A \sim 130$ and 195.

Decisive progress towards experimental information for r-process nuclei is expected from current and future radioactive ion-beam facilities like RIBF at RIKEN, FAIR at GSI and FRIB at NSCL/MSU. From these facilities we expect not only the direct determination of properties of r-process nuclei, but also stringent constraints to improve the theoretical description of such neutron-rich nuclei which are out of experimental reach even at these advanced facilities. We have witnessed such indirect progress due to data for neutron-rich nuclei for both, the global description of masses and the prediction of half-lives. The advances in experimental mass measurements are reviewed in Ref. [231]; recent mass evaluations can be found in [232, 233] (see also [234]). These data help to improve the predictions of nuclear mass models like the microscopic-macroscopic approach for many years pioneered by Möller [235, 236] (see also [237]), the Extended Thomas Fermi Model with Strutinski Integral [238], the shell-model guided approach by Duflo and Zuker [239] or studies based on the Hartree-Fock-Bogoliubov model [240]. Half-life measurements of r-process nuclei at or in the vicinity of the magic neutron numbers $N = 50$ and 82 have been reported in Refs. [241, 242, 243, 244] and [245, 246, 247], respectively. First half-life measurements towards r-process nuclei at the $N = 126$ shell closure have been performed at GSI [248], which are useful constraints for theoretical half-life predictions in this until yet unexplored part of the nuclear chart (e.g. [249, 250, 251] and the calculations of Borzov as quoted in [248]).

One of the fundamental questions in astrophysics is: where does the r-process operate? Although no conclusive answer can yet be given, crucial clues come from abundance observations in so-called metal-poor stars, i.e. stars with Fe/H ratios which are significantly (often by orders of magnitude) smaller than the solar Fe/H ratio. While hydrogen has mainly been produced by Big Bang nucleosynthesis, iron has gradually been synthesized by both types of supernovae (core-collapse and thermonuclear) during the history of the galaxy. The Fe/H abundance ratio can thus serve as a proxy of age and stars with Fe/H ratios much smaller than solar are supposed to be very old stars. Due to their abundance pattern, metal-poor stars can be classified roughly into two categories: So-called r-II stars [252] exhibit relative abundance patterns which agree nearly perfectly with the solar r-process abundances for elements with charge numbers $Z > 50$ [253, 254, 255]. Some other stars [256, 257] are depleted in elements with $Z > 50$, but enriched in lighter elements like Sr, Y and Zr, with the star HD 122563 being a famous

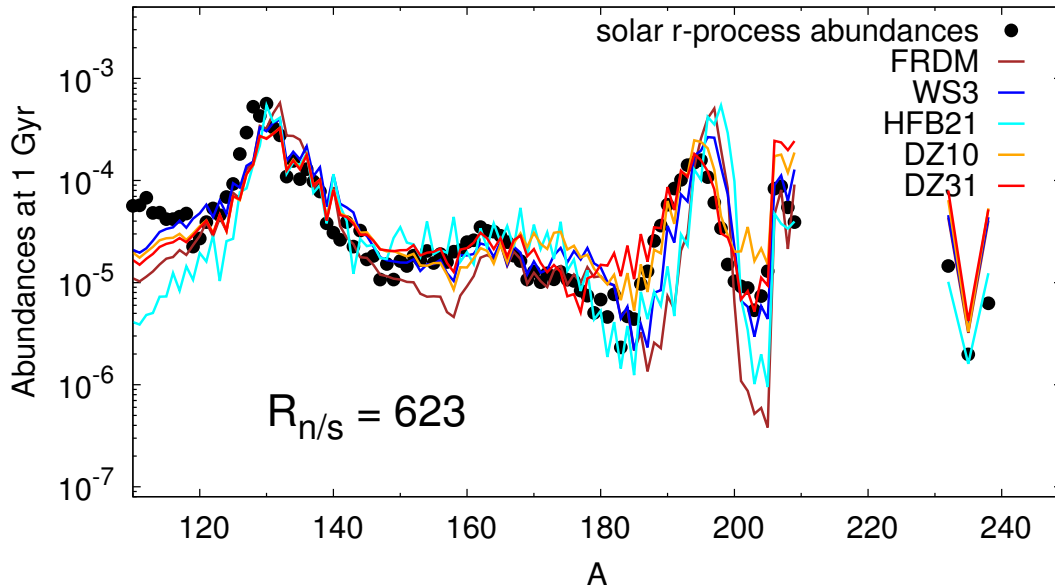


Figure 24: R-process abundances calculated for a neutron-star merger trajectory and different mass models (from [258]).

example [256]. One often denotes the process whose imprint is observed in stars like HD 122563 the 'weak r-process', while the 'main r-process' is related to the robust abundance pattern observed in the r-II stars.

It is tempting to identify potential astrophysical sites for the r-process. The main r-process might be attributed to neutron star mergers. Recent simulations [259, 260] show that the extreme neutron richness of the matter dynamically ejected during the merger ($Y_e \sim 0.05$) leads to fast mass flow to nuclei up to mass range $A \sim 280$ and the occurrence of fission cycling. In fact, the second r-process peak at $A \sim 130$ is produced by fission fragments in this scenario. Hence fission rates and yield distributions, including the production of free neutrons during the fission process and by β -delayed neutron emission of fission yields, are crucial ingredients in the simulations [261, 262]. Fig. 24 shows the abundance distribution obtained from r-process simulations based on neutron-star merger trajectories of Ref. [260] and using the fission fragment yields calculated on the basis of the ABLA code [263] which has been carefully adjusted against experimental fission data [111]. In fact the calculated abundance distributions reproduce quite nicely the solar r-process pattern in a quite robust way, i.e. basically independent on the nuclear mass models and the details of the merger trajectories [258]. Despite these intriguing results it is still an open question whether neutron-star mergers have already operated with sufficient frequencies at the early time of the galaxy to explain the observed r-process abundances in the oldest stars [264, 265, 266, 267, 268]. Furthermore, the impact of neutrinos in relativistic merger models requires further investigation [269]. Alternative sites for the r-process which are expected to operate mainly at low metallicities are jets from magnetorotational supernova [270] or an r-process in the He-shell of core-collapse supernovae [271]. In the latter scenario, the required neutrons are produced by charged-current reactions on ${}^4\text{He}$ via ${}^4\text{He}(\bar{\nu}_e, e^+){}^3\text{H}$ where the relevant cross sections are given in [272] based on an ab-initio calculation within the hyperspherical harmonics approach [273].

The weak r-process has been suggested to operate in the neutrino-driven wind developing in core-collapse supernovae after bounce. This scenario has actually been the favorite site for the r-process for many years [275, 276]. To achieve the neutron-to-seed ratio n/s necessary to produce the third r-process peak at $A \sim 195$ and the transactinides after freeze-out of charged-particle reactions, $n/s > 150$, puts

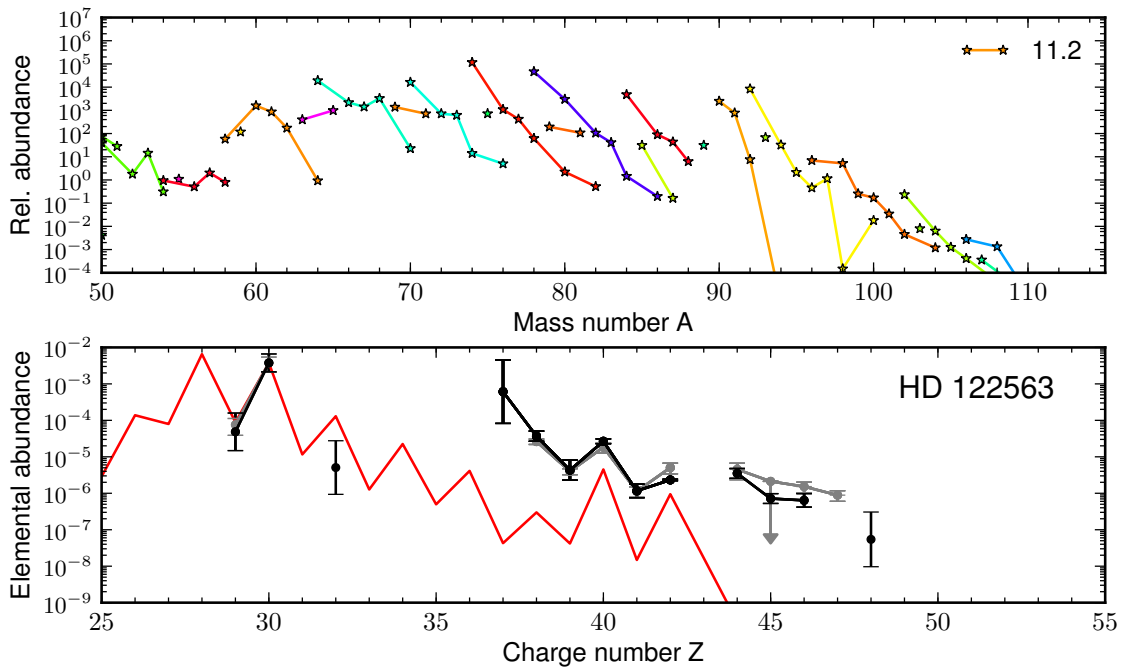


Figure 25: Mass-integrated abundances for the neutrino-driven wind of a core-collapse supernova (adapted from [274]).

stringent constraints on the wind properties. Such high ratios require either large entropies, small Y_e value or fast velocities of the ejected matter [277, 278]. Recent supernova simulations imply that such conditions are not met in the neutrino-driven scenario making the operation of the ‘main r-process’ unlikely in this scenario. However, the conditions might be sufficient to produce the light r-process elements up to Sr, Y, and Zr [279, 274]. This is demonstrated in Fig. 25 which shows the mass-integrated abundance distribution (upper panel) and elemental abundances (lower panel) obtained from a core-collapse supernova simulation of a $11.2M_\odot$ progenitor star [274] which followed the post-bounce evolution up to 9 s after bounce. The calculation adopted an Equation of State which consistently provided the mean-field corrections needed for the calculation of the charged-current neutrino reactions on nucleons which determine the Y_e value of the ejected matter (as discussed above). The ejected matter was found to be neutron rich at early times ($Y_e \sim 0.48$ for the first 3 seconds after bounce). At later times the matter becomes increasingly enriched in protons reaching $Y_e = 0.58$ after 9s. The early neutron-rich ejecta produce isotopes of the elements Sr to Mo ($Z = 38 - 42$), while nuclei with $Z > 42$ (or $A > 92$) are produced by the νp process in the later proton-rich ejecta. However, their production is quite inefficient due to low antineutrino luminosities (equivalently neutron production rates) at late times. Ref. [274] also finds relatively small amounts of matter ejected at late times. Thus, the νp process does not contribute much to the mass-integrated abundances. It is very interesting to note that the elemental abundances for the elements Sr, Y, Zr, Nb, Mo reproduce the abundance pattern observed in the star HD 122563 quite well (see lower panel in Fig. 25). However, the calculation clearly underproduces the observed abundances for the elements with $Z > 42$, including silver and palladium. The production site of these elements is yet an open question [274]. Active-sterile neutrino oscillations, that assume a sterile neutrino mass ~ 1 eV, help to achieve conditions suitable for the productions of elements in the range $Z = 42-50$ [280]

There have been several suggestions how neutrino-nucleus reactions might alter the r-process abundance in the neutrino-driven wind scenario (for a review see [281]). However, the impact of the reactions has mainly been explored choosing parametrizations of the wind which made it the site of

the main r-process. The studies include r-process calculations including neutrino-nucleus reactions [282, 283, 284, 285, 286], the exploration of the role of neutrino-induced fission [106, 107, 287] and potential fingerprints left by neutrino-induced spallation on the final r-process abundances [288, 289]. The recent calculations by Huther [218] indicate that neutrino-nucleus reactions have no noticeable impact on the abundance distribution of the weak r-process [274]. A potential exception is one of the variants of the so-called ‘ α effect’, proposed in Ref. [290]. In very strong neutrino fluxes neutral-current reactions on ${}^4\text{He}$ can trigger two-body reaction sequences (e.g. ${}^4\text{He}(\nu, \nu'p){}^3\text{H}({}^4\text{He}, \gamma){}^7\text{Li}({}^4\text{He}, \gamma){}^{11}\text{B}$ and ${}^4\text{He}(\nu, \nu'n){}^3\text{He}({}^4\text{He}, \gamma){}^7\text{iBe}({}^4\text{He}, \gamma){}^{11}\text{C}$) which compete with the three-body reaction $\alpha + \alpha + n \rightarrow {}^9\text{Be}$ which has been initially considered to bridge the mass gaps at $A = 5$ and 8 in the neutrino-driven wind r-process [275]. As a consequence of the more effective bridging the mass flow to heavier nuclei is faster, reducing in turn the neutron-to-seed ratio and thus throttling the subsequent r-process.

5.3 The ν process

When neutrinos, produced in the hot supernova core, pass through the outer shells of the star, they can induce nuclear reactions and in this way contribute to the synthesis of elements (the ν -process) [291, 292]. As pointed out by Woosley *et al.* [9], the nuclides ${}^{11}\text{B}$ and ${}^{19}\text{F}$ are produced by $(\nu, \nu'n)$ and $(\nu, \nu'p)$ reactions on the quite abundant nuclei ${}^{12}\text{C}$ and ${}^{20}\text{Ne}$. These reactions are dominantly induced by ν_μ and ν_τ neutrinos and their antiparticles due to their larger average energies than ν_e and $\bar{\nu}_e$ neutrinos. Also the synthesis of the odd-odd nuclides ${}^{138}\text{La}$ and ${}^{180}\text{Ta}$ are attributed to the ν process. However, they are produced mainly by the charged-current reaction ${}^{138}\text{Ba}(\nu_e, e^-){}^{138}\text{La}$ and ${}^{180}\text{Hf}(\nu_e, e^-){}^{180}\text{Ta}$ [293]. Hence, the ν -process is potentially sensitive to the spectra and luminosity of ν_e and ν_x neutrinos, which are the neutrino types not observed from SN1987A.

Neutrino nucleosynthesis studies are quite evolved requiring state-of-the-art stellar models with an extensive nuclear network [186, 294]. In the first step stellar evolution and nucleosynthesis is followed from the initial hydrogen burning up to the presupernova models. The post-supernova treatment then includes the passage of a neutrino flux through the outer layers of the star and of the shock wave which heats the material and also induces noticeable nucleosynthesis, mainly by photodissociation (the γ process [295]). Modelling of the shock heating is quite essential as the associated γ process destroys many of the daughter nuclides previously produced by neutrino nucleosynthesis.

The production of ${}^{138}\text{La}$ and ${}^{180}\text{Ta}$ by the ν process is caused by charged-current (ν_e, e^-) reactions on ${}^{138}\text{Ba}$ and ${}^{180}\text{Hf}$, respectively. At the energies involved the cross sections are dominated by the low-energy tail of the GT_- strength distribution. As large-scale shell model calculations are yet not feasible for these relatively heavy nuclei, the cross sections had to be calculated within the RPA model for both allowed and forbidden transitions [9, 294]. As a major improvement the GT_- strengths on ${}^{138}\text{Ba}$ and ${}^{180}\text{Hf}$ below the particle thresholds was measured at the RCNP in Osaka using the $({}^3\text{He}, t)$ charge-exchange reaction [296]. The left panel of Fig. 26 compares the running sum of the measured $\text{B}(\text{GT}_-)$ strength with the RPA prediction. Note that for the ν -process production of ${}^{138}\text{La}$ and ${}^{180}\text{Hf}$ one is only interested in the strength below the neutron threshold (indicated by S_n in Fig. 26) as the strength above S_n connects to states which will subsequently decay by neutron emission and hence not contribute to the ${}^{138}\text{La}$ and ${}^{180}\text{Hf}$ production. One finds that the RPA prediction are slightly smaller than the $\text{B}(\text{GT}_-)$ data for ${}^{138}\text{Ba}$ up to the neutron threshold, but underestimates the ${}^{180}\text{Hf}$ strength by nearly a factor of 3. The inversion of the $\text{B}(\text{GT}_-)$ strength into cross section is complicated by the fact that for both nuclei the proton decay channel opens below the neutron channel. The respective corrections have been derived from branching ratios obtained from the statistical model. Furthermore adding forbidden contributions to the cross sections derived from RPA calculations, one finds that the ${}^{138}\text{Ba}(\nu_e, e^-){}^{138}\text{La}$ and ${}^{180}\text{Hf}(\nu_e, e^-){}^{180}\text{Ta}$, calculated for a supernova spectrum for ν_e neutrinos with temperature $T = 4$ MeV and zero chemical potential, are about 25% and 30% larger than estimated solely on the basis of allowed transitions. The cross sections are shown, together with other relevant

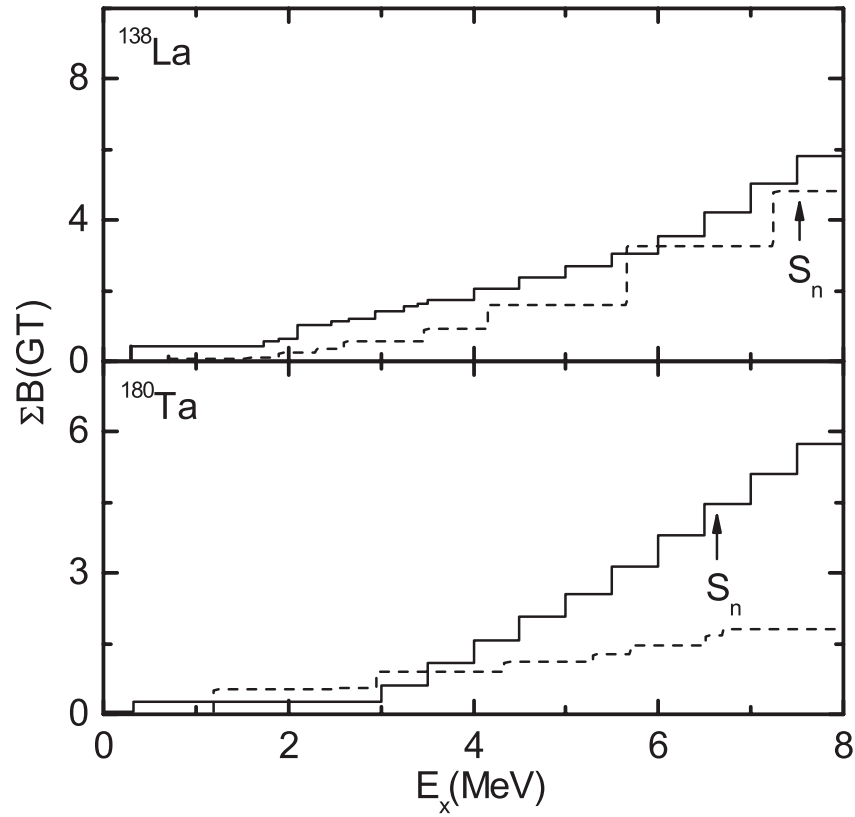


Figure 26: Summed $B(\text{GT})$ strength in ^{138}La and ^{180}Ta as a function of excitation energy up to the respective neutron emission thresholds. Solid lines: experimental data; dashed lines: RPA calculation [294] (from [296]).

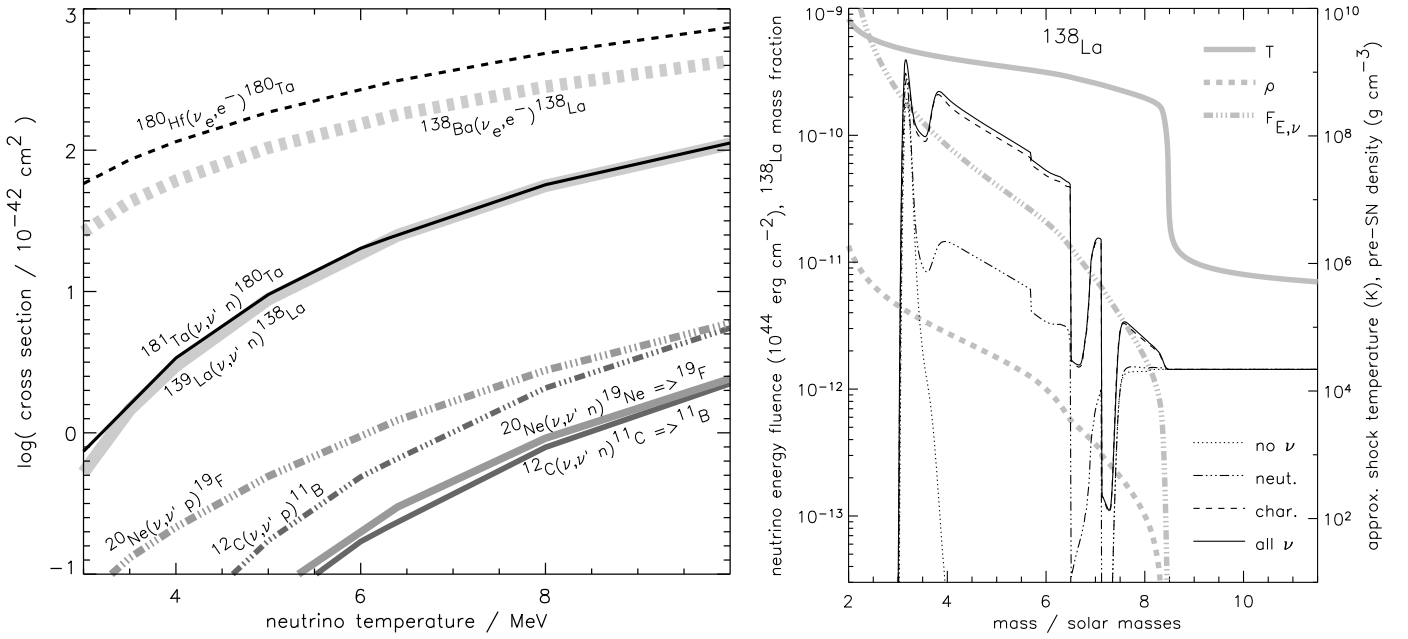


Figure 27: (Left) Electron neutrino charged-current cross sections on ^{138}Ba for cascades up to two particle emission. (right) Production of ^{138}La in a $25 M_{\odot}$ star. The figure shows the production of ^{138}La without neutrinos (dotted line), with the charged-current reaction $^{138}\text{Ba}(\nu_e, e^-)$ (dashed), with the neutral current reaction $^{139}\text{La}(\nu, \nu' n)$ (dashed-dotted) and with both reactions (solid). Additionally, the supernova shock temperature, the pre-supernova density, and the neutrino energy fluence $F_{E,\nu}$ assuming a total neutrino energy of 3×10^{53} erg are given (from [294]).

cross sections for the study of neutrino nucleosynthesis in the left panel of Fig. 27.

Incorporated into stellar models [186, 294] one finds indeed that ^{138}La is being produced by charged-current reactions on ^{138}Ba , This is demonstrated in Fig. 27 which shows the ^{138}La production in the oxygen/neon shell of a $25 M_{\odot}$ star [294]. The key is the enhancement of ^{138}Ba by an s-process prior to the supernova explosion. A ^{138}La abundance is basically not existing prior to the passing of the supernova neutrinos and is the mainly produced by the (ν_e, e^-) reaction on ^{138}Ba (right panel). In principle, ^{138}La can also be made by the neutral-current neutron-spallation reaction $(\nu, \nu' n)$, but its contribution to the total ^{138}La abundance is insignificant (right panel). The γ process produces also some ^{138}La when the shock passages through the oxygen/neon layer. But its contribution to the total ^{138}La yield is about an order of magnitude less than the charged-current contribution (right panel). In fact, ^{138}La appears to be co-produced with nuclides like ^{16}O and ^{24}Mg in massive stars. Using these nuclei as tracers for the contribution of massive stars to the solar abundance [186, 294, 296], the observed ^{138}La abundance appears to be mainly due to the ν process.

A comparison of the ^{180}Ta abundance calculated in stellar models is complicated by the fact that, on the time scales of the ν process, ^{180}Ta can exist in two states: the $J = 9^-$ isomeric state at excitation energy $E_x = 75.3$ keV with a half life of more than 10^{15} years and the ground state which decays with a half live of 8.15 hours. Also the B(GT₋) data cannot distinguish between the contributions to these two states. Furthermore in the finite temperature astrophysical environment the two states couple via excitation of states at intermediate energies [297, 298]. To treat this coupling, Hayakawa *et al.* have recently proposed a model [299, 300] in which they distinguish between states build on the ground and isomeric states (guided by data of Refs. [301, 302]) and assume these two band structures couple only weakly to each other. They then followed the decoupling of the two-band structure from thermal equilibrium to freeze-out in a time-dependent approach assuming an exponential decrease of

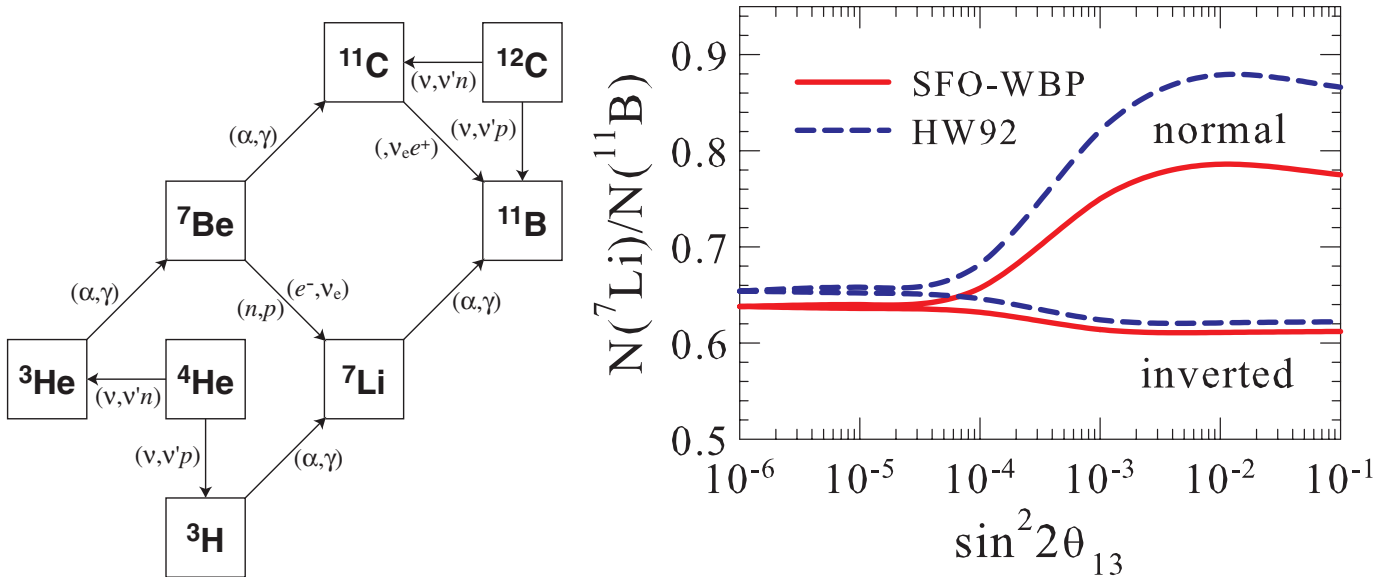


Figure 28: (left) Nuclear reaction flow path for the production of light elements induced by neutrino reactions on ^{12}C during a supernova explosion. (right) Dependence of the abundance ratio $^7\text{Li}/^{11}\text{B}$ on the neutrino mixing angle θ_{13} for normal and inverted neutrino mass hierarchies. The calculations have been performed for two sets of neutrino cross sections and branching ratios (from [128]).

temperature with time. In their calculation 39% of the ^{180}Ta produced in the ν process survives in the long-lived isomeric state. A similar branching ratio has been estimated earlier by Mohr *al.* [303]. Combining these branching ratios with the total ^{180}Ta ν process abundance as given in [296] makes the ν process a potential ^{180}Ta production site. We note, however, that also s-process nucleosynthesis has been suggested to produce nearly 100% of the solar ^{180}Ta abundance [304].

Following the work of Ref. [9], several studies have confirmed that the ν process can produce the nuclides ^{11}B and ^{19}F in solar abundances by $(\nu, \nu'n)$ and $(\nu, \nu'p)$ reactions on ^{12}C and ^{20}Ne . These studies considered improved stellar simulations [186, 305, 294] and more elaborate neutrino-induced spallation cross sections (e.g. [294, 306, 307]). The shell model has been shown to reproduce the GT distributions for nuclei in the p shell quite well [306]. Some ^7Li is produced by neutrino-induced reactions on ^4He in the He layer of the star (the $(\nu, \nu'p\alpha)$ reaction on ^{12}C can in principle also produce ^7Li in the oxygen/carbon layers, but the respective branching ratio is too small to be significant [18]).

Very recently Sieverding *et al.* have performed studies of neutrino-induced nucleosynthesis in supernovae for stars with solar metallicity and initial main sequence masses between 15 and 40 M_{\odot} [308]. These studies improve the previous investigations i) by using a global set of partial differential cross sections for neutrino-induced charged- and neutral-current reactions on nuclei with charge numbers $Z < 78$ and ii) by considering modern supernova neutrino spectra which are noticeably shifted to lower energies (i.e. $T_{\nu_e} = 2.8$ MeV, $T_{\bar{\nu}_e} = T_{\nu_x} = 4.0$ MeV assuming a Fermi-Dirac neutrino distribution with zero chemical potential) compared to spectra previously adopted and discussed above (e.g. [9, 294]). Mainly due to the change in neutrino spectra, Sieverding finds slightly smaller abundances for ^7Li , ^{11}B , ^{138}La and ^{180}Ta , however, he confirms the production of these nuclides by neutrino nucleosynthesis [308] (see Table 4).

Interestingly neutrino-induced reactions noticeably contribute to the production of ^{19}F in more massive stars with $M > 20 M_{\odot}$, while they are negligible in lower-mass stars [308]. This is related to the fact that ^{19}F is produced at two different stellar sites: in the C-O layer by the reaction sequence $^{18}\text{O}(p, \alpha)^{15}\text{N}(\alpha, \gamma)$, which is not sensitive to neutrino processes, and in the O-Ne layer by neutrino-induced spallation from the abundant ^{20}Ne . As in lower-mass stars the O-Ne layer is less massive

Table 4: Production factors relative to solar abundances normalized to ^{16}O production. The table shows results from calculations without neutrinos and with neutrinos assuming recent neutrino energy spectra. The highest temperature values correspond to the neutrino spectra adopted in [294].

Nucleus	no ν	$T_{\nu_e} = 2.8 \text{ MeV}$	$T_{\nu_e} = 4.0 \text{ MeV}$
		$T_{\bar{\nu}_e} = 4.0 \text{ MeV}$	$T_{\bar{\nu}_e} = 4.0 \text{ MeV}$
		$T_{\nu_{\mu,\tau}} = 4.0 \text{ MeV}$	$T_{\nu_{\mu,\tau}} = 6.0 \text{ MeV}$
15 M_{\odot} star			
^7Li	0.001	0.28	2.54
^{11}B	0.007	1.43	6.13
^{19}F	1.02	1.14	1.31
^{138}La	0.07	0.67	1.18
^{180}Ta	0.07	1.14	1.81
25 M_{\odot} star			
^7Li	0.0005	0.11	0.55
^{11}B	0.003	0.80	2.61
^{19}F	0.06	0.24	0.43
^{138}La	0.03	0.63	1.14
^{180}Ta	0.14	1.80	2.81

(about $1 M_{\odot}$ in the $15 M_{\odot}$ star) than in more massive stars (about $3 M_{\odot}$ in the $25 M_{\odot}$ star) the relative importance of neutrino-induced reactions for the total ^{19}F abundance depends strongly on the progenitor mass and the stellar evolution.

The studies of Ref. [308] find that neutrino-induced reactions, either directly or indirectly by providing an enhanced abundance of light particles, noticeably contribute to the production of the radioactive nuclides ^{22}Na and ^{26}Al , which are both prime candidates for gamma-ray astronomy. However, the studies do not find significant production of two other candidates, ^{44}Ti and ^{60}Fe , due to neutrino-induced reactions.

The neutrino-induced reactions on ^4He (in the He layer of the star) and on ^{12}C (in the oxygen/carbon layer) initiate a small nuclear network, which produces a few light elements, in particular ^7Li and ^{11}B (see left panel of Fig. 28). The main path for the ^7Li production is by $^4\text{He}(\nu, \nu'p)^3\text{H}(\alpha, \gamma)^7\text{Li}$ and $^4\text{He}(\nu, \nu'n)^3\text{He}(\alpha, \gamma)^7\text{Be}(e^-, \nu_e)^7\text{Li}$, while the ^{11}B production is mainly due to the neutral-current $(\nu, \nu'n)$ and $(\nu, \nu'p)$ reactions on ^{12}C . However, in both cases also charged-current reactions ($^4\text{He}(\nu_e, e^-p)^3\text{He}$ and $^4\text{He}(\nu_e, e^+n)^3\text{H}$ in the case of ^4He , and $^{12}\text{C}(\nu_e, e^-p)^{11}\text{B}$ and $^{12}\text{C}(\nu_e, e^+n)^{11}\text{C}$ for ^{12}C) contribute to the production of ^7Li and ^{11}B , respectively. This makes the abundance of these two nuclides sensitive to neutrino oscillations. Due to the expected hierarchy of average neutrino energies ($\langle E_{\nu_e} \rangle < \langle E_{\nu_x} \rangle$), neutrino oscillations are expected to increase the average ν_e energy and consequently also the charged-current cross section induced by supernova neutrinos. as pointed out by Kajino and collaborators, this makes the ratio of ^7Li and ^{11}B sensitive to the θ_{13} mixing angle and to the mass hierarchy [307, 310, 311] as is demonstrated in the right panel of Fig. 28. Despite this intriguing sensitivity, an accurate derivation of the $^7\text{Li}/^{11}\text{B}$ abundance ratio requires reliable stellar model calculations and neutrino and nuclear cross sections (see [312], but must also consider the production of the elements from other astrophysical sources; ^7Li is, for example, also produced by Big Bang nucleosynthesis [313].

Accounting for neutrino oscillations requires to consider the effect of collective neutrino oscillations. This has been recently done in ref. [97] based on neutrino spectra obtained in Boltzmann transport simulations [314]. Their results show that collective neutrino oscillations increase the average energy

of ν_e neutrinos assuming inverted hierarchy. Hence, the production of ^{138}La and ^{180}Ta , which are both generated by charged-current (ν_e, e^-) reactions, is enhanced. ^7Li and ^{11}B are produced in regions beyond the MSW resonance. Here the situation is different for normal or inverted hierarchy. In the case of normal hierarchy the increased average energy of ν_e neutrinos results in an enhancement of the production of ^7Li by the reaction $^4\text{He}(\nu_e, e^-p)^3\text{He}(\alpha, \gamma)^7\text{Be}(e^+\nu_e)^7\text{Li}$. For the case of inverted hierarchy the production of ^{11}B is enhanced by the reaction chain $^4\text{He}(\bar{\nu}_e, e^+n)^3\text{H}(\alpha, \gamma)^7\text{Li}(\alpha, \gamma)^{11}\text{B}$.

Woosley *et al.* also suggested that some medium-mass nuclei, most notably ^{51}V and ^{55}Mn , might be produced by neutral-current ($\nu, \nu'p$) reactions on ^{52}Fe and ^{56}Ni with subsequent beta decays of the daughters ^{51}Mn and ^{55}Co , respectively [9]. A recent calculation of the nucleosynthesis in a $25 M_\odot$ star, based on the stellar evolution of the star performed by Heger and for the first time taking the full set of neutrino-induced partial cross sections ([218], see above) into account, indeed confirms this suggestion showing that a sizable part of the abundances for ^{51}V , ^{55}Mn and ^{59}Co can be attributed to the ν process [315]. However, the production of these elements occurs close to the supernova core and therefore the amount, which might be ejected, will depend on the matter fallback during the onset of the supernova explosion requiring a more detailed study.

6 Detecting supernova neutrinos

The observation of neutrinos from supernova SN1987A by the earthbound detectors Kamiokande [1] and IMB [316] has confirmed and advanced the understanding of core-collapse supernovae. A similar boost is expected from the observation of the next near-by supernova which is likely to test the predictions of supernova models concerning the neutrino spectra for the different flavors, including the noticeable neutrino burst signal in electron neutrinos, originating from electron capture on protons set free by the shock, and the expected hierarchy in the average neutrino energies between the different flavors ($\langle E_{\nu_e} \rangle < \langle E_{\bar{\nu}_e} \rangle \lesssim \langle E_{\nu_x} \rangle$) reflecting the differences in the interaction of the neutrino flavors with the surrounding matter in the supernova core. To reach this goal, several supernova detectors are operational, with some more being in preparation or proposed.

Obviously translating the event rates of supernova neutrinos observed in the detectors requires a detailed understanding of these detectors, including the knowledge of the cross sections for the neutrino interaction with the detector materials. For a recent overview on the detectors and their scheme for observing supernova neutrinos the reader is referred to Ref. [191]. In accordance with the theme of the present review we will focus in the following on recent advances in describing neutrino-induced cross sections for those nuclei which serve as detector materials in current and future supernova neutrino detectors. Much of the early work on this topic has been described in [18]. We will briefly summarize these studies and discuss in some details the more recent calculations.

Besides neutrino-induced inelastic reactions on nuclei - as we will discuss in the following - supernova neutrinos can also be detected by their interaction with electrons and by elastic scattering on nuclei in the detector. The cross sections for the interaction of supernova neutrinos with electrons is well understood [317], but small. However, it has the advantage that the direction of the neutrino can be reconstructed if the electron track after the scatter can be reconstructed (like in Water Cerenkov detectors or liquid argon time-projection chambers) [191]. Elastic neutrino scattering on nuclei must be detected by the nuclear recoil. This can be a viable scheme for protons [318], but for nuclei the corresponding recoil energies are too small [319, 320, 191]. The cross section for this coherent process is well known and has been discussed above, see eq. (1).

Table 2 in Ref. [191] lists the present and future supernova neutrino detectors. Their main material are liquid scintillator (C_nH_{2n}), water, lead or liquid argon. Hence we will in the following discuss in turn reactions on ^{12}C , ^{16}O , ^{40}Ar and ^{208}Pb . Finally we add some remarks on neutrino-induced reactions for selected molybdenum and cadmium isotopes motivated by the ability of the MOON and COBRA

detectors to potentially also observe supernova neutrinos.

6.1 Carbon

The nucleus ^{12}C is an essential part of liquid scintillator detectors like Borexino, KamLAND, Mini-BooNe, LVD, Baksan. Electron neutrinos and antineutrinos can interact with ^{12}C by charged-current reactions (i.e. $^{12}\text{C}(\nu_e, e^-)^{12}\text{N}$ and $^{12}\text{C}(\bar{\nu}_e, e^+)^{12}\text{B}$), but for the relatively low-energy supernova neutrinos with $\langle E_{\nu_e} \rangle \approx 10$ MeV and $\langle E_{\bar{\nu}_e} \rangle \approx 15$ MeV both reactions are hindered due to the large Q values with 17.34 MeV for ν_e and 14.39 MeV for $\bar{\nu}_e$. The reactions leading to particle-bound states in the final nucleus can be tagged by the beta decays of the ^{12}N and ^{12}B ground states. The matrix element governing the neutrino-induced excitations of either ground state can be readily derived from the experimental value of the beta decay. We note that in RPA calculations of the $^{12}\text{C}(\nu_e, e^-)^{12}\text{N}$ and $^{12}\text{C}(\bar{\nu}_e, e^+)^{12}\text{B}$ inclusive cross sections the ground state transition is adjusted to the beta-decay data. Then the calculated $^{12}\text{C}(\nu_e, e^-)^{12}\text{N}$ cross section for electron neutrinos, produced by muon decay at rest and with somewhat higher energies than supernova ν_e neutrinos, agree quite well with the data from the KARMEN and LSND collaborations (see [18, 321]).

Recently shell model calculations have been performed for charged- and neutral-current neutrino reactions on ^{12}C using two different residual interactions in a $(0+2)\hbar\omega$ model space [306]. Two results of these studies are quite interesting. At first, the B(GT) strength is noticeably reduced if the model space is extended from the pure p shell ($0\hbar\omega$) to the $(0+2)\hbar\omega$ requiring for the latter case nearly no quenching of the GT strength anymore. Furthermore, the various neutrino-induced cross sections agree quite well with those obtained by RPA calculations (e.g. [322]). Shell model calculations performed in model spaces larger than the p shell, but employing different residual interactions than Ref. [306], have also been reported in [126, 127] again showing the importance of correlations beyond the RPA approach to describe the neutrino-induced transitions to the $T = 1$ triad in the $A = 12$ nuclei.

The detectors can observe neutral-current reactions, triggered by all neutrino flavors, by detecting the γ ray following the (ν, ν') excitation of the isospin $T = 1$ state at excitation energy $E_x = 15.11$ MeV. This state is the Isobaric Analog State of the ^{12}B and ^{12}N ground states. The Gamow-Teller matrix element needed to calculate the $^{12}\text{C}(\nu, \nu')^{12}\text{C}(15.11)$ cross section can be derived from the beta-decay of the ^{12}B and ^{12}N ground states after an appropriate isospin rotation or directly from the measured M1 strength between these states determined in inelastic electron scattering.

Due to the high thresholds for all neutrino reactions on ^{12}C the major detection channel is $\bar{\nu}_e$ absorption on free protons for liquid scintillator detectors. The respective event rate is estimated to be about an order of magnitude larger than the charged-current reactions on ^{12}C and about a factor of 5 larger for the neutral-current reactions [323] (although they can be induced by all neutrino flavors).

6.2 Oxygen

The double-magic nucleus ^{16}O is a potential neutrino target in water Cerenkov detectors like Superkamiokande. Like ^{12}C it has very large Q values for charged-current reactions. Furthermore, the closed-shell structure of the ^{16}O ground state strongly suppresses GT transitions (in the IPM limit the GT strength is zero). These two effects strongly reduce the neutrino cross sections on ^{16}O for supernova neutrinos. In fact, charged-current reactions have been estimated to give a negligible event rate in water Cerenkov detectors for galactical supernovae with a distance of 10 kpc or 30000 light years (the distance to the galactical center) [324, 325]. Due to their expected higher average energies ν_x neutrinos might excite the spin dipole resonances in ^{16}O which will then decay by emission of protons or neutrons. If this decay leaves the daughter nucleus, ^{15}N or ^{15}O , in particle-bound excited states (i.e. at excitation energies $E_x < 10.7$ MeV in ^{15}N and $E_x < 7.3$ MeV in ^{15}O) the subsequent γ decay cascade of these excited states might be observable in Superkamiokande, in particular as both daughter nuclei have no

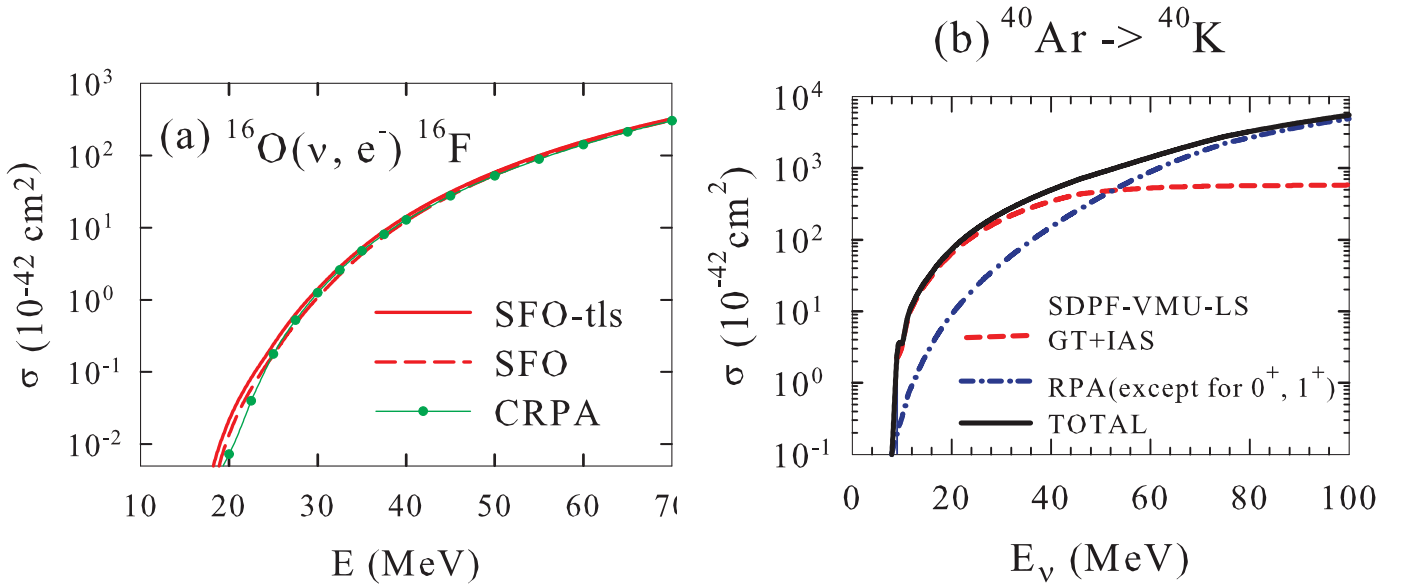


Figure 29: (left) Comparison of (ν_e, e^-) cross sections on ^{16}O calculated in shell model and RPA approaches (from [321]); (right) Contributions to the (ν_e, e^-) cross sections on ^{40}Ar from the IAS and from allowed (calculated in shell model) and forbidden (calculated by RPA) transitions (from [328]).

excited state below 5 MeV. In Ref. [326] this decay scheme has been estimated to yield about 700 events in Superkamiokande for a supernova in the galactical center. However, the estimate has been made for a ν_x Fermi-Dirac neutrino spectrum with temperature $T = 8$ MeV (and zero chemical potential). More modern supernova simulations indicate smaller average energies (temperatures) for ν_x neutrinos, which would noticeably reduce the expected event rate. The main observational channel of supernova ν_x neutrinos in water Cerenkov detectors appears to be coherent elastic scattering on protons [318].

As the Gamow-Teller contribution is very small, the charged- and neutral-current cross sections on ^{16}O are dominated by spin-dipole transitions. These have recently been modelled in a shell model calculation [321] considering the p and sd shells and modifying the residual interaction to account for effects of the tensor force [327]. This calculation finds the major dipole strength for the 2^- channel with excitations around $E_x = 15$ and 22 MeV. As is demonstrated in the left panel of Fig. 29, the calculated shell model $^{16}\text{O}(\nu_e, e^-)^{16}\text{F}$ cross sections agrees very well with results obtained within the Continuum RPA [190] for neutrino energies up to 100 MeV.

6.3 Argon

Liquid argon detectors are large time-projection chambers with a very good energy resolution and full particle track reconstruction [191]. For supernova neutrinos the main goal is to observe ν_e neutrinos from $^{40}\text{Ar}(\nu_e, e^-)^{40}\text{K}^*$ by tagging on the gamma's from the deexcitation of the final states in ^{40}K [191]. A similar detection scheme is possible for the observation of $\bar{\nu}_e$ neutrinos. However, as we will mention below, the respective cross section is reduced due to the suppression of Gamow-Teller distributions. The ICARUS detector is a currently operational liquid argon supernova neutrino detector [329, 330].

The $^{40}\text{Ar}(\nu_e, e^-)^{40}\text{K}$ cross section for supernova neutrinos is dominated by the Fermi contribution to the IAS in ^{40}K at $E_x = 4.38$ MeV and the Gamow-Teller transitions. The first can readily be calculated applying the $(N - Z)$ sum rule for Fermi transitions, while the second is constrained by the recent measurement of the $B(\text{GT}_-)$ strength of ^{40}Ar by a (p, n) charge-exchange experiment [331]. However, it has been found that the GT strengths assigned to transitions to two low-lying states at excitation energies $E_x = 2.289$ MeV and 2.730 MeV is relatively large, hence significantly contributing

to the charged-current cross section, but it is noticeably different than the B(GT) value derived from the β decay of the isospin-analog ^{40}Ti [332]. This difference has been recently investigated in a ($^3\text{He}, t$) experiment, which has determined the relative strength of the two transitions and found a value close to the (p, n) experiment and in clear contrast to the β -decay data (quoted in [333]). A shell model calculation performed in the pf - sd model space has nicely reproduced the B(GT) strength determined in the (p, n) experiment, including the relative transition strengths to the two low-lying states [328]. Recently a shell model calculation, including a residual interaction with consideration of Coulomb contributions, hence breaking isospin symmetry, has explored possible nuclear structure reasons for the differences between the B(GT) values derived from the (p, n) measurement and the ^{40}Ti β decay [333].

The authors of Ref. [333] recommend to use the Gamow-Teller strength determined from the (p, n) experiment to derive the $^{40}\text{Ar}(\nu_e, e^-)^{40}\text{K}$ cross section for supernova neutrinos. This has indirectly been done by Suzuki and Honma, as their shell model Gamow-Teller strength distribution gives a very good account of the one derived from the (p, n) data [328]. The calculation shows that there is additional GT strength outside of the experimental energy window explored by the (p, n) data. While theory and experiment give a B(GT) strength of about 5 units up to excitation energies of 8 MeV in ^{40}K , the calculated total strength is 7.21 units. The recent shell model calculation also gives a better account of the data than obtained in a model space restricted to 2p-excitations from the sd to the pf shell [334]. Based on a hybrid model approach (shell model GT strength distribution, the transition to the IAS from the Fermi sum rule and forbidden transition calculated within the RPA for multiplicities $\lambda = 1-5$ Suzuki and Honma have calculated the $^{40}\text{Ar}(\nu_e, e^-)^{40}\text{K}$ cross section for neutrino energies up to $E_\nu = 100$ MeV (see right panel of Fig. 29). As expected, the cross section is dominated by allowed contributions up to $E_\nu = 50$ MeV, which covers the range of supernova ν_e energies. It is interesting to note that the cross sections obtained within the hybrid model agrees well with calculations where all multipole contributions have been derived within the RPA [18] except at low neutrino energies where the hybrid model cross sections are larger by about 20-40 %. We note again that at low neutrino energies the cross section is sensitive to the detailed GT strength distribution which, in agreement with recent data, is well described by the shell model. Hence the results presented in Ref. [128] should be more reliable than the RPA results of ref. [18]. The neutrino-induced charged-current reactions have also been studied within the Local Density Approximation taking account of Pauli blocking and Fermi motion [335]. The results agree reasonably well with those from the hybrid model and the RPA approach for neutrino energies $E_\nu > 20$ MeV. Cross sections presented on the basis of a QRPA calculation [336] deviate from the values obtained in the hybrid model and the RPA study by about a factor of 3.

In the IPM, the GT_+ strength for ^{40}Ar (with 18 protons and 22 neutrons) vanishes as all GT transitions, in which a proton is changed into a neutron, are Pauli blocked. Cross-shell correlations might introduce a non-vanishing GT_+ strength, but it is expected to be small. Based on this assumption, the $^{40}\text{Ar}(\bar{\nu}_e, e^+)^{40}\text{Cl}$ cross section has been calculated solely within an RPA approach [18]. Due to the missing or highly suppressed allowed contributions, the $(\bar{\nu}_e, e^+)$ cross section on ^{40}Ar is much smaller than the (ν_e, e^-) cross section for supernova neutrino energies [18], making the observation of $\bar{\nu}_e$ neutrinos by liquid argon detectors a challenge. It would be still desirable to put the low energy $(\bar{\nu}_e, e^+)$ cross section on a more reliable basis by calculating the allowed and forbidden transitions to low-lying states within shell model calculations which take cross-shell correlations properly into account. Such studies have been proven to be up to the task in studying the M1 strength in ^{38}Ar [171] or the isotope shift in calcium [170].

6.4 Lead

The Fermi and Ikeda sum rules both scale with neutron excess ($N - Z$). As the charged-current response induced by supernova ν_e neutrinos (with average energies around 12 MeV) are dominated by Fermi and GT transitions, the charged-current cross sections on lead is expected to be significantly larger than

on other materials like iron or carbon. This makes ^{208}Pb an attractive target for supernova neutrino detectors like the HALO detector in Canada [337]. The main detection schemes are the (ν_e, e^-) and (ν_x, ν'_x) reactions where in both cases the final nuclei, ^{208}Bi and ^{208}Pb , respectively are left in excited states which mainly decay by particle emission. Due to the relatively low excitation energies involved and the large Coulomb barriers associated in the proton channel, the particle decay occurs mainly by emission of (one or two) neutrons. In HALO these neutrons can be detected from capture on ^3He , after they have been moderated in polypropylene [337, 191]. Hence the calculation of the partial neutrino-induced neutron spallation cross sections on ^{208}Pb are of relevance to interpret supernova neutrinos detected by HALO.

There have been several evaluations of the (ν_e, e^-) cross sections on ^{208}Pb , which is the dominating isotope of natural lead. Unfortunately the calculation of the allowed contributions to the cross sections within the shell model is yet computationally not feasible. The Fermi contribution to the cross section can be derived from the transition to the known IAS in ^{208}Bi and the Fermi sum rule $B(F) = (N - Z)$. All studies have calculated the contributions from the other multipoles on the basis of RPA variants which reproduce the strength and the position (around $E_x = 15$ MeV in ^{208}Bi) of the Gamow-Teller distribution as well as of the spin-dipole resonances [165, 338, 339]. The $B(\text{GT}_-)$ strength in ^{208}Pb is fixed by the Ikeda sum rule, however, it has been renormalized in Refs. [165, 339] (by $(0.7)^2$ and $(0.8)^2$, respectively) to account for the quenching of the GT strength at low excitation energies, while Ref. [338] used the unquenched g_A value. Despite these differences the calculations give quite similar cross sections (within 20 – 30%) as function of neutrino energy. The results are, however, noticeable smaller (by a factor 3) than those obtained in the first study of the (ν_e, e^-) reaction on ^{208}Pb [340] which is due to the differences in the nuclear model, the treatment of the multipole operator expansion and the Coulomb correction for the electron in the outgoing channel [165, 338]. A QRPA calculation, on top of a Hartree-Fock study with BCS pairing, has been presented in Ref. [160]. The obtained results are about a factor of 2 larger than in Refs. [165, 339] (also for ^{56}Fe), likely caused by the neglect of renormalization of the GT contribution to the cross section. Suzuki and Sagawa presented (ν_e, e^-) cross sections which have been obtained using GT data from a (p, n) experiment performed at Osaka [341] and adjusting their Hartree-Fock + Tamm-Dancoff approach for the first-forbidden response to the peaks of the spin-dipole resonances [342]. Furthermore, the spreading and quenching of the GT response has been considered by coupling to 2p-2h configurations. Although the calculations have been performed assuming a muon-decay-at-rest rather than a supernova neutrino spectrum, and are thus not directly relevant to the present discussion, the result, however, is satisfyingly: Suzuki and Sagawa obtain $(3.2 \times 10^{-39} \text{ cm}^2)$ for the (ν_e, e^-) cross sections [342], in close agreement to the RPA result of Ref. [165] $(3.62 \times 10^{-39} \text{ cm}^2)$.

Jachowicz and co-workers [343, 344] have investigated the influence of different neutrino spectra and of neutrino oscillations on the neutrino signal in lead-based supernova detectors. Total charged-current (ν_e, e^-) cross sections for the chain of lead isotopes for supernova neutrinos, assuming a Fermi-Dirac distribution with temperature $T = 4$ MeV and zero chemical potential, are reported in Refs. [104, 345] based on RPA calculations yielding quite similar cross sections. RPA-based studies have been performed for the neutral-current (ν, ν') cross sections on ^{208}Pb [165, 339]. Again the results agree quite well (within 10-15 %).

It might not be surprising that the RPA studies of Refs. [165, 338, 339] predict similar cross sections, as they are constrained by similar indirect data like the positions and strengths of the leading responses. However, the calculations differ noticeably in their treatment of the quenching of the GT strength. Here a recent measurement of the Gamow-Teller and spin-dipole responses by a (\vec{p}, \vec{n}) charge-exchange reaction with polarized protons and neutrons has determined the GT_- strength up to excitation energies of nearly 50 MeV. The data yield a GT_- strength of about 85 units up to an excitation energy of 25 MeV, which includes the GT resonance at about 15 MeV. This value is significantly smaller than the Ikeda sum rule, $3(N - Z) = 132$, corresponding to a quenching of the low-lying GT_- strength by a factor

of $(0.8)^2$ as assumed in Ref. [339]. Ref. [104] used too strong a quenching, hence the cross sections might be slightly too low, while Ref. [338] did not consider any quenching and might have overestimated the GT contribution to the cross section. The GT and spin-dipole data show another known shortcoming of RPA calculations as they often do not describe the observed fragmentation and spreading of the resonant strength well due to missing correlations. As we have discussed above this is not too relevant for the total cross sections if the neutrino energies are sufficiently large. However, these shortcomings are quite relevant if one wants to describe the neutron spallation cross sections as the GT resonance resides quite closely to the threshold of the $2n$ decay channel which opens at $E_x = 14.98$ MeV. Such studies have been performed for example in Refs. [165, 339] where the latter simply assumes that all states with excitation energies between 100 keV above the $1n$ threshold at $E_x = 6.9$ MeV to 2.2 MeV above the $2n$ threshold decay by emission of one neutron, while states at higher excitation energies decay by multiple neutron emission. Ref. [165] treats the various decay modes of excited states in ^{208}Bi as a cascade of decays followed on the basis of the statistical model. Ref. [165] uses the information from the statistical decays to calculate neutron spectra for various supernova neutrino spectra. These results, however, should be effected by the underestimation of the spreading and fragmentation of the resonant responses (see the discussions in Refs. [165, 18]). These references discuss whether the observation of the neutron count rate in a lead supernova detector might be a suitable tool to study neutrino oscillations as proposed in [340].

6.5 Molybdenium and cadmium

There have been recently several studies of neutral- and charged-current reactions on molybdenium and cadmium isotopes induced by supernova neutrinos. These investigations have been motivated to explore the sensitivity of the Cadmium Zinc Telluride 0-Neutrino Double-Beta Research Apparatus (COBRA) experiment [346] and the Molybdenium Observatory of Neutrinos (MOON) [347] to the observation of supernova neutrinos. The COBRA and MOON detectors are both designed and planned for the detection of neutrino-less double beta decay. If this mode is successfully observed it will establish the Majorana nature of the neutrino and, even more importantly, will establish violation of lepton number conservation (e.g. [348]). The COBRA detector is made out of CdZnTe crystals which serve as both source and detection material. Its potential to detect neutrino-less double beta decay rests mainly on the two nuclides ^{116}Cd and ^{130}Te . The MOON detector is a tracking-calorimeter detector which is highly enriched in ^{100}Mo [349]. Besides searching for neutrino-less double beta decay the MOON detector is also anticipated as solar neutrino detector.

Motivated by the relevance for double-beta decay, GT strength distributions for ^{100}Mo and ^{116}Cd have been determined by charge-exchange reactions. Using a $(^3\text{He}, t)$ experiment at RCNP Thies *et al* showed that the GT_+ strength on ^{100}Mo is basically concentrated in a single transition to the ^{100}Nb ground state [350], likely corresponding to the transformation of a $g_{9/2}$ proton into a $g_{7/2}$ neutron. The GT strength between these two ground states has independently been deduced from the ^{100}Tc electron capture branching ratios, obtained at the IGISOL facility [351]. We note that a similar domination of the GT strength by a single transition (to the 1^+ state at $E_x = 0.69$ MeV) has been observed in the GT_+ strength of ^{96}Mo , deduced by $(d, ^2\text{He})$ and $(^3\text{He}, t)$ charge-exchange experiments. For ^{116}Cd the GT_- strength has been determined recently using the (p, n) reaction [352, 353]. The centroid of the strength associated with the GT resonance is located at an excitation energy around $E_x = 14$ MeV, with some additional strength forming a shoulder in the GT distribution around $E_x = 8$ MeV. The GT_- strength on ^{116}Cd had previously been determined by a $(^3\text{He}, t)$ experiment [354] which turned out, however, to be erroneous due to the use of a natural cadmium target [355]. The GT strength between the ^{116}Cd and ^{116}In ground states has also been determined from the electron capture decay branch of ^{116}In [356] yielding a transition strength in agreement with the value deduced from the (p, n) charge-exchange experiment [353].

The experimental GT strength distributions are valuable constraints for calculations discussing the MOON and COBRA detectors as devices to observe supernova neutrino. A detailed study of neutrino- and antineutrino scattering off ^{116}Cd has recently been reported in Ref. [357] performed within the charge-changing mode of the QRPA. The authors performed detailed studies of the GT₋ strength distribution for several Skyrme interactions supplemented by finite-range (isovector and isoscalar) pairing interactions and compare it to the results obtained with the Bonn one-boson exchange potential. (Similar studies based on the Bonn potential have been previously reported in [358]. These authors adjusted the parameters of the force for each multipole individually.) Only the Bonn potential was found to reproduce the giant GT resonance at 14 MeV and its satellite around 8 MeV, while the calculations performed with the Skyrme forces missed these energies typically by 1-2 MeV [357]. These differences in the position of the strong GT transitions translate into different predictions for the (ν_e, e^-) cross section on ^{116}Cd for supernova neutrinos, which, as calculated in Ref. [357], is dominated by GT transitions. Using the cross section obtained with the Bonn potential as benchmark, the Skyrme interactions yield results which can deviate upto a factor of 2; however, most Skyrme interactions predict cross sections which agree within 50%. For the $(\bar{\nu}_e, e^+)$ cross section on ^{116}Cd for supernova antineutrinos the calculations predict results which agree within a factor of 2 among each other, with the Skyrme forces typically yielding a somewhat larger value than the Bonn interaction. The largest contribution to the cross sections arises from first-forbidden transitions to the $J = 1^-$ states in ^{116}Ag . The partial cross sections reported in Ref. [358] for the (differently parametrized) Bonn potential are very similar, except for the contribution of the $J = 0^+$ multipole to the (ν_e, e^-) cross section which is noticeably larger in the study of [358] than found in Ref. [357], in particular compared to the results for the Skyrme interactions.

The formalism of charge-changing QRPA has also been adopted to calculate the cross sections for neutral-current reactions on stable cadmium and molybdenum isotopes induced by supernova neutrinos of all flavor. For the cadmium isotopes the inelastic cross sections for supernova ν_e neutrinos are dominated by the contributions from the $J = 1^+$ multipole (GT₀ strength) [359]. For the odd-A isotopes $^{111,113}\text{Cd}$ Almosly *et al.* find a surprisingly large vector contribution to excited $J = 0^+$ states [359].

Also the calculation of neutral-current reactions on the stable molybdenum isotopes show a somewhat larger cross sections for the odd-A nuclei $^{95,97}\text{Mo}$ compared to their even-even neighbor isotopes [360]. The difference amounts to about 40% for neutrinos with energies typical for supernova ν_e 's and decreases with neutrino energy. The neutral-current response of supernova neutrinos on odd-A and even-even molybdenum isotopes has also been studied in Refs. [361, 362]. Interestingly the authors find a relatively large contribution of vector transitions to excited 0^+ states for the odd isotopes $^{95,97}\text{Mo}$ [361], which is less pronounced for the even-even isotopes [362]. The charged-current reactions on the odd isotopes $^{95,97}\text{Mo}$ for supernova neutrinos has been explored in Ref. [363]. The authors find the (ν_e, e^-) cross section dominated by allowed Fermi (to the IAS) and GT transitions, while the $(\bar{\nu}_e, e^+)$ cross section has some forbidden contributions arising from 1^- and 2^- multipoles, besides the dominating GT contribution.

Engel *et al.* [364] have studied the charged-current cross sections on ^{100}Mo , replacing in the dominating 1^+ channel the QRPA results with the GT strength measured by the $(^3\text{He}, t)$ charge-exchange reaction [354]. These authors discuss how the MOON detector might distinguish between charged- and neutral-current events, assuming that neutral-current reactions will excite the molybdenum isotopes to states which mainly decay by emitting neutrons and successive γ -rays [364]. Hence it appears useful if the studies reported in Refs. [361, 362] would be extended to calculations of the partial cross sections with particle emission in the final channel.

7 Summary

Neutrinos have been identified as one of the essential players in core-collapse supernovae. This insight - predicted by models - has been unambiguously verified by the observations from supernova SN1987A. The undisputably most important role of neutrinos for the supernova dynamics concerns the energy balance: due to their tiny cross sections with the surrounding matter neutrino emission efficiently cools the inner core of the collapsing core and, after bounce, carries away an overwhelmingly large portion of the gravitational binding energy released in the explosion. Even despite the tiny cross sections, the tremendously large number of neutrinos involved makes them an important means of energy transport during the explosion, reviving the stalled shock front.

Neutrinos also play a crucial role for the explosive supernova nucleosynthesis as their interaction with the hot matter surrounding the protoneutron star (mainly free nucleons, but also light nuclear clusters) determines the ratio of protons and neutrons available for synthesis of heavier nuclei in the νp process or potentially the r-process. While (anti)neutrino absorption on protons is at the very heart of the νp process, the role of neutrinos during the mass flow to heavy nuclides in the astrophysical r-process (if it occurs in the core-collapse supernova environment) is likely to be small. However, particle spallation induced by neutrino reactions on abundant nuclei in the outer layers of the star has been identified as the synthesis mechanism of selected isotopes like ^{11}B , ^{138}La and ^{180}Ta in a process called neutrino nucleosynthesis.

In several of these aspects of supernova dynamics and nucleosynthesis, neutrinos interact with free nucleons. The respective cross sections are well defined based on the framework of the electroweak theory. However, in the dense and hot supernova environment these interactions are modified by correlations which is a topic of ongoing research interest. Neutrino interactions with nuclei can occur during collapse as well as after bounce during the various nucleosynthesis processes. During collapse, an important neutrino process is coherent scattering on nuclei which leads to neutrino trapping in the final phase of the collapse. Except for small corrections induced by isospin breaking and additional Gamow-Teller contributions (at finite temperature and for odd- A and odd-odd nuclei), the coherent cross sections are determined by the Fermi transition to the Isobaric Analog State and hence well under control. Other neutrino processes during collapse include absorption on nuclei and inelastic neutrino scattering with nuclei. As electron capture on nuclei is the other very relevant weak-interaction process during collapse, mainly ν_e neutrinos are present in the core. They can be absorbed on neutrons in nuclei. As this is the inverse reaction of electron capture, the respective cross section is derived applying the principle of detailed balance. Hence, its accuracy has benefitted from the improved description of electron capture on nuclei made possible in recent years by more precise data from advanced charge-exchange experiments and from progress in nuclear modelling, mainly due to the application of shell model techniques.

The shell model has also been the many-body technique which has been applied in the first derivation of inelastic neutrino-nucleus scattering cross sections at finite supernova temperatures. The calculations have been validated against precision data derived from inelastic electron scattering. As these are taken for nuclear ground states only, the validation is restricted to cross sections at temperature $T = 0$. However, neutrino-induced deexcitation of nuclear states, thermally populated at finite temperatures, are found to strongly increase the inelastic cross sections at low neutrino energies. Although the shell model is expected to describe also the (Gamow-Teller) transitions on excited states adequately well, a full state-by-state summation to obtain the inelastic cross section at supernova temperatures is computationally unfeasible and some approximation has to be applied. However, it has been quite gratifying that calculations performed within the Thermal QRPA approach confirmed the strong increase of the cross sections at low neutrino energies at finite temperature. This method derives the cross sections consistently from a thermal ensemble and accounts for effects induced by the melting of nucleon pairs at finite temperature. It is important that both approaches - the TQRPA and the shell model - predict

very similar cross sections at higher neutrino energies as supernova simulations have indicated that inelastic scattering of such high-energy neutrinos off nuclei leads to down-scattering of the neutrinos and hence strongly reduces the tail of the neutrino spectra produced in the neutrino-burst just after bounce. As a consequence, this change in spectra reduces the expected event rates for the future observation of neutrinos from the burst phase by supernova neutrino detectors. Inelastic neutrino-nucleus scattering is also a mean of energy exchange between neutrinos and matter during collapse. But simulations have indicated that this process only adds rather mildly to neutrino thermalization, which is dominated by inelastic neutrino scattering on electrons.

Neutrino types other than electron neutrinos are produced during infall by deexcitation of thermally populated nuclear states by neutrino-pair emission. However, for the supernova dynamics this process has been recently shown as unimportant as the cross section for ν_e production by electron capture is several orders of magnitude larger and dominates the energy balance of the core during collapse. This finding is based on a reasonable, but quite schematic description of the neutrino-pair deexcitation process, but is unlikely to change if more accurate cross sections, for example derived on the basis of the Thermal QRPA model, become available.

Neutrino-induced reactions have been proposed to play roles in various supernova nucleosynthesis processes; e.g. in the νp and r-process nucleosynthesis and obviously in the process called neutrino nucleosynthesis. To allow for systematic and detailed investigations into the importance of neutrino-nucleus reactions for these various processes, a global set of partial differential cross sections for neutrino-induced charged- and neutral-current reactions on nuclei (up to charge number $Z = 78$) has been derived. Based on the observation that for the moderate supernova neutrino energies the initial neutrino-nucleus excitation function is dominated by the contributions of giant resonances, the calculation of the respective cross sections has been performed within the Random Phase Approximation, which is constructed to give a fair account of the energy and the total transition strength of these collective resonances. In these initial processes the neutrino excites the nucleus to levels which subsequently decay by particle or γ emission. The decay of the excited nuclear levels is followed within the Statistical Model considering a cascade of multi-particle decays.

Inserting these neutrino-nucleus cross sections into supernova nucleosynthesis simulations indicates that neutrino reactions on nuclei have only limited impact on the calculated abundances. For the νp process $\bar{\nu}_e$ absorption on protons bound in nuclei can in principle compete with the absorption on free protons, but is kinematically suppressed due to the relatively large Q values of the neutron-deficient nuclei encountered in the νp process mass flow. Current supernova simulations indicate only a ‘weak r-process’ which produces nuclides up to the second r-process peak (mass numbers $A < 130$). In this scenario neutrino-nucleus reactions are found unimportant. Uncertainties related to supernovae as r-process sites are introduced due to the yet insufficiently understood roles of collective neutrino oscillations and of sterile neutrinos as well as to the undetermined mass hierarchy of neutrinos.

More than two decades ago, neutrino-induced spallation of abundant nuclei in the outer layers of a supernova has been identified as a major nucleosynthesis source of selected nuclides. This finding has been confirmed over the years using improved stellar models, more accurate neutrino-nucleus cross sections and, last, but not least, refined spectra for the various types of supernova neutrinos. Although the predictions for these spectra shifted systematically to lower average energies (or temperatures if one describes the spectra as usual by a Fermi-Dirac distribution with zero chemical potential) stellar models still imply that the nuclides ${}^7\text{Li}$, ${}^{11}\text{B}$, ${}^{138}\text{La}$ and ${}^{180}\text{Ta}$ are produced by neutrino nucleosynthesis nearly in solar abundances. As ${}^{11}\text{B}$ is the product of neutral-current reactions on ${}^{12}\text{C}$ induced by ν_μ and ν_τ neutrinos and their anti-particles and ${}^{138}\text{La}$ and ${}^{180}\text{Ta}$ are made by (ν_e, e^-) reactions on ${}^{138}\text{Ba}$ and ${}^{180}\text{Hf}$, respectively, neutrino nucleosynthesis can serve as a thermometer for the spectra of those neutrino types, which have not been observed from supernova SN1987A.

The observation of neutrinos from a future close-by supernova, preferably from our galaxy, is the ultimate goal of the various neutrino detectors either operational or under construction. If the supernova

is indeed close enough, e.g. from the galactic center, these detectors have the ability to test the hierarchy of neutrino energies predicted by supernova models. Furthermore they will have the time resolution to probe the evolution of neutrino luminosities during collapse and explosion, including the prominent burst of electron neutrinos expected just after bounce when heavy nuclei are dissociated into free nucleons and the electrons, which have survived the collapse, are captured on free protons. To translate the observed neutrino event rates from a supernova requires the knowledge of the respective neutrino-induced reactions on the detector nuclei. These cross sections have been derived on the basis of nuclear models currently available to treat the related many-body problem. Hence for lead or cadmium targets only cross sections calculated within the frame work of the RPA are available, while for lighter target nuclei more sophisticated nuclear models have been applied. As a consequence for the lighter nuclei a more accurate description of the detailed nuclear response has been considered than for the heavier nuclei, which is of relevance if particle decays of levels in the daughter nucleus might serve as detection scheme. Furthermore some more fundamental questions like the quenching of higher multipoles, in relation to the one established for shell model calculations of the Gamow-Teller strength when compared to data, or the role of two-body currents has to be resolved.

Even if a few questions concerning the role of neutrino-induced reactions on nuclei for the supernova dynamics and nucleosynthesis remain insufficiently answered, the field has witnessed significant progress in recent years. The decisive push in this field in specific, and, of course, to our general understanding of supernovae globally would come from the observation of a nearby supernova by γ 's, neutrinos and the composition of the ejecta. Perhaps Nature is so kind and we do not have to wait for too long. The observers are ready.

Acknowledgments

The research presented in this review has strongly benefited from collaborations with A. Arcones, A. Bauswein, E. Caurier, T. Fischer, C. Fröhlich, A. Heger, L. Huther, H.-Th. Janka, A. Juodagalvis, E. Kolbe, M. Liebendörfer, B. Müller, J. J. Mendoza-Temis, P. von Neumann-Cosel, F. Nowacki, Y.-Z. Qian, A. Richter, K. Sieja, A. Sieverding, F.-K. Thielemann, P. Vogel, S. E. Woosley, M.-R. Wu, and Q. Zhi. This work was partly supported by the Deutsche Forschungsgemeinschaft through contract SFB 634, the Helmholtz International Center for FAIR within the framework of the LOEWE program launched by the state of Hesse, and the Helmholtz Association through the Nuclear Astrophysics Virtual Institute (VH-VI-417).

References

- [1] K. Hirata, T. Kajita, M. Koshiba, M. Nakahata, Y. Oyama, *Phys. Rev. Lett.* **58** (1987) 1490.
- [2] M. Koshiba, *Phys. Repts.* **220** (1992) 229.
- [3] H.A. Bethe, *Rev. Mod. Phys.* **62** (1990) 801
- [4] I. R. Seitenzahl, F. X. Timmes, G. Magkotsios, *Astrophys. J.* **792** (2014) 10.
- [5] K. Langanke, G. Martínez-Pinedo, B. Mller, H.-T. Janka, A. Marek, W. Hix, A. Juodagalvis, and J. Sampaio, *Phys. Rev. Lett.* **100** (2008) 1.
- [6] H.-T. Janka, *Annu. Rev. Nucl. Part. Sci.* **62**, 407 (2012).
- [7] A. Burrows, *Rev. Mod. Phys.* **85** (2013) 245.

- [8] G. Martínez-Pinedo, T. Fischer, and L. Huther, *J. Phys. G Nucl. Part. Phys.* **41**, 044008 (2014).
- [9] S.E. Woosley *et al.*, *Astrophys. J.* **356** (1990) 272
- [10] C. Gaarde *et al.*, *Nucl. Phys.* **A369** (1981) 258
- [11] I. Daito *et al.*, *Phys. Lett.* **B418** (1998) 27
- [12] R.G.T. Zegers *et al.*, *Phys. Rev.* **C74** (2006) 024309
- [13] M.C. Vetterli *et al.*, *Phys. Rev.* **C45** (1992) 997
- [14] D. Frekers, *Prog. Part. Nucl. Phys.* **57** (2006) 217
- [15] A. L. Cole, *et al.*, *Phys. Rev. C* **74** (2006) 034333.
- [16] J.G. Learned and K. Mannheim, *Ann. Rev. Nucl. Part. Sc.* **50** (2000) 679
- [17] J.K. Becker, *Phys. Rep.* **458** (2008) 173
- [18] E. Kolbe, K. Langanke, G. Martinez-Pinedo and P. Vogel, *J. Phys.* **G29** (2003) 1
- [19] E.M. Burbidge, G.R. Burbidge, W.A. Fowler and F. Hoyle, *Rev. Mod. Phys.* **29** (1957) 547
- [20] G. Wallerstein *et al.*, *Rev. Mod. Phys.* **69** (1997) 995
- [21] K. Langanke and M. Wiescher, *Rep. Prog. Phys.* **64** (2001) 1657
- [22] E.G. Adelberger *et al.* 1998, *Rev. Mod. Phys.* **70** 1265
- [23] E.G. Adelberger *et al.* 2011, *Rev. Mod. Phys.* **83** 195
- [24] H.A. Bethe, G.E. Brown, J. Applegate and J.M. Lattimer, *Nucl. Phys.* **A324** (1979) 487
- [25] A. Heger, K. Langanke, G. Martínez-Pinedo, and S. E. Woosley, *Phys. Rev. Lett.* **86** (2001) 1678.
- [26] A. Heger, S. E. Woosley, G. Martínez-Pinedo, and K. Langanke, *Astrophys. J.* **560** (2001) 307.
- [27] K. Langanke and G. Martínez-Pinedo, *Nucl. Phys. A* **673** (2000) 481
- [28] A. Juodagalvis, K. Langanke, W. R. Hix, G. Martínez-Pinedo, and J. M. Sampaio, *Nucl. Phys. A* **848** (2010) 454.
- [29] E. Caurier, K. Langanke, G. Martínez-Pinedo and F. Nowacki, *Nucl. Phys. A* **653** (1999) 439
- [30] K. Langanke, G. Martínez-Pinedo, *At. Data. Nucl. Data Tables* **79** (2001) 1.
- [31] E. Caurier, G. Martinez-Pinedo, F. Nowacki, A. Poves, A.P. Zuker, *Rev. Mod. Phys.* **77** (2005) 427
- [32] C.W. Johnson, S.E. Koonin, G.H. Lang and W.E. Ormand, *Phys. Rev. Lett.* **69** (1992) 3157
- [33] S.E. Koonin, D.J. Dean and K. Langanke, *Phys. Rep.* **278** (1997) 2
- [34] S. W. Bruenn, *Astrophys. J. Suppl.* **58** (1985) 771.
- [35] K. Langanke, *et al.*, *Phys. Rev. Lett.* **90** (2003) 241102.

- [36] R.W. Hix *et al.* Phys. Rev. Lett. **91** (2003) 210102
- [37] H.-T. Janka, K. Langanke, A. Marek, G. Martínez-Pinedo, B. Müller, Phys. Repts. **442** (2007) 38.
- [38] E.W. Grewe *et al.*, Phys. Rev. C **78** (2008) 044301
- [39] B.P. Kay *et al.*, Phys. Rev. C **79** (2009) 021301
- [40] Q. Zhi, K. Langanke, G. Martínez-Pinedo, F. Nowacki, and K. Sieja, Nucl. Phys. A **859** (2011) 172.
- [41] G.M. Fuller, W.A. Fowler and M.J. Newman, ApJS **42** (1980) 447
- [42] G.M. Fuller, W.A. Fowler and M.J. Newman, ApJS **48** (1982) 279
- [43] G.M. Fuller, W.A. Fowler and M.J. Newman, ApJ **252** (1982) 715
- [44] G.M. Fuller, W.A. Fowler and M.J. Newman, ApJ **293**
- [45] G. Martínez-Pinedo, M. Liebendörfer, D. Frekers, Nucl. Phys. A **777** (2006) 395.
- [46] P.Goldreich and S.V. Weber, Astrophys. J. **238** (1980) 991
- [47] A. Burrows, Annu. Rev. Nucl. Part. Sci. **40** (1990) 181.
- [48] A. Burrows, Astrophys. J. **334** (1988) 891.
- [49] H. A. Bethe, J. R. Wilson, Astrophys. J. **295** (1985) 14.
- [50] R. Buras, M. Rampp, H.-Th. Janka and K. Kifonidis, Phys. Rev. Lett. **90** (2003) 241101
- [51] H.Th. Janka and M. Rampp, Astrophys. J. **539** (2000) L33
- [52] A. Mezzacappa *et al.*, Phys. Rev. Lett. **86** (2001) 1935
- [53] T.D. Brandt, A. Burrows, C.D. Ott and E. Livne, Astrophys. J. **728** (2011) 8
- [54] M. Herant, W. Benz, W.R. Hix, C.L. Fryer, S.A. Colgate, Astro. J. **435** (1994) 339
- [55] B. Müller, H.-T. Janka and A. Marek, Astrophys. J. **756** (2012) 84
- [56] J. Nordhaus, A. Burrows, A. Almgren and J. Bell, Astrophys. J. **720** (2010) 694
- [57] C.L. Fryer and M.S. Warren, Astrophys. J. **574** (2002) L65
- [58] A. Takiwaki, K. Kotake and Y. Suwa, Astrophys. J. **749** (2012) 98
- [59] F. Hanke, A. Marek, B. Müller and H.-T. Janka, Astrophys. J. **755** (2012) 138
- [60] A. Burrows, J.C. Dolence and J.W. Murphy, Astrophys. J. **759** (2012) 5
- [61] C.D. Ott *et al.*, Astrophys. J. **768** (2013) 115
- [62] A. Burrows, J. Hayes and B.A. Fryxell, Astrophys. J. **450** (1995) 830
- [63] C.L. Fryer, Astrophys. J. **522** (1999) 413

- [64] C.L.Fryer and M.S. Warren, *Astrophys. J.* **601** (2004) 391
- [65] J.M. Blondin, A. Mezzacappa and C. DeMarino, *Astrophys. J.* **584** (2003) 971
- [66] L. Scheck, T. Plewa, H.-Th. Janka, K. Kifonidis and E. Müller, *Phys. Rev. Lett.* **92** (2004) 011103
- [67] L. Scheck, K. Kifonidis, H.-Th. Janka and E. Müller, *Astron. Astrophys.* **457** (2006) 963
- [68] A. Burrows *et al.*, *Astrophys. J.* **640** (2006) 878
- [69] L. Scheck, H.-T. Janka, T. Foglizzo and K. Kifonidis, *Astron. Astrophys.* **477** (2008) 931
- [70] T. Foglizzo, F. Masset, J. Guilet and G. Durand, *Phys. Rev. Lett.* **108** (2012) 051103
- [71] J.M. Lattimer and F.D. Swesty, *Nucl. Phys.* **A535** (1991) 331
- [72] H. Shen, H. Toki, K. Oyamatsu and K. Sumiyoshi, *Nucl. Phys.* **A637** (1998) 435
- [73] W. Hillebrandt, R.G. Wolff and K. Nomoto, *Astron. Astrophys.* **133** (1984) 175
- [74] M. Hempel, J. Schaffner-Bielich, *Nucl. Phys. A* **837** (2010) 210.
- [75] A. W. Steiner, M. Hempel, T. Fischer, *Astrophys. J.* **774** (2013) 17.
- [76] Y. Suwa, T. Takiwaki, K. Kotake, T. Fischer, M. Liebendörfer, K. Sato, *Astrophys. J.* **764** (2013) 99.
- [77] T. Fischer, M. Hempel, I. Sagert, Y. Suwa, J. Schaffner-Bielich, *Eur. Phys. J. A* **50** (2014) 46.
- [78] M. Voskresenskaya and S. Typel, *Nucl. Phys.* **A887** (2012) 42
- [79] I. Sagert *et al.*, *Phys. Rev. Lett.* **102** (2009) 081101
- [80] T. Fischer, *et al.*, *Astrophys. J. Suppl.* **194** (2011) (2) 39.
- [81] A. Burrows, S. Reddy, T. A. Thompson, *Nucl. Phys. A* **777** (2006) 356.
- [82] C.J. Horowitz, *Phys. Rev.* **D55** (1997) 4577
- [83] S.W. Bruenn and A. Mezzacappa, *Phys. Rev.* **D56** (1997) 7529
- [84] A. Marek, H.-Th. Janka, R. Buras, M. Liebendörfer and M. Rampp, *Astron. Astrophys.* **443** (2005) 201
- [85] S. Bacca, K. Hally, C.J. Pethick and A. Schwenk, *Phys. Rev.* **C80** (2009) 032802
- [86] S. Bacca, K. Hally, M. Liebendörfer, A. Perego, C.J. Pethick and A. Schwenk, *Astrophys. J.* **758** (2012) 34
- [87] S. Hannestad and G. Raffelt, *Astrophys. J.* **507** (1998) 339
- [88] R. Buras, H.-Th. Janka, M. Keil, G. Raffelt and M. Rampp, *Astrophys. J.* **587** (2003) 320
- [89] M. Rampp and H.-Th. Janka, *Astron. Astrophys.* **396** (2002) 361
- [90] R. Buras, M. Rampp, H.-Th. Janka and K. Kifonidis, *Astron. Astrophys.* **447** (2006) 1049
- [91] T. Fischer, G. Martínez-Pinedo, M. Hempel, M. Liebendörfer, *Phys. Rev. D* **85** (2012) 083003.

- [92] A.S. Dighe and A. Yu. Smirnov, Phys. Rev. D **62** (2000) 033007
- [93] H. Duan, G.M. Fuller and Y.-Z. Qian, Ann. Rev. Nucl. Part. Sci. **60** (2010) 569
- [94] B. Dasgupta, A. Dighe, G.G. Raffelt and A. Yu. Smirnov, Phys. Rev. Lett. **103** (2009) 051105
- [95] H. Duan and A. Friedland, Phys. Rev. Lett. **106** (2011) 091101
- [96] M.-R. Wu and Y.-Z. Qian, Phys. Rev. D **84** (2011) 045009
- [97] M.-R. Wu, Y.-Z. Qian, G. Martínez-Pinedo, T. Fischer, L. Huther, Phys. Rev. D **91** (2015) 065016.
- [98] J.D. Walecka, Semi-leptonic weak interactions in nuclei, in Muon, physics, eds. V.W. Hughes and C.S. Wu (Academic Press, New York).
- [99] J.S. Connell, T.W. Donnelly and J.D. Walecka, Phys. Rev. C **6** (1972) 719
- [100] W.C. Haxton, G.J. Stephenson, Jr. and D. Strottman, Phys. Rev. D **25** (1982) 2360
- [101] H. Behrens, W. Bühring, *Electron Radial Wave Functions and Nuclear Beta-decay* (Clarendon, Oxford, 1982).
- [102] J. Engel *et al.*, Phys. Rev. D **48** (1993) 3048
- [103] J. Engel, Phys. Rev. **C57** (1998) 2004
- [104] K. Langanke and E. Kolbe, ATom. Data Nucl. Data Tables, **79** (2001) 293
- [105] K. Langanke and E. Kolbe, ATom. Data Nucl. Data Tables, **82** (2002) 191
- [106] Y.-Z. Qian, Astrophys. J. **569** (2002) L103
- [107] E. Kolbe, K. Langanke and G.M. Fuller, Phys. Rev. Lett. **92** (2004) 2569
- [108] J.J. Cowan, F.-K. Thiememann and J.W. Truran, Pys. Rep. 208 (1991) 267
- [109] T. Rauscher, Int. J. Mod. Phys. **E20** (2011) 1071
- [110] A.J. Koning and D. Rochman, Nucl. data sheets **113** (2012) 2841
- [111] A. Kelic, M.V. Ricciardi and K.-H. Schmidt, ABLA07 - towards a complete description of the decay channels of a nuclear system from spontaneous fission to multifragmentation. Technic Report, GSI Helmholtzzentrum für Schwerionenforschung, Darmstadt, 2010, arXiv:0906.4193 [nucl-th]
- [112] F. Weisskopf, Phys. Rev. **52** (1937) 295
- [113] B. Jurado, K.-H. Schmidt and J. Benlliure, Phys. Lett. **B533** (2003) 186
- [114] A. R. Junghans, M. de Jong, H.-G. Clers, A. V. Ignatyuk, G. A. Kudyaev and K.-H. Schmidt, Nucl. Phys. **A629** (1998) 635
- [115] K.-H. Schmidt, H. Delagrange, J. P. Dufour, N. Carjan, A. Fleury, Z. Phys. **A308** (1982) 215
- [116] A.V. Ignatyuk, G.N. Smirenkin and A.S. Tishin, Sov. J. Nucl. Phys. **21** (1975) 255
- [117] A.J. Sierk, Phys. Rev. **C33** (1986) 2039

- [118] J. Benlliure, A. Grewe, M. de Jong, K.-H. Schmidt and S. Zhdanov, Nucl. Phys. **A628** (1998) 458
- [119] N. Paar, D. Vretenar, T. Marketin and P. Ring, Phys. Rev. C **77** (2008) 024608
- [120] I.S. Towner and J.C. Hardy, in: W.C. Haxton, E.M. Henley (Eds), *Symmetries and Fundamental Interactions in Nuclei* (World Scientific, Singapore, 1995) p. 183
- [121] A.R. Edmonds, *Angular Momentum in Quantum Mechanics* (Princeton University Press, Princeton (New Jersey), 1960)
- [122] F. Osterfeld, Rev. Mod. Phys. **64** (1992) 491
- [123] B.A. Brown and B.H. Wildenthal, Ann. Rev. Nucl. Part. Sci. **38** (1988) 29
- [124] K. Langanke *et al.*, Phys. Rev. **C52** (1995) 718
- [125] G. Martinez-Pinedo, A. Poves, E. Caurier and A.P. Zuker, Phys. Rev. **C55** (1997) 187
- [126] A.C. Hayes and I.S. Towner, Phys. Rev. C **61** (2000) 044603
- [127] C. Volpe *et al.*, Phys. Rev. C **62** (2000) 015501
- [128] T. Suzuki and T. Kajino, J. Phys. G Nucl. Part. Phys. **40** (2013) 083101
- [129] J. Sampaio, K. Langanke, G. Martinez-Pinedo and D.J. Dean, Phys. Lett. B **529** (2002) 19
- [130] A. Juodagalvis *et al.*, Nucl. Phys. A **747** (2005) 87
- [131] W. Misch, B.A. Brown and G.M. Fuller, Phys. Rev. C **90** (2014) 065808.
- [132] P.B. Radha *et al.*, Phys. Rev. C **56** (1997) 3079
- [133] A. Dzhioev, A. Vdovin, V. Ponomarev and J. Wambach, Phys. At. Nucl. **74** (2011) 1162
- [134] A.A. Dzhioev, A.I. Volovin, J. Wambach and V. Yu. Ponomarev, Phys. Rev. C **89** (2014) 035805
- [135] V. Gudkov and K. Kubodera, J. Phys. G: Nucl. Part. Phys. **29**, 2597 (2003)
- [136] L.E. Marcucci, K.M. Nollett, R. Schiavilla and R.B. Wiringa, Nucl. Phys. **A777** (2006) 111
- [137] P. Vogel, Proceedings of *Nucleosynthesis - Making the Elements in the Universe* (432. WE-Heraeus Seminar, Bad Honnef, 2009): <http://www.theory.gsi.de/Heraeus-432/Talks/Vogel.pdf>
- [138] R. Schiavilla *et al.*, Phys. Rev. C **58** (1998) 1263
- [139] P. Butler, J.W. Chen and P. Vogel, Phys. Lett. B **549** (2002) 26
- [140] J.W. Chen, K.M. Heeger and R.G.H. Robertson, Phys. Rev. **C67** (2003) 025801
- [141] K.I.T. Brown, M.N. Butler and D.B. Guenther, nucl-th/0207008
- [142] S. Nakamura, T. Sato, V. Gudkov, and K. Kubodera, Phys. Rev. C **63**, 1 (2001).
- [143] G. Drexlin *et al.*, Phys. Lett. **B267** (1991) 321
- [144] B. Zeitnitz *et al.*, Prog. Part. Nucl. Phys. **32** (1994) 351

- [145] M. Albert *et al.*, Phys. Rev. **C51** (1995) 1065
- [146] C. Athanassopoulos *et al.*, Phys. Rev. **C55** (1997) 2078; Phys. Rev. **C56** (1997) 2806
- [147] , R. Imlay, Nucl. Phys. **A629** (1998) 531c
- [148] R. Maschuw, Prog. Part. Nucl. Phys. **40** (1998) 183
- [149] E. Kolbe, K. Langanke and G. Martinez-Pinedo, Phys. Rev. **C60** (1999) 052801(R)
- [150] E. Kolbe, K. Langanke and S. Krewald, Phys. Rev. **C49** (1994) 1122
- [151] E. Kolbe, K. Langanke and P. Vogel, Nucl. Phys. **A652** (1999) 91
- [152] A.C. Hayes, P. Navratil and J.P. Vary, Phys. Rev. Lett. **91** (2003) 012502
- [153] P. Navratil, V.G. Gueorguiez, J.P. Vary, W.E. Ormand and A. Nogga, Phys. Rev. Lett. **99** (2007) 042501
- [154] P. Maris, J.P. Vary, A. Calci, J. Langhammer, S. Binder and R. Roth, Phys. Rev. C **90** (2014) 014314
- [155] T. Otsuka *et al.*, Phys. Rev. Lett. **104** (2010) 012501
- [156] N.T. Zinner, K. Langanke and P. Vogel, Phys. Rev. **C74** (2006) 024326
- [157] T. Marketin, N. Paar, T. Niksic and D. Vretenar, Phys. Rev. **C79** (2009) 054323
- [158] A.R. Samana and C.A. Bertulani, Phys. Rev. **C78** (2008) 024312
- [159] M.S. Athar, A. Ahmad and S.K. Singh, Nucl. Phys. **A764** (2006) 551
- [160] R. Lazauskas and C. Volpe, Nucl. Phys. **A792** (2007) 219
- [161] J. Rapaport *et al.*, Nucl. Phys. **A410** (1983) 371
- [162] H. Fujita *et al.*, OULNS Annual Report, Osaka University (2006) 91
- [163] Y. Fujita, B. Rubio and W. Gelletly, Prog. Part. Nucl. Phys. **66** (2011) 549
- [164] N. Paar, T. Suzuki, M. Honma, T. Marketin and D. Vretenar, Phys. Rev. C **84** (2011) 047305
- [165] E. Kolbe and K. Langanke, Phys. Rev. **C63** (2001) 025802
- [166] T. Rönning *et al.*, Nucl. Phys. **A563** (1993) 225
- [167] S. El-Kateb *et al.*, Phys. Rev. **C49** (1994) 3128
- [168] M. Scott *et al.*, Phys. Rev. C **90** (2014) 025801
- [169] A.L. Cole *et al.*, Phys. Rev. C **86** (2012) 015809
- [170] E. Caurier *et al.*, Phys. Lett. **B522** (2001) 240
- [171] A.F. Lisetzky *et al.*, Nucl. Phys. **A789** (2007) 114
- [172] L.B. Auerbach *et al.*, Phys. Rev. **C64** (2001) 065501

- [173] A. Richter, Progress in Particle and Nuclear Physics **44** (2000) 3 .
- [174] P.J. Mohr and B.N. Taylor, Rev. Mod. Phys. **72** (2000) 351
- [175] P. von Neumann-Cosel, A. Poves, J. Retamosa, A. Richter, Phys. Lett. B **443** (1998) 1.
- [176] T. Guhr *et al.*, Z. Phys. **A336** (1990) 159
- [177] J. Enders *et al.*, Phys. Rev. **C59** (1999) R1851
- [178] D. Bohle *et al.*, Phys. Lett. **B137** (1984) 27
- [179] R.W. Fearick *et al.*, Nucl. Phys. **A727** (2003) 41
- [180] K. Langanke, G. Martinez-Pinedo, P. von Neumann-Cosel and A. Richter, Phys. Rev. Lett. **93** (2004) 202501
- [181] V. Chasioti, T.S. Kosmas and P. Divari, Prog. Part. Nucl. Phys. **59** (2007) 481
- [182] H. Dapo and N. Paar, Phys. Rev. **C86** (2012) 035804
- [183] W.C. Haxton, Phys. Rev.Lett. **60** (1988) 1999
- [184] S.W. Bruenn and W.C. Haxton, Astrophys. J. **376** (1991) 678
- [185] J. Toivanen *et al.*, Nucl. Phys. **A694** (2001) 395
- [186] S.E. Woosley, A. Heger and T.A. Waever, Rev. Mod. Phys. **74** (2002) 1015
- [187] W.R. Hix and F.-K. Thielemann, astr. J. **460** (1996) 869
- [188] G. 't Hooft, Phys. Lett. **37** (1971) 195
- [189] S. Nakamura *et al.*, Nucl. Phys. **A707** (2002) 561
- [190] E. Kolbe, K. Langanke and P. Vogel, Phys. Rev. **D66** (2002) 013007
- [191] K. Scholberg, Ann. Rev. Nucl. Part. Science **62** (2012) 81
- [192] T.A. Thompson, A. Burrows and P.A. Pinto, Astrophys. J. **A592** (2003) 434
- [193] M. Kachelriess *et al.*, Phys. Rev. **D71** (2005) 063003
- [194] G.M. Fuller and B.S. Meyer, Astrophys. J. **376** (1991) 701
- [195] T. Fischer, K. Langanke and G. Martinez-Pinedo, Phys. Rev. C **88** (2014) 065804
- [196] G.W. Misch, B.A. Brown and G.M. Fuller, Phys. Rev. **C88** (2013) 015807
- [197] Y.-Z. Qian and G.M. Fuller, Phys. Rev. **D52** (1995) 656
- [198] C. Fröhlich *et al.*, Astrophys. J. **637** (2005) 415
- [199] L.F. Roberts, S. Reddy and G. Shen, Phys. Rev. **C86** (2012) 065803
- [200] G. Martinez-Pinedo, T. Fischer, A. Lohs and L. Huther, Phys. Rev. Lett. **109** (2012) 251104
- [201] A. Arcones *et al.*, Phys. Rev. **78** **78** (2008) 015806

- [202] N. Barnea and D. Gazit, *Few Body Systems* **43** (2008) 5
- [203] D. Gazit and N. Barnea, *Phys. Rev. Lett.* **98** (2007) 192501
- [204] E. O'Connor *et al.*, *Phys. Rev.* **C75** (2007) 055803
- [205] E. Kolbe and K. Langanke, *Phys. Rep.* **227** (1993) 37
- [206] M. Liebendörfer *et al.*, *Phys. Rev.* **D63** (2001) 103004
- [207] H.Th. Janka, R. Buras and M. Rampp, *Nucl. Phys.* **A718** (2003) 269
- [208] T.A. Thompson, E. Quataert and A. Burrows, *Astrophys. J.* **620** (2005) 861
- [209] I.R. Seitenzahl *et al.*, *Astrophys. J. Lett.* **685** (2008) L129
- [210] C. Fröhlich, G. Martinez-Pinedo *et al.*, *Phys. Rev. Lett.* **96** (2006) 142502
- [211] J. Pruet *et al.*, *Astrophys. J.* **623** (2005) 325
- [212] F.-K. Thielemann, K. Nomoto and M. Hashimoto, *Astrophys. J.* **460** (1996) 408
- [213] R. Cayrel *et al.*, *Astrophys. Astrophys.* **416** (2004) 1117
- [214] R.G. Gratton and C. Sneden, *Astrophys. Astrophys.* **241** (1991) 501
- [215] H. Schatz *et al.*, *Phys. Rep.* **294** (1998) 167
- [216] M. Wiescher and H. Schatz, *Nucl. Phys.* **A693** (2001) 269
- [217] J. Pruet, R. D. Hoffman, S. E. Woosley, H.-T. Janka, R. Buras, *Astrophys. J.* **644** (2006) 1028.
- [218] L. Huther, PhD thesis, Technische Universität Darmstadt, (2014)
- [219] S. Wanajo, H.-T. Janka, S. Kubono, *Astrophys. J.* **729** (2011) 46.
- [220] A. Arcones, C. Fröhlich, G. Martínez-Pinedo, *Astrophys. J.* **750** (2012) 18.
- [221] S. Wanajo, *Astrophys. J.* **647** (2006) 1323
- [222] G. Fogli, E. Lisi, A. Marrone and I. Tamborra, *J. Cosmol. Astropart. Phys.* **10** (2009) 002
- [223] G. Martinez-Pinedo *et al.*, *Eur. Phys. J.* **47** (2011) 98
- [224] S. Wanajo, H.-Th. Janka and B. Müller, *Astrophys. J. Lett.* **726** (2011) L15
- [225] C. Weber *et al.*, *Phys. Rev.* **C78** (2008) 054310
- [226] E. Haettner *et al.*, *Phys. Rev. Lett.* **106** (2011) 122501
- [227] X.L. Tu *et al.*, *Phys. Rev. Lett.* **106** (2011) 112501
- [228] J. Fallis *et al.*, *Phys. Rev.* **C84** (2011) 045807
- [229] C. Fröhlich and T. Rauscher, *AIP Conference Series* **1484** (2012) 232
- [230] A.G.W. Cameron, *Stellar evolution, Nuclear Astrophysics and Nucleogenesis*, Report CRL-41 (Chalk River, 1957)

- [231] K. Blaum, Phys. Rep. **425** (2006) 1
- [232] G. Audi *et al.*, Nucl. Data Sheets **120** (2014) 1; Chin. Phys. **C36** (2012) 1603
- [233] G. Audi *et al.*, Nucl. Phys. **A729** (2003) 337
- [234] B. Pfeiffer, K. Venkataramaniah, U. Czok and C. Scheidenberger, At. Data Nucl. Data Tables **100** (2014) 403
- [235] P. Möller, J.R. Nix, W.D. Myers and W.J. Swiatecki, At. Data Nucl. Data Tables **59** (1995) 185
- [236] P. Möller *et al.*, Phys. Rev. Lett. **108** (2012) 052501
- [237] M. Liu, N. Wang, Y. Deng and X. Wu, Phys. Rev. **84** (2011) 014333
- [238] J.M. Pearson, R.C. Nayak and S. Goriely, Phys. Lett. **B387** (1996) 455
- [239] J. Duflo and A.P. Zuker, Phys. Rev. **C52** (1995) R23
- [240] S. Goriely, N. Chamel and J.M. Pearson, Phys. Rev. **C82** (2010) 035804
- [241] P.T. Hosmer *et al.*, Phys. Rev. Lett. **94** (2005) 112501
- [242] M. Madurga *et al.*, Phys. Rev. Lett. **109** (2012) 112501
- [243] M. Quinn *et al.*, Phys. Rev. **C85** (2012) 035807
- [244] P.T. Hosmer *et al.*, Phys. Rev. **C82** (2010) 025806
- [245] K.-L. Kratz *et al.*, Zeit. f. Phys. **A325** (1986) 489
- [246] B. Pfeiffer, K.-L. Kratz, F.-K. Thielemann and W.B. Walters, Nucl. Phys. **A693** (2001) 282
- [247] N. Nishimura *et al.*, Phys. Rev. **C85** (2012) 048801
- [248] T. Kurtukian-Nieto *et al.*, Eur. Phys. J. (2014)
- [249] P. Möller, B. Pfeiffer and K.-L. Kratz, Phys. Rev. **C66** (2003) 055802
- [250] T. Suzuki *et al.*, Phys. Rev. **C85** (2012) 015802
- [251] Q. Zhi *et al.*, Phys. Rev. **C87** (2013) 025803
- [252] N. Christlieb *et al.*, Astrophys. J. **428** (2004) 1027
- [253] J.J. Cowan and C. Sneden, Nature **440** (2006) 1151
- [254] C. Sneden, J.J. Cowan and R. Gallino, Ann. Rev. Astron. Astrophys. **46** (2008) 241
- [255] I.U. Roederer and J.E. Lawler, Astrophys. J. **750** (2012) 76
- [256] S. Honda, W. Aoki, Y. Ishimaru, S. Wanajo and S.G. Ryan, Astrophys. J. **643** (2006) 1180
- [257] I.U. Roederer *et al.*, Astrophys. J. Suppl. **203** (2012) 27
- [258] J. de Jesus Mendoza-Temis, Ph.D. thesis, Technische Universität Darmstadt (2014)

- [259] O. Korobkin, S. Rosswog, A. Arcones and C. Winteler, *Mon. Not. Roy. Astrophys. Soc.* **426** (2012) 1940
- [260] A. Bauswein, S. Goriely and H.-Th. Janka, *Astrophys. J.* **773** (2013) 78
- [261] S. Goriely *et al.*, *Phys. Rev. Lett.* **111** (2013) 242502
- [262] M. Eichler *et al.*, *Astrophys. J.* (2014) submitted
- [263] J.-J. Gaimard and K.-H. Schmidt, *Nucl. Phys.* **A531** (1991) 709
- [264] Y.Z. Qian, *Astrophys. J.* **534** (2000) L67
- [265] D. Argast, M. Samland, F.-K. Thielemann and Y.Z. Qian, *Astrophys. J.* **416** (2004) 997
- [266] S. Shen, R. Cooke, E. Ramirez-Ruiz, P. Madau, L. Mayer, J. Guedes, ArXiv e-prints (2014), arXiv:1407.3796 [astro-ph.GA].
- [267] F. van de Voort, E. Quataert, P. F. Hopkins, D. Kereš, C.-A. Faucher-Giguère, *Mon. Not. Roy. Ast. Soc.* **447** (2015) 140.
- [268] B. Wehmeyer, M. Pignatari, F.-K. Thielemann, ArXiv e-prints (2015), arXiv:1501.07749 [astro-ph.GA].
- [269] S. Wanajo, Y. Sekiguchi, N. Nishimura, K. Kiuchi, K. Kyutoku, M. Shibata, *Astrophys. J.* **789** (2014) L39.
- [270] C. Winteler *et al.*, *Astrophys. J.* **750** (2012) L22
- [271] P. Banerjee, W.C. Haxton and Y.Z. Qian, *Phys. Rev. Lett.* **106** (2011) 201104
- [272] D. Gazit and N. Barnea, *Phys. Rev. Lett.* **98** (2007) 192501
- [273] N. Barnea, W. Leidemann and G. Orlandini, *Phys. Rev.* **C61** (2000) 054001
- [274] G. Martinez-Pinedo, T. Fischer and L. Huther, *J. Phys.* **G41** (2014) 044008
- [275] S.E. Woosley *et al.*, *Astrophys. J.* **433** (1994) 229
- [276] J. Wittl, H.-Th. Janka and K. Takahashi, *Astrophys. J.* **286** (1994) 841
- [277] Y.-Z. Qian and S.E. Woosley, *Astrophys. J.* **471** (1996) 331
- [278] R.D. Hoffman, S.E. Woosley and Y.Z. Qian, *Astrophys. J.* **482** (1997) 951
- [279] L.F. Roberts, S.E. Woosley and R.D. Hoffman, *Str. J.* **722** (2010) 954
- [280] M.-R. Wu, T. Fischer, L. Huther, G. Martínez-Pinedo, and Y. Qian, *Phys. Rev. D* **89**, 061303 (2014).
- [281] K. Langanke and G. Martinez-Pinedo, *Rev. Mod. Phys.* **75** (2003) 819
- [282] G.M. Fuller and B.S. Meyer, *Astrophys. J.* **453** (1995) 792
- [283] G.C. McLaughlin and G.M. Fuller, *Astrophys. J.* **455** (1995) 202
- [284] M. Terasawa *et al.*, *Astrophys. J.* **562** (2001) 470

- [285] M. Terasawa *et al.*, Nucl. Phys. **A688** (2001) 581c
- [286] M. Terasawa *et al.*, Astrophys. J. **608** (2004) 470
- [287] A. Kelic *et al.*, Phys. Lett. **B616** (2005) 48
- [288] Y.-Z. Qian *et al.*, Phys. Rev. **C55** (1997) 1532
- [289] W.C. Haxton *et al.*, Phys. Rev. Lett. **78** (1997) 2694
- [290] B.S. Meyer, Astrophys. J. Lett. **449** (1995) L55
- [291] G.V. Domogatskii and D.K. Nadyozhin, Sov. Astron. **22** (1978) 297
- [292] S.E. Woosley and W.C. Haxton, Nature **334** (1988) 45
- [293] S. Goriely, M. Arnould, I. Borzov and M. Rayet, Astrophys. J. **375** (2001) 35
- [294] A. Heger *et al.*, Phys. Lett. **B606** (2005) 258
- [295] W.M. Howard, B.S. Meyer and S.E. Woosley, Astrophys. J. **373** (1991) L5
- [296] A. Byelikov *et al.*, Phys. Rev. Lett. **98** (2007) 082501
- [297] D. Belic *et al.*, Phys. Rev. Lett. **83** (1999) 5242
- [298] D. Belic *et al.*, Phys. Rev. **C65** (2001) 035801
- [299] T. Hayakawa, T. Kajino, S. Chiba and G.M. Mathews, Phys. Rev. **C81** (2010) 052801
- [300] T. Hayakawa, T. Kajino, S. Chiba and G.M. Mathews, Phys. Rev. **C82** (2010) 058801
- [301] T.R. Saitoh *et al.*, Nucl. Phys. **A660** (1999) 121
- [302] G.D. Dracoulis *et al.*, Phys. Rev. **C58** (1998) 1444
- [303] P. Mohr, F. Käppeler and R. Gallino, Phys. Rev. **C75** (2007) 012802(R)
- [304] K. Wisshak *et al.*, Phys. Rev. Lett. **87** (2001) 251102
- [305] T. Rauscher, A. Heger, R.D. Hoffman and S.E. Woosley, Astrophys. J. **576** (2002) 323
- [306] T. Suzuki, S. Chiba, T. Yoshida, T. Kajino and T. Otsuka, Phys. Rev. **C74** (2006) 034307
- [307] T. Yoshida *et al.*, Astrophys. J. **686** (2008) 448
- [308] A. Sieverding, L. Huther, G. Martinez-Pinedo and K. Langanke, submitted to Physical Review Letters (2015)
- [309] K. Loders, ApJ **591**, 1220 (2003)
- [310] G.J. Mathews *et al.*, Phys. Rev. **D85** (2012) 105023
- [311] M.K. Cheoun *et al.*, Prog. Theor. Phys. Suppl. **196** (2012) 476
- [312] T. Kajino, G.J. Mathews and T. Hayakawa, J. Phys. **G41** (2014) 044007
- [313] S.G. Ryan, J.E. Norris and T.C. Beers, Astrophys. J. **523** (1999) 654

- [314] T. Fischer, S. C. Whitehouse, A. Mezzacappa, F.-K. Thielemann, and M. Liebendörfer, *Astron. Astrophys.* **517**, A80 (2010).
- [315] A. Sieverding, Master Thesis, technische Universität Darmstadt (2014)
- [316] R.M. Biontaet *et al.*, *Phys. Rev. Lett.* **58** (1987) 1494
- [317] W.J. Marciano and Z. Parsa, *J. Phys.* **G29** (2003) 2629
- [318] J.F. Beacom, W.M. Farr and P. Vogel, *Phys. Rev.* **D66** (2002) 033001
- [319] D.Z. Freedman, D.N. Schramm and D.L. Tubbs, *Ann. rev. Nucl. Part. Sci.* **27** (1977) 167
- [320] A. drukier and L. Stodolsky, *Phys. Rev.* **D30** (1984) 2295
- [321] T. Suzuki, *J. Phys.: Conf. Ser.* **321** (2011) 012041
- [322] E. Kolbe *et al.*, *Nucl. Phys.* **A540** (1992) 599
- [323] A. Ianni, *Journal of Physics Conf. Ser.* **309** (2011) 012027
- [324] W.C. Haxton, *Phys. Rev.* **D36** (1987) 2283
- [325] W.C. Haxton, *Phys. Rev.* **C37** (1988) 2660
- [326] K. Langanke, P. Vogel and E. Kolbe, *Phys. Rev. Lett.* **76** (1996) 2629
- [327] T. Suzuki and T. Otsuka, *Phys. Rev. C* **78** (2008) 061301(R)
- [328] T. Suzuki and M. Honma, *Phys. Rev. C* **87** (2013) 014607
- [329] A. Bueno, I. Gil Bottella and A. Rubbia, arXiv:hep-ph/0307222 (2003)
- [330] I. Gil Botella and A. Rubbia, *J. Cosmol. Astr. Phys.* (2004) 0408:001
- [331] M. Bhattacharya, C.D. Goodman and A. Garcia, *Phys. Rev. C* **80** (2009) 055501
- [332] M. Bhattacharya *et al.*, *Phys. Rev. C* **58** (1998) 3677
- [333] M. Karakoc *et al.*, *Phys. Rev. C* **89** (2014) 064313
- [334] W.E. Ormand *et al.*, *Phys. Lett. B* **345** (1995) 343
- [335] M. Sajjad Athar and S.K. Singh, *Phys. Lett. B* **591** (2004) 69
- [336] M.-K. Cheoun, E. Ha and T. Kajino, *Phys. Rev. C* **83** (2011) 028801
- [337] C.A. Duba *et al.*, *J. Phys. Conf. Ser.* 136:042077 (2008)
- [338] C. Volpe, N. Auerbach, G. Colo and N. Van Giai, *Phys. Rev.* **C65** (2002) 044603
- [339] J. Engel, G.C. McLaughlin and C. Volpe, *Phys. Rev.* **D67** (2003) 013005
- [340] G.M. Fuller, W.C. Haxton and G.C. McLaughlin, *Phys. Rev.* **D59** (1999) 085005
- [341] A. Krasznahorkay *et al.*, *Phys. Rev.* **C64** (2001) 067302
- [342] T. Suzuki and H. Sagawa, *Nucl. Phys.* **A718** (2003) 446c

- [343] N. Jachowicz and K. Heyde, Phys. Rev. **C68** (2003) 055502
- [344] N. Jachowicz, G.C. McLaughlin and C. Volpe, Phys. Rev. **C77** (2008) 055501
- [345] N. Paar, H. Tutman, T. Marketin and T. Fischer, Phys. Rev. **C87** (2013) 025801
- [346] K. Zuber, Phys. Lett. **519** (2001) 1
- [347] M. Nomachi *et al.*, Nucl. Phys **B138** (2005) 221
- [348] W. Rodejohann, Int. J. Mod. Phys. **20** (2011) 1833
- [349] H. Ejiri and S.R. Elliott, Phys. Rev. **C89** (2013) 055501
- [350] H.J. Thies *et al.*, Phys. Rev. **C86** (2012) 044309
- [351] A. Garcia *et al.*, Hyperfine Interact **223** (2014) 201
- [352] M. Sasano *et al.*, Nucl. Phys. **A788** (2007) 76
- [353] M. Sasano *et al.*, Phys. Rev. **85** (2012) 061301(R)
- [354] H. Akimune *et al.*, Phys. Lett. **B394** (1997) 23
- [355] H. Akimune *et al.*, Phys. Lett. **B665** (2008) 424
- [356] C. Wrede *et al.*, Phys. Rev. **C87** (2013) 031303(R)
- [357] W. Almosly *et al.*, Phys. Rev. **C89** (2014) 024308
- [358] W. Almosly, E. Ydrefors and J. Suhonen, J. Phys. **G40** (2013) 095201
- [359] W. Almosly, E. Ydrefors and J. Suhonen, J. Phys. **G42** (2015) 025106
- [360] E. Ydrefors, K.G. Balasi, T.S. Kosmas and J. Suhonen, Nucl. Phys. A **896** (2012) 1
- [361] E. Ydrefors, K.G. Balasi, T.S. Kosmas and J. Suhonen, Nucl. Phys. A **866** (2011) 67
- [362] K.G. Balasi, E. Ydrefors and T.S. Kosmas, Nucl. Phys. A **868** (2011) 82
- [363] E. Ydrefors and J. Suhonen, Phys. Rev. C **87** (2013) 034314
- [364] H. Ejiri, J. Engel and N. Kudomi, Phys. Lett. B **530** (2002) 27